

Yield stress materials in soft condensed matter

Daniel Bonn

*Van der Waals-Zeeman Institute, Institute of Physics, University of Amsterdam,
Science Park 904, 1098 XH Amsterdam, The Netherlands*

Morton M. Denn

*Benjamin Levich Institute and Department of Chemical Engineering, City College of New York,
CUNY, New York, New York 10031, USA*

Ludovic Berthier

*Laboratoire Charles Coulomb, UMR 5221, CNRS and Université Montpellier,
Montpellier, France*

Thibaut Divoux

*Centre de Recherche Paul Pascal, CNRS UPR 8641–115 avenue Schweitzer,
33600 Pessac, France and MultiScale Material Science for Energy and Environment,
UMI 3466, CNRS-MIT, 77 Massachusetts Avenue, Cambridge, Massachusetts 02139, USA*

Sébastien Manneville

*Univ Lyon, Ens de Lyon, Univ Claude Bernard, CNRS, Laboratoire de Physique,
F-69342 Lyon, France*

(published 21 August 2017)

A comprehensive review is presented of the physical behavior of yield stress materials in soft condensed matter, which encompasses a broad range of materials from colloidal assemblies and gels to emulsions and non-Brownian suspensions. All these disordered materials display a nonlinear flow behavior in response to external mechanical forces due to the existence of a finite force threshold for flow to occur: the yield stress. Both the physical origin and rheological consequences associated with this nonlinear behavior are discussed and an overview is given of experimental techniques available to measure the yield stress. Recent progress is discussed concerning a microscopic theoretical description of the flow dynamics of yield stress materials, emphasizing, in particular, the role played by relaxation time scales, the interplay between shear flow and aging behavior, the existence of inhomogeneous shear flows and shear bands, wall slip, and nonlocal effects in confined geometries.

DOI: [10.1103/RevModPhys.89.035005](https://doi.org/10.1103/RevModPhys.89.035005)

CONTENTS

I. Introduction to Yield Stress Materials	2	a. Mode-coupling theories and trap models	12
II. General Concepts about Yield Stress Fluids	3	b. Shear transformation zones and elastoplastic models	12
A. Popular rheological models for yield stress materials	3	3. Theoretical flow curves	12
B. Physical origin of the yield stress in soft materials	4	a. Soft glassy rheology	13
1. Simple colloidal systems: Soft glassy materials	4	b. Mode-coupling theories	13
2. Non-Brownian suspensions: Jammed materials	5	c. Jamming rheology	15
3. Role of attractive forces: Colloidal gels	7	III. Physical Insights from Yield Stress Measurements	17
a. Nonequilibrium gels	7	A. Experiments probing the liquid-to-solid transition	17
b. Attractive glasses	7	1. Extrapolating the flow curve in the limit of vanishing shear rates	17
c. Athermal adhesive systems	8	2. Determining the residual stress after flow cessation	18
C. Is the yield stress real?	8	B. Experiments probing the solid-to-liquid transition	18
1. A historical debate	8	1. Analyzing the transient stress response during shear start-up	18
2. Theoretical considerations about the existence of a yield stress	9	2. Creep experiments	20
D. Thixotropy in yield stress fluids	10	3. Large-amplitude oscillatory shear experiments	20
E. Theoretical descriptions of yield stress materials	11	4. Nonviscometric flows	22
1. Why a theory of yield stress solids is difficult	11	C. Wall slip in yield stress materials	22
2. Theoretical approaches	11		

1. Impact on flow-curve measurements	22
2. Physical origin of wall slip in yield stress fluids	22
a. Wall slip in the case of soft particles	23
b. Wall slip in the case of hard particles	24
3. Dealing with wall slip in practice	24
IV. Steady-state Flow Dynamics of Yield Stress Fluids:	
Flow Curves and Shear Banding	25
A. Flow curves of simple and thixotropic yield stress fluids	25
1. Distinction between flow curves	25
2. Existence of a “viscosity bifurcation”	25
3. Consequences for local measurements	26
B. Causes of steady-state shear banding	27
1. Competition between aging and shear rejuvenation	27
2. Static versus dynamic yielding	28
3. Flow-concentration coupling	29
C. Emerging topics: Confinement and transient regimes	29
1. Yield stress materials in confined geometries	29
a. Cooperative effects in simple yield stress fluids	30
b. Shear-induced structuration of attractive yield stress fluids	30
2. Origin and scaling of the yielding time scales	31
a. Power-law scalings of the fluidization time and transient shear banding	31
b. Exponential scalings: Activated processes and brittlelike failure	32
c. Dynamics induced by wall slip in transient and steady-state flows	32
D. Open questions	33
V. Summary and Outlook	33
Acknowledgments	34
References	34

I. INTRODUCTION TO YIELD STRESS MATERIALS

Many of the materials that we encounter in our daily life are neither perfectly elastic solids nor simple Newtonian fluids, and attempts to describe these materials as being either fluid or solid often fail. Take, for instance, whipped cream and thick syrup. When moving a spoon through these two materials, one would conclude that syrup is the more viscous fluid. However, when left at rest, the syrup will readily flatten and become horizontal under the force of gravity, while whipped cream will retain its shape for a long time, suggesting that, actually, the whipped cream is more viscous than syrup (Fig. 1). This paradox stems from the fact that the syrup is a Newtonian fluid, whereas whipped cream is not a simple fluid at all, and its flow properties cannot be reduced to a single number such as its viscosity. Whipped cream does not flow if the imposed stress is below a threshold value and flows rather easily after this value is exceeded. This threshold rheology is the defining feature of *yield stress materials*. Classical, everyday examples of yield stress materials include paints, foams, wet cement, cleansing creams, mayonnaise, and tooth paste.

Besides pharmaceutical and cosmetic applications, yield stress materials are also used in the oil industry, where estimating the minimum pressure required to restart a gelled crude-oil pipeline is crucial (Chang, Nguyen, and Rønning, 1999). The yield stress is also relevant to the concrete



FIG. 1. Which fluid is more viscous: whipped cream or thick maple syrup? Slowly stirring both materials with a spoon suggests that syrup is more viscous, while observing the flattening of piles of each material with time suggests the opposite. In fact, the question is ill posed. The flow properties of whipped cream cannot be reduced to a single viscosity value because it is a yield stress material, whereas syrup is simply a very viscous fluid.

and dairy product industries, where its value is related to the size of air bubbles that may remain trapped in the material and directly affect its properties (van Aken, 2001; Kogan *et al.*, 2013). In all these fields, it is of paramount importance to characterize as quantitatively as possible the force threshold needed to make the material flow, i.e., the yield stress.

We review recent progress concerning the fundamental understanding of the yield stress as well as the physical processes relevant to experimental studies of the yielding transition in a broad range of materials across soft condensed matter. The existence of a threshold for flow suggests that these materials respond in a highly nonlinear manner, which has a dramatic impact on their dynamical properties under flow, which we also discuss extensively. Yield stress phenomena are of key importance both from a fundamental point of view and for practical situations involving amorphous solids, spanning a wide range of materials and spanning the fields of hard and soft condensed matter physics.

There are a number of topical reviews available dealing with specific aspects of yield stress materials (Coussot, 2005, 2014; Møller, Mewis, and Bonn, 2006; Denn and Bonn, 2011; Mansard and Colin, 2012; Balmforth, Frigaard, and Ovarlez, 2014). In addition, a collection of relevant papers appeared very recently in a special issue celebrating the anniversary of the first paper by Bingham describing yield stress fluids (Cloitre and Bonnecaze, 2017; Coussot, 2017; Coussot, Malkin, and Ovarlez, 2017; Dinkgreve, Denn, and Bonn, 2017; Ewoldt and McKinley, 2017; Frigaard, Paso, and de Souza Mendes, 2017; Malkin, Kulichikhin, and Ilyin, 2017; Mitsoulis and Tsamopoulos, 2017; Saramito and Wachs, 2017). The present review attempts to give a concise overview of the physics of yield stress materials taking a very broad perspective encompassing fundamental, experimental, and practical issues, along with a discussion of some important open questions.

The review is organized as follows. In Sec. II, we give a general overview of the various physical concepts and issues raised by the existence of a yield stress, with emphasis on model systems and theoretical approaches. In Sec. III, we provide a critical review of the experimental issues that arise due to the yield stress and of their physical causes, with emphasis on the ubiquitous phenomenon of apparent slippage of yield stress materials at the walls. Section IV is devoted to the most recent developments and emerging topics regarding flow dynamics of yield stress fluids, including time

dependence and shear banding, as well as the effects of confinement and transient fluidization behaviors. We close our review with a summary in Sec. V.

II. GENERAL CONCEPTS ABOUT YIELD STRESS FLUIDS

A. Popular rheological models for yield stress materials

Quantifying the steady-state flow properties of a non-Newtonian fluid requires the measurement of its full *flow curve* as the shear viscosity is not a unique number. For a simple shear geometry, the flow curve is a representation of the dependence of the shear stress σ on the shear rate $\dot{\gamma}$. For a Newtonian fluid, these functions are linearly related, $\sigma = \eta\dot{\gamma}$, where η is a constant viscosity. For a yield stress material, the viscosity formally becomes a function of the shear rate $\sigma = \eta(\dot{\gamma})\dot{\gamma}$, and the flow curve $\sigma = \sigma(\dot{\gamma})$ is not a simple straight line crossing the origin. As discussed later, for a number of materials, the viscosity also becomes a function of the entire measurement procedure, resulting in a complex time dependence, which can make practical measurements challenging.

The most elementary model capturing the existence of a finite yield stress is the Bingham model (Bingham, 1922):

$$\sigma < \sigma_y \Rightarrow \dot{\gamma} = 0, \quad (1)$$

$$\sigma \geq \sigma_y \Rightarrow \sigma = \sigma_y + \eta_p \dot{\gamma}, \quad (2)$$

where $\sigma_y > 0$ is the yield stress, and η_p is a model parameter describing the slope of the flow curve in the fluid region, which is defined by $\dot{\gamma} > 0$. The Bingham model is equivalently described by an effective viscosity which is asymptotically equal to η_p at large stresses and diverges continuously as the stress decreases toward the yield stress $\eta_{\text{eff}}(\dot{\gamma}) \equiv \sigma/\dot{\gamma} = \eta_p + \sigma_y/\dot{\gamma}$. Its simplicity stems from the fact that it uses only a single material-dependent number, the yield stress σ_y , to describe complex, nonlinear behavior incorporating a threshold force.

In Fig. 2 we return to the examples of whipped cream and syrup, showing flow curves for both materials. Figure 2(a) illustrates the fact that the Bingham model gives a reasonable description of the measured flow curve of whipped cream with a yield stress of about $\sigma_y \approx 33$ Pa, while Fig. 2(b) shows that it makes little sense to compare the viscosity of these two “fluids” as, in fact, only one of them is really a fluid with a constant viscosity.

Figure 2 also illustrates that whereas the Bingham model appears to be an excellent fit to the flow curve of whipped cream [Fig. 2(a)], it actually fails at low shear rates, which becomes obvious once the resolution is improved [Fig. 2(b)]. From the latter plot, one concludes that the yield stress is about $\sigma_y \approx 10$ Pa, rather than 33 Pa. This highlights one of the many practical problems encountered when working with complex fluids: before a question about the flow properties of a complex material can be satisfactorily answered, one needs to carefully consider the exact experimental protocol as well as the range and resolution of shear rates and stresses over which the data are analyzed.

Two popular generalizations of the Bingham fluid model in shear flow are the Herschel-Bulkley (Herschel and Bulkley, 1926) and Casson equations given as

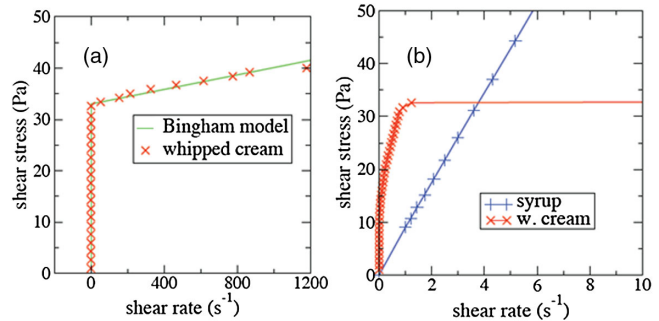


FIG. 2. (a) The Bingham model (solid line) provides a reasonable fit to the experimental flow curve of whipped cream (crosses), with yield stress $\sigma_y \approx 33$ Pa. (b) The flow curves of syrup (plusses) and whipped cream (crosses) at low shear rates. Data points are connected by lines as guides to the eye. For stresses above 33 Pa, whipped cream flows more easily than syrup, while the opposite is true below 33 Pa. Using this enlarged scale, one can see that the flow curve of whipped cream below the yield stress is in fact not well described by the Bingham model [Eq. (1)], which simply predicts zero shear rate all the way up to σ_y .

$$\text{Herschel-Bulkley : } \sigma = \sigma_y + K\dot{\gamma}^n, \quad \sigma \geq \sigma_y, \quad (3)$$

$$\text{Casson : } \sigma^{1/2} = \sigma_y^{1/2} + (\eta_p \dot{\gamma})^{1/2}, \quad \sigma \geq \sigma_y, \quad (4)$$

where K and n are additional parameters. Obviously, the Bingham model is a specific instance of the Herschel-Bulkley equation, obtained by imposing $n = 1$.

The Herschel-Bulkley model is popular as it offers more flexibility for fitting experimental data than the Bingham model. It describes both the yield stress regime $\sigma \approx \sigma_y$ at low shear rate, and a power-law shear-thinning behavior $\sigma \approx K\dot{\gamma}^n$, with $n < 1$ for larger shear rates. Across a large variety of systems, the shear-thinning exponent n is found to have a value in the range $n = 0.2–0.8$, rather than the $n = 1$ value imposed in the Bingham model. Frequently, n changes very little with either the density or the temperature of the material (Vinogradov, Froishteter, and Trilisky, 1978), so that it appears to be a relevant “material parameter,” for instance for microgels (Roberts and Barnes, 2001; Oppong *et al.*, 2006; Nordstrom *et al.*, 2010; Gutowski *et al.*, 2012), emulsions (Mason, Bibette, and Weitz, 1996; Bégu, Manneville, and Colin, 2006), and foams (Princen and Kiss, 1989; Pratt and Dennin, 2003; Höhler and Cohen-Addad, 2005; Gilbreth, Sullivan, and Dennin, 2006). As such, its determination (or prediction) has become a question of theoretical interest as well, as discussed later.

The crossover between the yield stress and the shear-thinning regimes in the Herschel-Bulkley model occurs for a typical shear rate $\dot{\gamma}^* \approx (\sigma_y/K)^{1/n}$. It is therefore tempting to interpret the corresponding time scale $1/\dot{\gamma}^*$ as a relevant microscopic time scale for the material (Bonnecaze and Cloitre, 2010). The Herschel-Bulkley equation also predicts the existence of a diverging time scale τ governing the relaxation to steady state in stress-controlled experiments in the vicinity of the yield point, i.e., for $\sigma \gtrsim \sigma_y$, since one gets $\tau \sim \dot{\gamma}^{-1} \approx [K/(\sigma - \sigma_y)]^{1/n}$, which readily suggests an interpretation of the yielding transition observed in steady-state

simple shear flows in terms of a critical point (Divoux *et al.*, 2012; Chaudhuri and Horbach, 2013). This topic will be discussed extensively in Sec. IV.C.

B. Physical origin of the yield stress in soft materials

To elucidate the physical origin of yield stress rheology in a given material, ideally one wants to know under what conditions the material exhibits a yield stress, what microscopic mechanisms are responsible for the emergence of a yield stress, and whether general rules can be formulated to predict the actual value of the yield stress for instance as a function of the composition and structural organization (constituents, interactions) of the material. The emergence of a finite yield stress is frequently referred to as a “jamming transition” (Liu and Nagel, 2001; Trappe *et al.*, 2001; van Hecke, 2010): a broad range of dense amorphous materials (from foams and grains to dense liquids) shares the important similarity that they do not flow unless a large enough shear stress is applied. This idea was popularized via a schematic jamming phase diagram by Liu and Nagel (1998).

However, the existence of a similar type of transition between fluid and amorphous solid states does not imply that a single physical mechanism should be at work: soft condensed materials may become solid by crossing a variety of phase transitions, and the jamming transition is now understood as being only one of them (Liu and Nagel, 2010; van Hecke, 2010). In the following, we describe three important classes of yield stress materials whose solid behavior originates from qualitatively different types of phase transitions (or sharp dynamical crossovers), which are usually described by different types of theoretical approaches as well.

1. Simple colloidal systems: Soft glassy materials

Suspensions of nearly hard-sphere colloidal particles are among the most studied experimental systems in soft condensed matter (Pusey and van Megen, 1986; Hunter and Weeks, 2012), as they represent good model systems to study a large variety of physical phenomena also occurring in atomic

and molecular systems, from first-order crystallization to glassy dynamics (Royall, Poon, and Weeks, 2013). For colloidal particles, thermal fluctuations and Brownian motion play key roles since they ensure that the system can reach thermal equilibrium. However, when the volume fraction ϕ of colloidal hard spheres is increased, the system undergoes a colloidal glass transition that shares important similarities with the glass transition observed upon decreasing the temperature in molecular supercooled liquids (Pusey and van Megen, 1987). Experimentally, above a “glass transition” packing fraction of about $\phi_G \approx 0.58\text{--}0.60$ (in three-dimensional suspensions), the equilibrium relaxation time of the colloidal suspension becomes so large that the particles do not significantly diffuse over a typical experimental time scale and the system is effectively dynamically arrested (Brambilla *et al.*, 2009). At packing fractions above ϕ_G , colloidal particles simply perform localized back-and-forth “vibrational” motion inside the cage formed by their neighbors. This empirical definition of the glass transition density demonstrates that its actual location is not very well defined experimentally, in the sense that deciding whether a material is “solid” or simply “very viscous” depends on the observation time scale or the explored range of shear rates in steady-state flow curves.

The rheological consequences of the glass transition are readily observed in the flow curves shown in Fig. 3(a) (Petekidis, Vlassopoulos, and Pusey, 2004). An extended Newtonian regime is observed for $\phi < \phi_G$, which defines a density-dependent viscosity $\eta(\phi)$ that is seen to increase very rapidly as the density increases toward ϕ_G . A finite yield stress σ_y emerges as the glass transition is crossed for $\phi > \phi_G$, which increases as the colloidal glass concentration is increased further. In the vicinity of the glass transition $\phi \approx \phi_G$, a shear-thinning regime is observed, where $\sigma \approx \dot{\gamma}^n$ with $n < 1$, illustrating the general fact that glassy suspensions are easily driven out of the linear rheological regime. In fact, accurate measurements of the linear viscosity in hard-sphere suspensions are scarce and often limited to a modest dynamic regime (Cheng *et al.*, 2002), precisely because it is challenging to access the linear rheological regime. In the glass phase, the flow

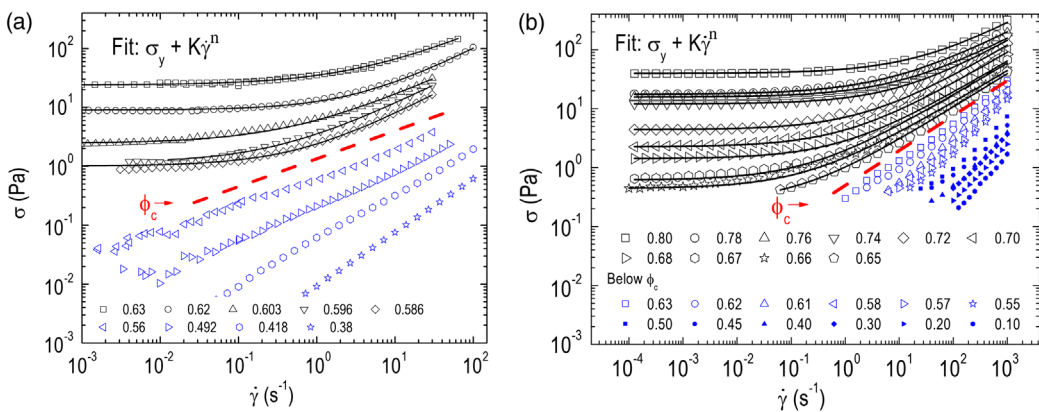


FIG. 3. (a) Soft glassy rheology. Evolution of the flow curves across the thermal colloidal glass transition for a suspension of PMMA hard spheres of size $a \approx 200$ nm. From Petekidis, Vlassopoulos, and Pusey, 2004. (b) Jamming rheology. Evolution of the flow curves for an oil-in-water emulsion with droplet size $a \approx 3.2$ μm across the athermal jamming transition. From Paredes, Michels, and Bonn, 2013. In both cases, a yield stress appears above a certain critical density ϕ_c (dashed line), which corresponds to the glass transition ϕ_G for thermal systems in (a), and to the jamming transition ϕ_J for athermal particles in (b). Although the emergence of solid behavior in both cases is conceptually very different, the flow curves of both materials are surprisingly similar.

curves are typically well described by the Herschel-Bulkley law, which efficiently incorporates both the yield stress and shear-thinning behaviors in a single empirical model.

Similar flow curves are observed in many systems undergoing a glass transition, from dense molecular liquids (Berthier and Barrat, 2002) to colloidal suspensions with soft and hard repulsion between the particles (Petekidis, Vlassopoulos, and Pusey, 2004; Nordstrom *et al.*, 2010; Siebenbürger, Fuchs, and Ballauff, 2012). In all these systems, a finite yield stress emerges when the shear viscosity becomes so large (upon changing density or temperature) that the system cannot flow anymore on experimentally accessible time scales. Physically, the yield stress results from the fact that particles move too slowly and cannot rearrange the structure fast enough to relax the stress introduced by an external deformation. Therefore, a simple criterion for the emergence of a yield stress is when the time scale for the spontaneous equilibrium relaxation, usually called the “alpha-relaxation” time scale τ_α , becomes larger than the time scale of the external deformation given by $1/\dot{\gamma}$. In the regime where $\tau_\alpha \dot{\gamma} \gg 1$, spontaneous relaxation cannot occur over the rheologically relevant time window and the system appears solid. Empirically, τ_α closely follows the behavior of the Newtonian viscosity $\tau_\alpha \propto \eta(\phi)$, which explains why the linear regime $\tau_\alpha \dot{\gamma} \ll 1$ becomes difficult to study near the glass transition, where the viscosity increases dramatically.

In such glassy materials, the yield stress is typically a function of temperature and density. This dependence simplifies considerably for the hard-sphere model, because the hard-sphere potential contains no energy scale. In that case, the relevant stress scale controlling solidity is $\sigma_T = k_B T / a^3$, where k_B is Boltzmann’s constant, T is the temperature, and a is the particle diameter, so that the yield stress can be rewritten as $\sigma_y = \sigma_T f(\phi)$, where $f(\phi < \phi_G) = 0$. This behavior emphasizes the entropic origin of the solidity in colloidal hard spheres, and therefore the crucial role played by thermal fluctuations in the emergence of a yield stress in colloidal particles with purely repulsive interactions (Petekidis, Vlassopoulos, and Pusey, 2004; Ikeda, Berthier, and Sollich, 2012).

Finally, when the colloidal glass is compressed far above the glass transition, the interparticle distance decreases and particles eventually come into near contact as the “random close-packing” fraction is approached (Bernal and Mason, 1960). For rheology, this critical packing fraction is more commonly called the “jamming” density (Liu and Nagel, 2010). As a consequence, the colloidal glass becomes stiffer when density increases. For pure hard spheres, this results in a strong increase of the yield stress, which appears to diverge as a power law $\sigma_y \sim \sigma_T (\phi_J - \phi)^{-\gamma}$, with an exponent $\gamma \approx 1$ and a jamming density $\phi_J > \phi_G$. This functional form shows that the yield stress vanishes for fully non-Brownian suspensions of hard particles due to the entropic prefactor $\sigma_T = k_B T / a^3$ which vanishes when the particle size becomes macroscopic, $a \rightarrow \infty$. Therefore, suspensions of non-Brownian hard particles such as granular particles do not belong to the family of yield stress materials. The density dependence of mechanical properties is much smoother for particles with non-hard-sphere interactions, such as soft repulsive particles (Koumakis, Pamvouxoglou *et al.*, 2012; van der Vaart *et al.*, 2013), for which the concept of a sharp jamming transition

cannot be defined in the presence of thermal fluctuations (Ikeda, Berthier, and Sollich, 2013).

2. Non-Brownian suspensions: Jammed materials

When the typical size a of colloidal particles increases, Brownian motion becomes negligible and thermal fluctuations are less relevant. This is because the typical time scale for a Brownian particle to diffuse over a distance comparable to its own size scales as a^2/D_0 , where D_0 is the single-particle diffusion constant. For an observation time scale of the order of 1 s, the crossover typically occurs for a particle diameter of about $a \approx 1 \mu\text{m}$.

Non-Brownian suspensions of soft particles, such as foams and large emulsion droplets, become solid when the density is increased above a critical packing fraction, which corresponds to a genuine jamming transition; in this case, glassy dynamics are not observed. For soft, repulsive spherical particles in three dimensions, the transition takes place near the random close-packing density, $\phi_J \approx 0.64\text{--}0.66$. Apart from experimental difficulties, an important source of the uncertainty concerning the jamming density is size polydispersity. It is empirically found that ϕ_J increases systematically with the size polydispersity of the sample (Hermes and Dijkstra, 2010; Torquato and Stillinger, 2010).

In contrast with the glass transition, thermal fluctuations play strictly no role in this process, and the emergence of solid behavior can be obtained in model systems directly at $T = 0$. If the packing fraction is large enough, non-Brownian particles come into contact and possibly deform, therefore supporting local stresses. The key concept for jamming is the existence of a sufficiently large number of contacts between the particles such that mechanical equilibrium can be maintained throughout the sample (van Hecke, 2010), but the detailed nature of this geometrical transition is different from a simple percolation transition.

A second major difference with the glass transition is that the jamming transition can in principle be defined and located with arbitrary precision, as its definition does not rely on an observation time scale, although, of course, additional experimental difficulties might intervene (van Hecke, 2010; Ikeda, Berthier, and Sollich, 2013). The reason is that the emergence of solidity does not result from the competition between an equilibrium relaxation time scale defined at rest and a finite shear rate, as for glasses, because non-Brownian suspensions have no spontaneous dynamics at rest. The jamming transition and existence of a yield stress in soft materials can therefore be described as “static” transitions resulting from a sharp qualitative change in the microstructural properties of the material (Parisi and Zamponi, 2010).

Another important consequence of the absence of thermal fluctuations is the fact that the jamming transition, unlike the glass transition, necessarily takes place far from thermal equilibrium. In particular, this implies that the preparation protocol of the non-Brownian packings in the vicinity of the jamming transition becomes a relevant parameter controlling the location of the transition (Donev *et al.*, 2004; Berthier and Witten, 2009) but, quite importantly, not its physical nature and properties (Chaudhuri, Berthier, and Sastry, 2010).

In experiments and model systems studied in computer simulations, it is found that the yield stress emerges continuously with increasing packing fraction past the jamming transition (Durian, 1995). This has been reported for foams and emulsions, which are well described (at least near the transition) by simple models of soft repulsive spheres interacting via truncated harmonic or Hertzian potentials of the form

$$V(r < a) = \frac{\epsilon}{\alpha} (1 - r/a)^\alpha, \quad (5)$$

where r is the distance and α gives the power-law exponent for the decay of the interactions; ϵ is an energy scale governing the mechanical property (essentially, the softness) of the particles; the potential is zero when particles are not in contact, $V(r > a) = 0$. In that case, the relevant stress scale controlling the behavior of the yield stress is of energetic (rather than entropic) nature: $\sigma_0 = \epsilon/a^3$. As a result, the yield stress can now be written $\sigma_y = \sigma_0 g(\phi)$, where $g(\phi < \phi_J) = 0$. A robust finding for the behavior of the yield stress above the jamming transition is a power-law behavior $\sigma_y = \sigma_0(\phi - \phi_J)^\Delta$ for $\phi \geq \phi_J$ (Durian, 1995; Olsson and Teitel, 2007). The exponent Δ can be seen as a critical exponent characterizing the rheology of jammed materials; we now discuss whether such scalings can be retrieved in experiments, and how universal these would be.

Emulsions are systems for which the packing fraction can be changed relatively easily, without changing other system parameters much. Probably the first systematic study of flow curves across a range of volume fractions was performed by Mason, Bibette, and Weitz (1996), using a droplet size which is however not quite large enough for thermal fluctuations to be fully irrelevant. Figure 3(b) shows similar data taken over a broader range of parameters and larger droplets so that thermal effects are fully irrelevant (Paredes, Michels, and Bonn, 2013). The similarity with the soft glassy rheology in Fig. 3(a) is striking, as the material crosses over from a Newtonian fluid at low enough density and shear rate to a yield stress solid above jamming, where the flow curves are again well described by the Herschel-Bulkley model with a shear-thinning exponent $n < 1$. Exactly at the jamming density, a power-law shear-thinning behavior is observed. A detailed discussion of the exponent appearing in the Herschel-Bulkley law can be found in Olsson and Teitel (2012). A careful determination of n requires a power-law fit of $\sigma - \sigma_y$ as a function of $\dot{\gamma}$. It is found in simple numerical models that such a plot actually displays two distinct power-law regimes with two different exponents: n at small shear rates and n' at larger shear rates (Olsson and Teitel, 2011, 2012; Lerner, Düring, and Wyart, 2012; Kawasaki *et al.*, 2015). It is likely that the fitting of experimental flow curves is dominated by the second of these two exponents, and comparison to theory is thus somewhat delicate. Additionally, at finite shear rates, it is also possible that other ingredients, such as friction between particles (Katgert, Möbius, and van Hecke, 2008; Katgert *et al.*, 2009; Bonnecaze and Cloitre, 2010) or energy dissipation of the interstitial liquid [or in plateau borders for foams (Schwartz and Princen, 1987)], start to play a significant role and also affect the value of the shear-thinning exponent.

It is interesting to consider the limit of infinitely hard non-Brownian (i.e., granular) suspensions, which are also often

described as possessing a yield stress. As should be clear from the previous discussion, a yield stress can exist only in non-Brownian repulsive objects if they can be compressed strictly above the jamming density $\phi > \phi_J$. This is by definition not possible when particles are truly hard, such as in granular suspensions that exist only in the fluid state $\phi < \phi_J$ (Andreotti, Forterre, and Pouliquen, 2013). Careful measurements on suspensions of spherical particles (Fall *et al.*, 2009, 2013) have indeed revealed that if the particles and suspending liquid are carefully density matched, there is no yield stress up to random close packing, where all the particles start to touch each other. However, as soon as there is the slightest density mismatch, the particles cream or sediment, so that $\phi \rightarrow \phi_J$, which is indeed the only density where hard particles can be fully arrested. This makes non-density-matched suspensions similar to dry granular systems: a sand pile has a clear, finite angle of repose, which is equivalent to stating that it has a yield stress (Vanel *et al.*, 1999). As for sedimenting suspensions, this is due to the gravitational forces that push the grains together and in this way activate the frictional contacts between the grains (Vanel *et al.*, 1999).

A direct consequence of the hard-particle limit is then that no time scale can be constructed from the particle interaction, and the flow curves obtained at constant density therefore simplify considerably and become fully Newtonian. Very different from the flow curves shown in Fig. 3, the rheology of this regime is described by simpler constitutive laws (with no yield stress) that have been carefully studied and validated by many experiments in the community of granular media (MiDi, 2004; Andreotti, Forterre, and Pouliquen, 2013).

In Fig. 4 we summarize the evolution of yield stress with temperature T and packing fraction ϕ for several types of three-dimensional assemblies of harmonic repulsive particles, determined using computer simulations (Ikeda, Berthier, and Sollich, 2013). This demonstrates the emergence of a yield stress in thermalized colloidal assemblies at a packing fraction ϕ_G , which depends weakly on the particle softness. This softness is quantified by the adimensional temperature scale $k_B T/\epsilon$, which compares thermal energy to particle repulsion. Colloidal poly(methyl methacrylate) (PMMA) hard spheres are typically characterized by $k_B T/\epsilon \sim 10^{-8}$, whereas soft microgels are usually much softer, $k_B T/\epsilon \sim 10^{-4}$, emulsions being typically intermediate, $k_B T/\epsilon \sim 10^{-6}$. All these systems display a yield stress above the colloidal glass transition, and the yield stress increases with density in the glass phase. For hard spheres, it diverges at the jamming transition, for emulsions it shows a strong crossover behavior, and it has a smooth density dependence for soft microgels. In soft systems such as foams, $k_B T/\epsilon \sim 10^{-8}$ is again small because thermal fluctuations become irrelevant for such large particles, and the emergence of the yield stress is associated with the jamming transition, with no influence of thermal fluctuations on the rheology. The jamming transition controls the $T \rightarrow 0$ limit of the jamming phase diagram in Fig. 4. Such a diagram is experimentally useful as it allows one to locate systems such as microgels, emulsions, foams, and colloidal hard spheres on the same graph, and to elucidate the origin of the yield stress observed in rheological experiments.

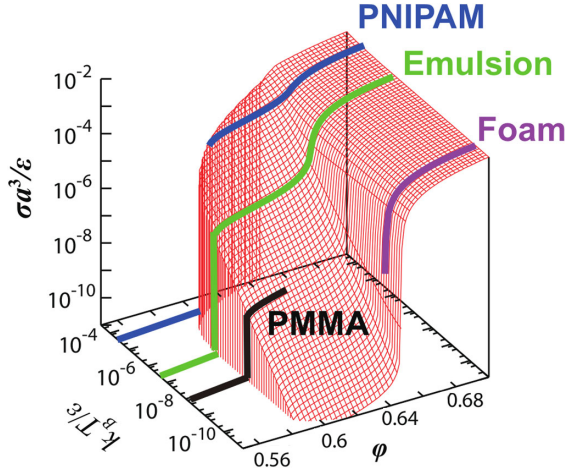


FIG. 4. Three-dimensional “jamming phase diagram” showing the reconstructed yield stress surface from numerical simulations as a function of the thermodynamic parameters temperature and density in a dimensionless representation (particle softness $k_B T/\epsilon$, volume fraction φ , and stress $\sigma a^3/\epsilon$) for a model of soft harmonic particles. The thick lines represent the location of typical experimental measurements in various materials: foams (rightmost line) are mainly sensitive to jamming physics; PMMA hard spheres (black line) to glass physics; emulsions display an interesting interplay between glass and jamming transitions; poly(*N*-isopropylacrylamide) (p-NIPAM) microgels (leftmost line) undergo a colloidal glass transition far from the jamming limit with no particular signature across the jamming density. From Ikeda, Berthier, and Sollich, 2013.

3. Role of attractive forces: Colloidal gels

In the previous section, particle systems with solely repulsive forces were described from a theoretical perspective, in which case temperature can only compete with the particle softness, and the main control parameter is the packing fraction. The situation becomes more complex when attractive forces come into play. Adhesion and attractive forces are relevant for a large number of model systems and real materials. For instance, dense liquids do not interact via hard-sphere potentials, but typically also possess longer-range attractive forces, modeled for instance via a Lennard-Jones potential (Hansen and McDonald, 2006). In colloidal systems, attractive forces can be easily induced and tuned, using for instance colloid-polymer mixtures (Royall, Poon, and Weeks, 2013). Many real-material systems, such as clay suspensions or more generally colloidal gels, are Brownian systems with attractive interactions between the colloidal particles (Larson, 1999).

Regarding the glass transition phenomenon in simple systems, attractive forces only weakly affect the physics, in the sense that they contribute quantitatively to the relaxation dynamics and details of the phase diagram, but do not change the physical behavior qualitatively (Berthier and Tarjus, 2009, 2011).

Attractive forces in simple liquids start to change the physics when they are strong enough to induce a nontrivial dynamical arrest in a regime that would otherwise be characterized by a simple fluid behavior. The simplest case is when very strong bonds are present, which might result in a

percolating particle network that can sustain a finite stress, as in chemical gels (Larson, 1999). Here a yield stress emerges and coincides with a percolation transition. When the gel is dense enough, such a network can confer a macroscopic elasticity to the system and hence be responsible for a yield stress. However, if the thermal energy is sufficient to break and reform bonds within the network, for a small applied stress the system will eventually flow at long time scales, and the system is simply viscoelastic (it is a “transient” gel).

Percolation represents only one of the possible routes to the production of physical gels; several other examples have been studied in recent years (Zaccarelli, 2007). Here we mention three examples.

a. Nonequilibrium gels

A well-described example concerns colloidal gels that are formed by increasing the strength of short-ranged adhesive depletion forces, starting from an initially purely repulsive system. It has been empirically found that “nonequilibrium gels” can be formed over a broad range of densities as the adhesion between particles is increased (Manley *et al.*, 2005; Lu *et al.*, 2008; Royall *et al.*, 2008). These gels are heterogeneous, dynamically arrested structures, which thus behave mechanically as soft solids. The current understanding of the gelation process is that adhesion induces the analog of a liquid-gas phase separation in the colloidal system, which may phase separate into colloid-rich and colloid-poor phases. However, because the attraction is very short ranged, the coexistence curve on the colloid-rich region at large density may hit the colloidal glass transition. The emergence of slow, glassy dynamics may be able, in some cases, to slow down dramatically and even fully arrest the kinetics of the phase-separation process (Foffi *et al.*, 2005; Lu *et al.*, 2008; Testard, Berthier, and Kob, 2011). At long times, the system may thus acquire a percolating bicontinuous structure, which is mechanically rigid and does not flow if a small shear stress is applied. A consensus has been reached regarding the formation of these nonequilibrium gels as reviewed by Zaccarelli (2007), whose structure can be controlled by tuning the flow cessation dynamics (Ovarlez, Tocquer *et al.*, 2013; Koumakis *et al.*, 2015; Helal, Divoux, and McKinley, 2016). However, the steady-state rheology of attractive gels is still a topic of intense research (Helgeson *et al.*, 2014; Romer *et al.*, 2014; Zia, Landrum, and Russel, 2014; Capellmann *et al.*, 2016). Indeed, colloidal gels show a pronounced time-dependent response (Ovarlez and Chateau, 2008) and a strong propensity to wall slip that appears to be nontrivially coupled to spatially heterogeneous flows (Gibaud, Barentin, and Manneville, 2008; Grenard *et al.*, 2014), which makes it difficult to measure flow curves and even questions the very existence of a unique constitutive equation. The transient and steady-state rheology of these systems is discussed in more detail in Sec. IV.

b. Attractive glasses

The behavior of dense assemblies of attractive colloids has also attracted a large experimental interest in the recent decade (Sciortino and Tartaglia, 2005; Puertas and Fuchs, 2009).

In this situation, a complex physical interplay is to be expected, due to the competition between the nonequilibrium kinetic arrest arising at moderate densities (leading to non-equilibrium gelation) and the glassy physics emerging at large densities without adhesive interaction (leading to glass formation). Early studies advocated that this competition produces a novel state of arrested matter, named “attractive glass” (Fabbian *et al.*, 1999; Dawson *et al.*, 2000; Pham *et al.*, 2002; Sciortino, 2002), actively studied both numerically and experimentally (Pham *et al.*, 2002, 2004; Sciortino, Tartaglia, and Zaccarelli, 2003; Puertas, Zaccarelli, and Sciortino, 2005; Zaccarelli *et al.*, 2005). For a discussion on how to experimentally differentiate a glass from both a gel and an attractive glass, see Bonn *et al.* (1999) and Tanaka, Meunier, and Bonn (2004). Because the dynamics is controlled by at least two microscopic length scales (the adhesion range responsible for initiating phase separation and the cage size responsible for the glassy dynamic arrest), complex relaxation patterns have been predicted (Fabbian *et al.*, 1999; Dawson *et al.*, 2000) and observed (Pham *et al.*, 2004; Zaccarelli *et al.*, 2005), including in rheological studies (Koumakis and Petekidis, 2011). Whereas early interpretation relied on the existence of an underlying peculiar form of glass singularity predicted by mode-coupling theory (Fabbian *et al.*, 1999; Dawson *et al.*, 2000), additional work has shown that such singularity is not needed for complex time dependences to occur (Chaudhuri, Hurtado, and Kob, 2010). The existence of a genuine attractive glass phase has also been called into question (Zaccarelli and Poon, 2009; Royall, Williams, and Tanaka, 2015), and indeed the idea of a specific type of attractive glass does not seem needed to interpret the rheology of all concentrated attractive glasses; see, e.g., Data *et al.* (2011) for an example of an attractive emulsion. From a practical (rather than fundamental) viewpoint, the idea that glasses with different types of frozen-in disorder may exist in models with adhesive interactions remains valuable (Pham *et al.*, 2004).

c. Athermal adhesive systems

Finally, the role of attractive forces in non-Brownian suspensions is also relevant but necessarily has a different nature, as the adhesive forces by construction cannot compete with thermal fluctuations. A few studies explored the emergence of solidity in athermal adhesive particle systems, to understand, in particular, how the jamming transition is affected when adhesion is present (Lois, Blawzdziewicz, and O’Hern, 2008; Chaudhuri, Berthier, and Bocquet, 2012; Irani, Chaudhuri, and Heussinger, 2014). This point is relevant for instance in the context of humid granular materials.

In particular, because adhesion creates bonds between particles, it seems physically clear that adhesive forces can only enhance solidity above jamming, and in this dense regime adhesion acts as a small perturbation. On the other hand, it appears that solid behavior can be maintained in a density range even below the jamming transition $\phi < \phi_J$, which opens a novel regime for solid behavior which has no analog for purely repulsive systems. In particular, a recent numerical study suggests that a small amount of attractive force is indeed able to generate a material with a finite yield

stress below the jamming transition, with a potentially interesting interplay between the imposed shear flow and the microstructure of the system, eventually giving rise to large-scale flow inhomogeneities (Irani, Chaudhuri, and Heussinger, 2014). This points to a possible mechanism for shear banding, which is a topic that we discuss further later.

C. Is the yield stress real?

1. A historical debate

For many years, there has been a controversy about whether the yield stress marks a transition between a solid and a fluid state, or between two fluid states with drastically different viscosities (Hartnett and Hu, 1989; Astarita, 1990; Schurz, 1990; Evans, 1992; Spaans and Williams, 1995; Barnes, 1999, 2007). Numerous experimental studies argued that yield stress materials actually flow like very viscous Newtonian liquids at low stresses (Macosko, 1994; Barnes, 1999). Barnes and Walters (1985) presented data on Carbopol microgels to demonstrate the existence of a finite viscosity at very low shear stresses (Fig. 5), rather than an infinite viscosity below the yield stress, and later published a review with numerous flow curves suggesting that yield stress materials should rather be described as Newtonian fluids with a very large viscosity (Barnes, 1999).

Møller, Fall, and Bonn (2009) reproduced the experiments used to demonstrate Newtonian limits at low stresses and indeed observed finite apparent viscosities at low stresses; see Fig. 5. However, while all measurements collapse at high stresses, below the yield stress they no longer do, and the apparent viscosity depends in fact on the delay time between the application of the stress and the viscosity measurement. Each individual curve resembles the curves of Barnes and others, but if all the points that do not seem to correspond to a steady state are removed, one is left with a simple Herschel-Bulkley material with a well-defined yield stress. The large viscosity values obtained at low stress in fact correspond to shear rates of the order of 10^{-6} s^{-1} or less, which are not only reaching the accuracy limits of ordinary rheometers, but also show that within a reasonable experimental measurement time,

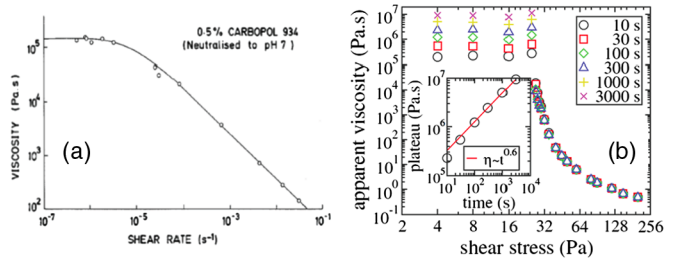


FIG. 5. Viscosity vs shear stress in Carbopol. (a) From Barnes and Walters, 1985. (b) A subsequent study of the same system. From Møller, Fall, and Bonn, 2009. The latter showed that the values of the low-stress viscosity plateau increase with measurement time (from 10 to 3000 s, colored symbols). The insets show that the plateau value increases as a power law with time, with exponent of about 0.6, indicating that the measured viscosities do not correspond to steady-state shear flows for shear stresses below the yield stress.

no steady state is reached where the deformation increases linearly with time, and the total deformation imposed on the sample remains well below unity. Consequently, the instantaneous shear rate cannot be interpreted as representative of a well-defined steady-state viscosity.

Besides this fundamental problem, debates about the existence of a yield stress demonstrate that the most ubiquitous practical problem encountered by scientists and engineers dealing with everyday materials such as food products, powders, cosmetics, crude oils, or concrete is that the yield stress of a given material is very difficult to determine experimentally (Barnes, 1999; Mujumdar, Beris, and Metzner, 2002; Møller, Mewis, and Bonn, 2006). Indeed, James, Williams, and Williams (1987), Zhu *et al.* (2001), and Nguyen *et al.* (2006) demonstrated that a variation of the yield stress of more than 1 order of magnitude can be obtained, depending on the way it is measured. This cannot be attributed to different resolution powers of different measurement techniques, but hinges on more fundamental complexities resulting from the physical processes responsible for the flow of yield stress materials.

2. Theoretical considerations about the existence of a yield stress

Can theory and simulations shed light on the debate regarding the existence of a true yield stress in amorphous materials? This is a difficult question, which cannot have a simple generic answer, as it amounts to asking first whether genuine amorphous solid states exist, and second whether such states can support a finite shear stress without flowing over arbitrarily long time scales. Moreover, as detailed earlier, different materials exhibit solid properties for distinct fundamental reasons under various experimental conditions and due to various particle interactions. Let us disentangle all these issues.

Clearly, the existence of a “real” yield stress in materials undergoing a glass transition is at least as ambiguous as that of a genuine fluid-to-glass phase transition, which remains an open fundamental question. There exist theoretical approaches and simple models, which describe the glassy phase of matter as a genuine thermodynamic singularity accompanied by a diverging viscosity. However, there are competing theoretical perspectives based on the opposite idea that the glass region is accessed by a dynamic crossover, and where the equilibrium relaxation time scale does not truly diverge (Berthier and Biroli, 2011). Therefore, the existence of glassy phases with truly infinite viscosity is not settled theoretically, or, for that matter, experimentally.

Of course, this fundamental question is not relevant in practice, as glassy phases are experimentally produced by going through a dynamic crossover in a nonequilibrium manner, as explained in Sec. II.B.1. As a consequence, in the vicinity of the experimental glass transition, flow curves might display an apparent yield stress value when measured over a given window of shear rates, even though the material might eventually flow at much longer time scales. Deeper in the glassy region, when the relaxation time has become larger than any relevant experimental time scale, the distinction between a slowly flowing fluid and a kinetically arrested material is essentially irrelevant, and the question of the existence of a genuine glassy phase may appear rather academic.

In glassy materials, a system prepared in the glass region slowly ages with time because thermal fluctuations allow for a slow exploration of its complex free-energy landscape (Berthier and Biroli, 2011). Importantly, this also implies that the rheological properties of glasses might depend on the time scale used to perform the measurements. For instance, the yield stress of the system has been observed to increase logarithmically with the preparation time in model systems (Varnik, Bocquet, and Barrat, 2004). Additionally, the aging behavior observed in glasses at rest might be affected in a nontrivial manner by an imposed shear flow, possibly resulting in a steady-state situation where aging is prevented by the external shear flow, a situation coined “shear rejuvenation” (Cloitre, Borrega, and Leibler, 2000; Bonn, Tanase *et al.*, 2002; Viasnoff and Lequeux, 2002; Ianni *et al.*, 2007). The roles played by the preparation protocol and by the aging dynamics are similarly crucial for colloidal gels that might be formed through nonequilibrium processes, such as kinetically arrested phase separation. In that case, it is unclear how such a nonequilibrium competition is affected by an externally imposed shear stress, which could for instance either “mix” the material or break the bicontinuous structure and accelerate the phase separation.

Assuming that genuine amorphous phases exist (where for instance ergodicity is truly broken and the Newtonian viscosity is infinite), is it necessarily obvious that such phases should display a finite yield stress? To answer this question one should ask whether there exists a physical dynamical process allowing the system to relax and flow on a finite time scale after a finite shear stress has been imposed. This problem was addressed by Sausset, Biroli, and Kurchan (2010). Using a simple nucleation-type argument, a stress-dependent free-energy barrier for relaxation was constructed, which could then be crossed using thermal fluctuations. By connecting the constructed activation time scale to the imposed stress, a limiting flow curve $\sigma(\dot{\gamma})$ was obtained, which in three spatial dimensions is of the form

$$\dot{\gamma} = \frac{\sigma}{G\tau_0} \exp \left[-c \left(\frac{\sigma_0}{\sigma} \right)^4 \right], \quad (6)$$

where G is the elastic shear modulus, c is a constant, τ_0 is a characteristic relaxation time, and σ_0 is a temperature-dependent stress scale. Equation (6) suggests that the shear rate should actually be finite at any imposed shear stress even in the solid phase. This result is not inconsistent with the existence of measured flow curves with an apparent yield stress, as it predicts that the shear stress decreases logarithmically (very) slowly with the shear rate. It might therefore be difficult to detect such behavior in an experiment and to discriminate it, for instance, from a Herschel-Bulkley functional form with a finite yield stress (where the yield stress value is approached algebraically with decreasing $\dot{\gamma}$). Interestingly, the result is not specific to amorphous materials, but applies equally to ordered systems such as crystalline materials. This discussion shows that despite the translational symmetry breaking observed during the formation of the crystal, which contrasts with the absence of such a symmetry breaking in amorphous solids, a yield stress is conceptually

not better defined in ordered systems. Therefore, the absence of a real yield stress is not due to the “messy” nature of soft amorphous materials, but has a more profound origin.

The reasoning leading to Eq. (6) and the conclusion that a finite yield stress cannot exist even in dynamically arrested phases rely heavily on a barrier-crossing argument, and therefore on the presence of thermal fluctuations. Therefore, the situation might be different in non-Brownian suspensions undergoing a jamming transition at zero temperature. For soft jammed particle systems such as foams and large-droplet emulsions, the transition to the jammed phase is not a dynamic crossover and the “solidity” is thus not destroyed by (nonexisting) thermal fluctuations. In this case, there is *a priori* no deep theoretical argument against the existence of a finite yield stress, so that the flow curves shown in Fig. 3(b) might be true examples of genuine yield stress materials. Of course, as mentioned several times, these experimental results do not seem to differ dramatically from measurements performed in thermal materials, which suggests that the experimental debate regarding the existence of a yield stress presumably revolves around practical issues, with little connection to the present discussion putting forward more fundamental arguments.

D. Thixotropy in yield stress fluids

Most yield stress fluids have an underlying microstructure that confers a macroscopic elasticity to the system. This microscopic structure may be (partly) destroyed by the flow, causing a reversible decrease of the viscosity with time, in which case the system is said to be *thixotropic* (Mewis and Wagner, 2009). The yield stress will be different following flow application, with a value that may be dependent on the rest time prior to shearing, during which the structure may also reform. It is therefore useful in practical terms to distinguish between thixotropic and simple (nonthixotropic) yield stress fluids as follows:

- Simple yield stress fluids: the shear stress (and hence the viscosity) depends only on the imposed shear rate. Examples include nonadhesive emulsions, foams, and Carbopol microgels (Bertola *et al.*, 2003; Bécu, Manneville, and Colin, 2006; Møller *et al.*, 2009; Ovarlez, Cohen-Addad *et al.*, 2013).
- Thixotropic yield stress fluids: both the yield stress and the viscosity depend on the shear history of the sample. Examples include particle and polymer gels (Møller *et al.*, 2008), attractive glasses (Møller *et al.*, 2009), “soft” colloidal glasses (Bonn, Coussot *et al.*, 2002), adhesive emulsions (Ragouilliaux *et al.*, 2007), non-Brownian gels (Kurokawa *et al.*, 2015), pastes (Huang *et al.*, 2005), and hard-sphere colloidal glasses (Møller, Fall, and Bonn, 2009).

The distinction is straightforward, at least in principle: one can measure the flow curve by using up and down stress ramps, for instance, and check for reproducibility (Fig. 6). In Fig. 6(b), we show that if the material is thixotropic, in general the flow will have significantly “liquefied” the material at high stresses, and the branch obtained upon decreasing the stress is significantly below the one obtained while increasing the stress. Hysteresis is mostly negligible for simple yield

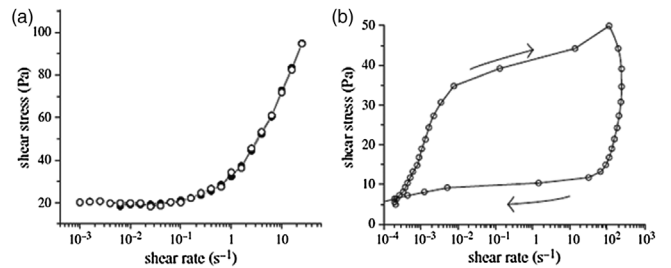


FIG. 6. (a) The behavior of 0.1% wt Carbopol microgel under increasing and decreasing shear stresses shows that this material is nonthixotropic (filled circles, up; open circles, down). (b) Thixotropy of a 10% wt bentonite solution under an increasing and then decreasing stress ramp. From Møller *et al.*, 2009.

stress fluids; see Fig. 6(a). The response of a thixotropic yield stress fluid will depend on the rate at which the stress is ramped up and down, and the rest time in between subsequent sweeps.

Figure 7 shows a direct qualitative observation of the effect of stress-dependent structural organization in a colloidal gel. At rest [Fig. 7(a)], the gel exhibits a percolated structure and exhibits a yield stress of about 5 Pa. Just after flow [Fig. 7(b)], the gel has broken up into individual flocs and there is no measurable yield stress. Detailed images of the shear-induced breakup of two-dimensional colloidal gels at interfaces for different values of the shear rate and strain were shown by Masschaele, Fransaer, and Vermant (2011), who quantified the effect of surface coverage and deformation on the morphology (i.e., transient networks or individual deformed aggregates); the undeformed structures in these experiments undoubtedly exhibit a yield stress, but direct mechanical measurements are not available.

The distinction between the two main families of simple yield stress fluids and thixotropic yield stress fluids is at present mostly driven by empirical considerations. It would be interesting to determine if it can also be rationalized at a more fundamental level. Experimentally, it would be useful to develop model systems allowing both types of behaviors to be observed and controlled, for instance by devising materials

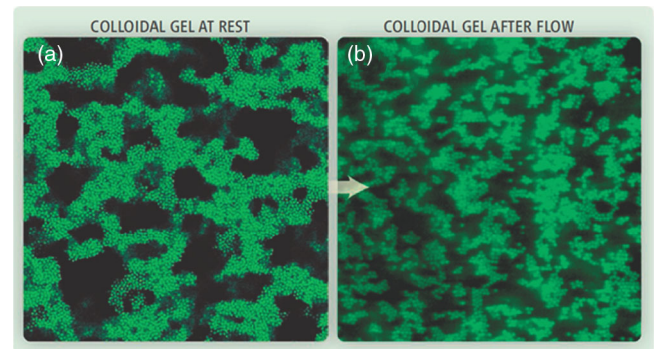


FIG. 7. (a) A colloidal gel at rest, with a percolated structure and a yield stress of 5 Pa, and (b) just after flow, with individual flocs and no measurable yield stress. The gel is made up of 1.3 μm fluorescent PMMA particles and 3 × 10⁷ Mw polystyrene in a mixture of decalin and cyclohexyl bromide. From Bonn and Denn, 2009.

that are only weakly thixotropic and where simple yield stress behavior can be continuously recovered in some well-controlled limit.

E. Theoretical descriptions of yield stress materials

1. Why a theory of yield stress solids is difficult

While properly defining and measuring a yield stress is a debated issue from an experimental point of view, as emphasized throughout this review, in theoretical work one usually identifies the yield stress as the shear stress measured in steady-state shear flow in the limit where the deformation rate goes to zero:

$$\sigma_y = \lim_{\dot{\gamma} \rightarrow 0} \sigma(\dot{\gamma}). \quad (7)$$

Thus, the challenge for theoreticians does not lie in the practical definition of the yield stress or its best quantitative determination, but in the conceptual difficulty to describe the nonlinear mechanical properties of disordered complex solids.

An additional difficulty can be appreciated by comparing the situation of disordered materials to that of crystalline solids. Crystals are formed through a phase transition across which translational invariance is broken. Because the broken symmetry is easily identified, it is not difficult to recognize the associated defects (such as dislocations) directly from the structure of an imperfect crystalline system. It is well established that nonlinear flow and mechanical deformation in crystalline materials are mostly driven by these defects, so that an understanding of the flow defects of crystals is indeed the key to understanding their rheology. So, we are led to ask what the “defects” are in an amorphous material that is formed without breaking any obvious symmetry. Are there at least equivalent localized structures allowing us to efficiently describe flow and mechanical deformation in amorphous solids? These are two long-standing questions in the area of amorphous material rheology, which have received some constructive answers in the last decades, mostly from numerical and experimental studies (Barrat and Lemaître, 2011).

It has been demonstrated in many different studies that flow in amorphous materials occurs at the microscopic scale in very localized “zones,” sometimes identified as “shear transformation zones” (STZ) (Falk and Langer, 1998). These zones are best observed in studies of amorphous systems which are sheared so slowly that individual events can be resolved in space and time, such as computer simulations in quasistatic shear conditions (Maloney and Lemaître, 2006) or confocal microscopy experiments on slowly deformed colloidal glassy systems (Schall, Weitz, and Spaepen, 2007). It has been observed that flow occurs mostly near zones comprising a small number of particles (say, 5 to 10) undergoing the largest irreversible rearrangements. However, because the material is globally an elastic solid, these local plastic events additionally induce a long-range redistribution of the stress field in their surroundings (Picard *et al.*, 2004), which, in turn, can couple to a different zone, or trigger further relaxation elsewhere in the system. An example of such an event detected in the numerical simulation of a slowly sheared glass model (Tanguy, Leonforte, and Barrat, 2006) is shown in Fig. 8. Notice however that both computational studies and colloidal

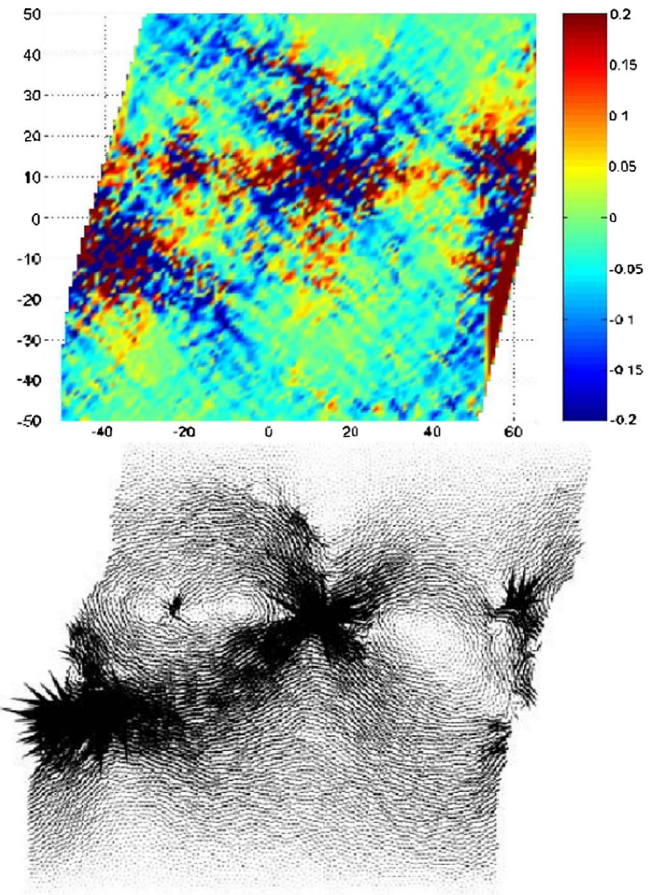


FIG. 8. Changes in the local shear stresses (as indicated by the color coding) during a localized plastic event (top); the color coding gives the amplitude of the stress changes, and associated displacement field (bottom) observed in the numerical simulation of a quasistatically sheared model of atomic glass. Adapted from Tanguy, Leonforte, and Barrat, 2006.

experiments are performed on disordered systems that are prepared in physical conditions that are vastly different from the ones relevant for molecular and polymeric glasses (i.e. “hard” glasses), for which these ideas remain to be experimentally validated.

2. Theoretical approaches

The previous section suggests that theory still has trouble describing the transition between a fluid and an amorphous solid (glass, gel, and jammed states), and that describing the rheology of these materials requires in addition a description of a nonlinear response to flow, which is typically accompanied by strong spatial fluctuations and localized flow defects that may induce long-range correlations, intermittent relaxations, and even catastrophic responses with complex time dependences. It should therefore come as no surprise that no complete, well-accepted, first-principle theoretical approach exists that can account for all aspects of the rheology of yield stress materials. Instead, several layers of (potentially complementary) theoretical descriptions are found in the literature. In the following, we distinguish two main types of theoretical approaches.

a. Mode-coupling theories and trap models

In the first category of theoretical models, the focus is primarily on a detailed description of the rheological consequences of the existence of a fluid-to-amorphous solid phase transition. In particular, numerous theoretical approaches to the description of the glass transition in dense fluids and colloidal systems have now been extended to account for the mechanical properties in the vicinity of the glass transition (Berthier and Biroli, 2011), such as for instance mode-coupling theories (Götze, 2008) and Bouchaud's trap model (Bouchaud, 1992). Even in this restricted context, these approaches differ widely.

On the one hand, mode-coupling theories were developed as truly microscopic or “first-principle” approaches to understand the dynamics of simple liquids near a glass transition (Bengzelius, Götze, and Sjolander, 1984; Götze, 2008). A large amount of work has been performed to develop tractable equations of motion that can attack complex flow histories while retaining aspects of the driven dynamics of the microscopic degrees of freedom.

On the other hand, trap models correspond to more phenomenological descriptions of the glass phenomenon and have attracted a lot of attention, in particular, in the context of aging phenomena inside glassy phases. The rheological trap model is called the “soft glassy rheology” (SGR) model and has been studied extensively (Sollich *et al.*, 1997; Sollich, 1998), both in steady-state conditions, in the context of rheological aging, and in even more complicated time-dependent situations, with interesting connections to the physics of thixotropic materials (Fielding, Sollich, and Cates, 2000). By introducing spatial dependences, the SGR model has also been studied to give insight into spatially inhomogeneous flows (Fielding, Cates, and Sollich, 2009; Moorcroft, Cates, and Fielding, 2011; Moorcroft and Fielding, 2013).

b. Shear transformation zones and elastoplastic models

A second family of theoretical models actually postulates from the start that a solid amorphous state exists, which is characterized by a finite yield stress. These models are then able to explore in more detail how such a solid system might flow under an applied shear stress larger than the yield stress.

The starting point for these models is the observation that flow occurs in a spatially inhomogeneous manner, and occurs mostly at localized shear transformation zones as illustrated in Fig. 8. This empirically well-established observation made in different systems suggests a theoretical pathway to model the mechanical properties of yield stress amorphous solids.

A well-studied model constructed in this manner is the shear transformation zone model, pioneered by Falk and Langer (1998, 2011). Building upon their numerical observations, they devised a set of minimal equations of motion for the dynamic evolution of a sparse population of shear transformation zones. In later refinements and theoretical reformulations of the model, spatiotemporal aspects were introduced in the original mean-field version of the model, allowing it to attack a large variety of physical situations, from simple and time-dependent flows to shear-banding phenomena and fractures in amorphous materials (Manning, Langer, and Carlson, 2007; Manning *et al.*, 2009). The shear

transformation zone model has also been used to understand the thermodynamic properties of sheared amorphous solids (Langer, 2004; Bouchbinder and Langer, 2009a, 2009b, 2009c), and has been generalized to also include the effects of thermal fluctuations (Falk, Langer, and Pechenik, 2004; Langer and Manning, 2007). The model continues to be actively developed to more complex situations; see, e.g., Rycroft and Bouchbinder (2012) and Hinkle and Falk (2016).

An alternative modeling effort gaining increasing attention builds on the observation of localized shear transformation zones to construct “mesoscopic” elastoplastic descriptions of the rheology of amorphous materials (Baret, Vandembroucq, and Roux, 2002; Picard *et al.*, 2002, 2005; Bocquet, Colin, and Ajdari, 2009; Cheddadi *et al.*, 2011; Rodney, Tanguy, and Vandembroucq, 2011). These models are coarse-grained descriptions in the sense that no attempt is made to describe the microscopic origins of the yield stress. Instead, they assume that a yield stress exists and directly explore the consequences of deforming a solid material. The clear advantage of such models is that they open up the possibility to explore large-scale consequences of the dynamics of shear transformation zones. For instance, numerical simulations have revealed that elastic deformation in the vicinity of a local rearrangement induces long-range spatial correlations, which may induce correlations between plastic events (Vandembroucq and Roux, 2011; Martens, Bocquet, and Barrat, 2012). These correlations have been observed to lead to system-spanning avalanches in quasistatic deformations that are sometimes also described as precursors for the formation of permanent shear bands or strong flow localization (Falk, Langer, and Pechenik, 2004; Maloney and Lemaître, 2006; Shi *et al.*, 2007; Barrat and Lemaître, 2011; Falk and Langer, 2011). The obvious drawback is that no information can be gained about the dependence of the yield stress on external control parameters, but these models can more efficiently explore the consequences of nonlinear flow curves, and might be able to describe in a relevant manner more complex situations such as shear bands, kinetic heterogeneities under flow, fractures, time-dependent phenomena, or flow in confined geometries, as discussed in more detail in Sec. IV.

3. Theoretical flow curves

In the preceding section, we provided two broad classes of methods to describe the fluid-amorphous solid transition. In the following we ask how we can quantitatively describe and compare their outcomes. We consider mode-coupling and soft glassy rheology-type “trap models” separately, and therefore consider three families of theoretical paradigms to analyze steady-state flow curves in yield stress materials. These approaches go beyond (or in some cases justify) the popular Herschel-Bulkley model described in Sec. II.A, which provides an efficient fitting model but is essentially empirical.

Note that flow curves in steady-state simple shear flows only represent one of the many aspects of the rheology of yield stress materials, and some models also make detailed predictions for, e.g., time-dependent flows or more complex geometries. Reviewing model predictions for all these phenomena would however require a review article of its own (Voigtmann, 2014).

a. Soft glassy rheology

The SGR model is a direct extension of Bouchaud's trap model (Bouchaud, 1992) that incorporates mechanical degrees of freedom in a minimal manner to describe the interplay between glassy dynamics and shear deformation (Sollich *et al.*, 1997). The original trap model was mainly devised to study the physics of the glass transition and the aging dynamics in systems quenched suddenly into a glassy phase (Bouchaud, 1992; Bouchaud and Dean, 1995). The SGR model provides an evolution equation for the probability distribution of the system in terms of energy and stress variables. In the presence of a constant shear stress, steady-state flow curves can be predicted, with a behavior that is governed by the only control parameter of the model, namely, the “temperature” T . Whereas the initial trap model for aging glasses explicitly refers to T as the temperature of a thermal bath coupled to the system, the SGR model differs somewhat on the precise interpretation of the temperature and uses the words “effective temperature” in order to include athermal materials such as foams or emulsions in the same framework. The temperature T is then thought as quantifying the strength of “mechanical noise” triggered by the flow itself. More detailed discussions of effective temperatures in driven materials can be found in Cugliandolo, Kurchan, and Peliti (1997), Berthier, Barrat, and Kurchan (2000), Bouchbinder and Langer (2009a, 2009b, 2009c), and Sollich and Cates (2012). Recent work critically revisited the properties of the mechanical noise triggered by shear transformation zones (Nicolas, Martens, and Barrat, 2014), offering, in particular, a detailed comparison between the SGR model and an alternative mean-field modeling proposed by Hébraud and Lequeux (1998), where a Langevin dynamics is studied in which noise is directly related to the amount of plastic deformation generated in the material.

Despite its simplicity, the SGR model offers a rich variety of possible flow curves, depending on the considered temperature regime (Sollich, 1998). In the absence of a flow, the system undergoes a glass transition at some critical temperature T_c , below which ergodicity breaking occurs. With an imposed shear flow, three temperature regimes are observed as follows:

- First, when $T > 2T_c$, the system exhibits a Newtonian flow, as expected for a simple fluid state.
- A second, somewhat unexpected regime occurs when $T_c < T < 2T_c$, where the system displays a pure power-law rheology of the form $\sigma \approx \dot{\gamma}^n$, with a “shear-thinning” exponent $0 < n = T/T_c - 1 < 1$. This regime is peculiar as it corresponds to a solid system with an infinite viscosity at rest when $\dot{\gamma} \rightarrow 0$, but with no yield stress. When the shear-thinning exponent n becomes small, it might be difficult to distinguish this behavior from a Herschel-Bulkley functional form. A peculiarity of this regime is the infinite shear viscosity for temperatures that are strictly above the glass transition temperature where the system actually reaches thermal equilibrium. See Lequeux and Ajdari (2001) for a detailed discussion of this curious issue.
- In the third regime, for temperatures below the critical temperature $T < T_c$, the rheology can be described by

the Herschel-Bulkley model $\sigma \approx \sigma_y(T) + K\dot{\gamma}^n$ and the shear-thinning exponent obeys $0 < n = 1 - T/T_c < 1$. A temperature-dependent yield stress $\sigma_y(T)$ emerges continuously at the glass temperature, with a linear onset $\sigma_y(T \lesssim T_c) \approx 1 - T/T_c$ and a smooth approach to a finite limit at zero temperature, $\sigma_y(T \rightarrow 0) > 0$.

Overall, within the SGR model, the behavior of the flow curves is smooth at the transition temperature $T = T_c$, where the system has no yield stress but the shear-thinning exponent vanishes—a situation that could easily be confused experimentally with a finite yield stress.

Moreover, since all the characteristic exponents of the model are temperature-dependent quantities, they carry no deep physical meaning but simply reflect the complex interplay between the broad distribution of relaxation times in the equilibrium model and the external mechanical forcing in the presence of thermal fluctuations. This remark implies that no particular scaling form is predicted to describe the flow curves derived within the SGR model in any of the temperature regimes, or even in the close vicinity of the critical temperatures of the model.

b. Mode-coupling theories

The mode-coupling theory of the glass transition is now understood as a building block of a larger theoretical construction to understand the physics of glassy materials called random first-order transition theory, which aims at describing dynamic and thermodynamic aspects of the statistical mechanics of materials undergoing a fluid-to-glass transition (Lubchenko and Wolynes, 2007; Berthier and Biroli, 2011).

The mode-coupling approach itself is not a unique theory, and several related lines of research coexist, which differ in their microscopic starting point but often provide similar predictions. A few of these approaches were extended to also include mechanical degrees of freedom, much in the spirit of the SGR model. There are at present two main starting points for solving the dynamics in the amorphous solid state.

- A first approach (Cugliandolo *et al.*, 1997; Berthier, Barrat, and Kurchan, 2000) consists of exactly solving the driven dynamics of simple, but rather abstract, glass models that are known to exhibit an equilibrium dynamics that is in the same universality class as other mode-coupling approaches, such as, for instance, the p -spin glass models or other disordered models (Kirkpatrick and Thirumalai, 1987).
- A second line of work starts from microscopic equations of motion for particles in a dense fluid, and develops mode-coupling approximations to derive closed, but approximate, dynamical equations for microscopic correlation functions based on density fluctuations (Fuchs and Cates, 2002; Miyazaki and Reichman, 2002; Brader *et al.*, 2007; Fuchs and Cates, 2009).

Both approaches have been extended to include external driving forces and shear flows in order to study the interplay between glassy dynamics and rheology. In mode-coupling theories, the equilibrium dynamics (without shear flow) is characterized by a critical temperature T_c where the (alpha) relaxation time $\tau_\alpha(T)$ diverges as a power law. Near the glass transition, time-correlation functions develop a two-step

decay with an intermediate plateau reflecting the transient caging of the particles in the dense fluid. In rheological terms, this simply signals that very viscous fluids near a glass transition are viscoelastic and behave as solids at intermediate time scales and flow at long times, associated with complex frequency spectra for the linear rheological response. The approach to, and departure from, this plateau regime involve nontrivial power laws for time-correlation functions, which are characteristic signatures of mode-coupling theories (Götze, 2008). A known limitation of the theory is that the algebraic divergence that it predicts for the equilibrium relaxation time is not observed in experiments, where it is replaced by a smooth crossover. The current view is that mode-coupling theories describe the initial regime of slow dynamics in glassy materials well, but fail closer to the glass transition. Interestingly, this “mode-coupling” regime coincides with the physically relevant one for colloidal systems (Götze, 2008; Siebenbürger, Fuchs, and Ballauff, 2012), which justifies why the mode-coupling approach is included in this soft-matter review article.

In both mode-coupling approaches, the glass transition is destroyed by the imposed shear flow, and the microscopic relaxation time scale is never infinite in the presence of a finite driving force, but rather becomes dependent on the imposed shear rate $\dot{\gamma}$. However, the resulting flow curves differ somewhat in their details, as we discuss in the following.

In the first class of models, namely, schematic mean-field models, the rheology exhibits Newtonian behavior at temperatures above T_c at very low shear rates, but the dynamics become strongly dependent on $\dot{\gamma}$ when the “dressed” Péclet number $\text{Pe} \equiv \tau_\alpha \dot{\gamma}$ becomes larger than unity. Since the shear flow accelerates the microscopic structural relaxation, the viscosity decreases as $\dot{\gamma}$ increases, a shear-thinning behavior. As a result, one obtains the following scaling form for the flow curves:

$$\eta(\dot{\gamma}, T) = \frac{\eta_0(T)}{[1 + \dot{\gamma}/\dot{\gamma}_0(T)]^{1-n}}, \quad (8)$$

where $\eta_0(T) \sim \tau_\alpha(T)$ is the Newtonian viscosity, $\dot{\gamma}_0(T)$ is a critical shear rate separating Newtonian from shear-thinning regimes, and n is the usual shear-thinning exponent, whose value is $n = 1/3$ in the specific family of models studied by Berthier, Barrat, and Kurchan (2000), but may be different in different models (Yamamoto and Onuki, 1997).

At the glass transition, a pure power-law rheology is thus obtained, $\sigma(\dot{\gamma}, T = T_c) \sim \dot{\gamma}^n$, whereas a temperature-dependent power-law rheology is obtained in the glass phase $\sigma(\dot{\gamma}, T < T_c) \sim \dot{\gamma}^{n(T)}$ with a shear-thinning exponent decreasing from $n(T = T_c) = 1/3$ to $n(T \rightarrow 0) = 0$, but with no finite yield stress. Therefore, the rheology of the glass phase is very similar to the intermediate temperature regime of the SGR model, with the difference being that here the viscosity divergence coincides with the equilibrium glass transition of the model.

The absence of a yield stress is natural in the context of mean-field approaches whose aging dynamics in the glass phase is well understood (Cugliandolo and Kurchan, 1993). In the absence of external flow, the system slowly relaxes along the flat or “marginal” regions of its free-energy landscape, but

does not penetrate deeper free-energy minima. This is a general feature of mean-field glassy dynamics (Kurchan and Laloux, 1996). The power-law rheology found in the glass phase directly results from this marginal dynamics, and non-mean-field effects are believed to manifest themselves by the emergence of a finite yield stress, as explored by Berthier (2003).

Using liquid-state theory to derive mode-coupling equations for glassy fluids under flow results in a set of dynamical equations that reduce to the usual mode-coupling phenomenology described for the equilibrium dynamics. However, the driven dynamics under shear flow provides a set of predictions that differ somewhat from the schematic mean-field models, for reasons that are more technical than physical and presumably stem from the application of different types of “mean-field” approximations. These mode-coupling equations have been derived in a number of ways that are technically quite involved, but all derivations essentially provide similar predictions for the flow curves (Fuchs and Cates, 2002, 2009; Miyazaki and Reichman, 2002). The predicted flow curves in the vicinity of the glass transition closely reflect the complexity of the time regimes observed for time-correlation functions, as illustrated in Fig. 9.

Specifically, the flow curves predicted by this second class of models in the fluid region exhibit a Newtonian regime at sufficiently small $\dot{\gamma}$ followed by a strong shear-thinning regime for large Péclet numbers $\text{Pe} = \dot{\gamma}\tau_\alpha$, as found in the mean-field and SGR models. The flow curve at the critical temperature $T = T_c$ obeys a Herschel-Bulkley functional form with a finite yield stress $\sigma_y(T = T_c) > 0$ and a shear-thinning exponent that takes a nonuniversal value [specific approximations give $n \approx 0.15$ (Fuchs and Cates, 2003)]. The power-law approach to a finite yield stress closely mimics the power-law approach to a finite plateau found for time-correlation functions.

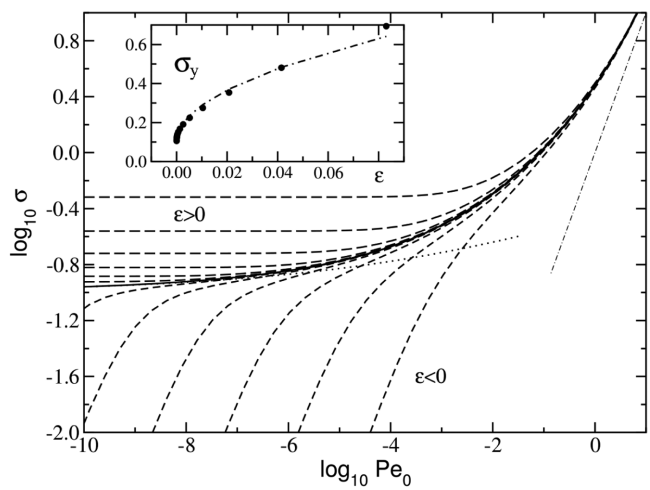


FIG. 9. Flow curves predicted for a range of temperatures T across the mode-coupling critical temperature T_c ; $\epsilon = T_c - T$ is the distance to the critical temperature, and the shear rate is rescaled by a microscopic time unit τ to form a Péclet number $\text{Pe}_0 = \dot{\gamma}\tau$. The inset shows the discontinuous emergence of the yield stress at T_c . From Fuchs and Cates, 2003.

Just below the glass transition, the yield stress increases algebraically with decreasing temperature $\sigma_y(T \lesssim T_c) \approx \sigma_y(T_c) + c\sqrt{T_c - T}$, which again mimics the temperature behavior of the plateau in time-correlation functions (indeed the two are intimately connected within the theory). Note, however, that the yield stress emerges discontinuously at the critical temperature T_c , a prediction that seems unique to this approach. However, this abrupt emergence of a yield stress cannot exist in experiments, where a true mode-coupling transition is not observed. In practice it is replaced by a crossover between flow curves where the Newtonian regime of the flowing liquid slowly shifts outside the experimental time window, so that by construction the “first” measurable value of the yield stress must indeed be a finite number (Varnik and Henrich, 2006; Wittmer *et al.*, 2013). Therefore, the question of the (dis)continuous nature of the emergence of a yield stress at the glass transition is ill posed. Of course, when analyzing experimental and numerical flow curves (which do not have a real transition) within the framework of the mode-coupling approach (which has a real transition), the discontinuous emergence of a yield stress is needed (Siebenbürger, Fuchs, and Ballauff, 2012; Voigtmann, 2011).

In the glass regime, the flow curves are again well described by a Herschel-Bulkley functional form. The limit of low temperatures is, however, problematic within the theory as it makes the unphysical prediction that the yield stress eventually vanishes in the $T \rightarrow 0$ limit (Ikeda and Berthier, 2013). This implies that the theory is actually not well suited to describe the yield stress of glassy systems deep in the glass phase, which is perhaps not surprising as its starting point is actually an equation of motion for the fluid.

It should thus be kept in mind that mode-coupling theories are to be used to describe the interplay of glassy dynamics and shear flow in the immediate vicinity of kinetic arrest, over a modest window of shear rates. All the detailed predictions of the theory have been tested in great detail in both numerical and experimental studies (Brader *et al.*, 2010; Siebenbürger, Fuchs, and Ballauff, 2012; Amann *et al.*, 2013; Ballauff *et al.*, 2013; Amann *et al.*, 2015). We emphasize that despite the presence of a genuine critical temperature in the mode-coupling approach and the existence of power laws controlling the divergence of the viscosity and the discontinuous emergence of a finite yield stress, no specific “critical data collapse” of the flow curves is obtained within the theory.

The theoretical limitations of mode-coupling approaches are fully understood in the broader context of random first-order transition theory, where the structure and dynamics of the glass phase are treated analytically using a completely different method based on an approximate treatment involving replica calculations (Mézard, Parisi, and Virasoro, 1988) to describe the complex free-energy landscape characterizing glassy materials (Yoshino and Mézard, 2010). Recent progress in this direction has been substantial (Parisi and Zamponi, 2010; Charbonneau, 2014), as the nature of the equilibrium glass transition has been analytically elucidated for particle systems in the (abstract) limit of a large number of spatial dimensions. This approach opens new ways to analytically treat the nature of the glass phase, of the dynamics of the viscous liquid near the glass transition, and potentially of its

rheological properties. Currently, the theory is being developed to treat mechanical properties, such as the shear modulus (Yoshino and Zamponi, 2014). Recently, stress-strain curves in quasistatic deformation protocols have been obtained analytically (Rainone *et al.*, 2015), thus pushing the theory closer to being able to describe the yielding transition in glassy solids (Urbani and Zamponi, 2017). Reconciling these thermodynamic replica calculations to dynamic equations derived within mode-coupling theories remains an open issue (Szamel, 2010). Another promising route is the possibility to perform a systematic treatment of non-mean-field effects, thus paving the way for a generalization of mode-coupling approaches that do not suffer from the shortcomings described previously.

c. Jamming rheology

In Sec. II.B.2, we provided a qualitative description of the flow curves obtained from simple computational models undergoing an ideal jamming transition, in connection with the experimental results displayed in Fig. 3(b) for emulsions with sufficiently large (i.e., non-Brownian) droplets. In the vicinity of the jamming transition, these flow curves can display a number of scaling features that are fully specific to non-Brownian assemblies of particles. Upon compression toward ϕ_J , the system exhibits a Newtonian viscosity that diverges algebraically, accompanied by a power-law shear-thinning behavior. Above ϕ_J , a finite yield stress emerges continuously at the transition, and its increase with packing fraction is also described by a power law.

We emphasize that the presence of these power-law behaviors is unique to athermal rheology, and that the situation differs qualitatively from the behaviors observed in Brownian systems sheared across their glass transition. There has been some confusion in the literature about the distinction between the two types of yield stress rheology. The scaling behavior proposed for athermal systems has for instance been incorrectly applied to Brownian and thermal systems as well. As mentioned, the distinction is readily made by looking at adimensional shear rates (Péclet numbers) and stress scales (Ikeda, Berthier, and Sollich, 2012, 2013, 2016).

The scaling properties of the jamming rheology near the zero-temperature jamming transition have been fully elucidated in computer simulations of soft repulsive potentials, such as harmonic or Hertzian pair potentials; see Eq. (5). These flow curves have now been characterized numerically in great detail (Olsson and Teitel, 2007, 2012; Hatano, 2010; Ikeda, Berthier, and Sollich, 2012; Vagberg, Olsson, and Teitel, 2014).

An approximate scaling form similar to Eq. (8) is obtained below the jamming transition in the non-Brownian suspension regime, where the Newtonian viscosity diverges as $\eta_0(\phi) \sim (\phi_J - \phi)^{-m}$, with $m \approx 1.5\text{--}2.5$ (Boyer, Guazzelli, and Pouliquen, 2011; Andreotti, Barrat, and Heussinger, 2012). A series of recent large-scale numerical studies for nonfrictional particles report $m \approx 2.55$ (Vagberg, Olsson, and Teitel, 2014; Kawasaki *et al.*, 2015), but note that this power law only holds extremely close to the jamming density, with strong corrections further away from the critical point, which presumably explain the large spread in literature values for the exponent m of the viscosity divergence. Because the Newtonian regime is reached at very low shear stresses where particles barely

overlap, the particle softness does not affect the value of m , which thus remains pertinent to describe the hard-sphere limit.

In the jammed region, the density increase of the yield stress is well described by a power law $\sigma_y(\phi) \sim (\phi - \phi_J)^\Delta$, where Δ is a critical exponent. Because this exponent describes the solidity of a compressed assembly of soft overlapping particles, it is not surprising that it is found to depend on the chosen form of the pair repulsion between the particles. In particular, simulations show if α is the exponent describing the pair repulsion $V(r)$ in Eq. (5) (with $\alpha = 2$ for harmonic sphere, and $\alpha = 5/2$ for Hertzian potential), then Δ is very close to the value $\Delta = \alpha - 1$, with small but measurable deviations from this estimate (for instance $\Delta \approx 1.15$ for harmonic spheres) (Olsson and Teitel, 2012). This estimate is reasonable as $\alpha - 1$ is also the exponent controlling the increase of the pressure in compressed packings, as predicted by dimensional analysis (O'Hern *et al.*, 2003). Systematic deviations $\Delta \gtrsim \alpha - 1$ have now been reported in several numerical studies (Hatano, 2010; Olsson and Teitel, 2011, 2012; Kawasaki *et al.*, 2015).

Finally, above jamming, the flow curves are well described by a Herschel-Bulkley model, with a shear-thinning exponent $n \approx 0.38$ which is also independent of the form of the soft potential (Olsson and Teitel, 2012). Exactly at the jamming transition, a pure power-law rheology is obtained $\sigma \sim \dot{\gamma}^{n'}$, with another nontrivial shear-thinning exponent n' , which depends on the form of the pair potential and is thus not universal (Olsson and Teitel, 2012). We emphasize that a precise determination of the various scaling regimes and the precise values of all these critical exponents (m, Δ, n, n') is a difficult numerical task, which is in addition plagued by strong finite-size effects (Vagberg *et al.*, 2011; Kawasaki *et al.*, 2015). These difficulties also suggest that direct comparison to experimental results should be done with some caution.

An important consequence of these multiple scaling regimes is that despite the presence of power laws in the rheology of model assemblies of soft particles, the flow curves measured over a large domain of densities and shear rates cannot be rescaled onto master curves, as initially proposed by Olsson and Teitel (2007). These deviations have been described with great analytic precision as a form of correction to scaling in a series of studies (Vagberg *et al.*, 2011; Vagberg, Olsson, and Teitel, 2014); see Kawasaki *et al.* (2015) for a specific illustration of a “failed” data collapse for a fully athermal assembly of soft particles.

In addition, there is currently a large theoretical activity to better understand the physical origin of these exponents and to relate them to more microscopic quantities characterizing the structure of athermal packings in the vicinity of the jamming transition (Tighe *et al.*, 2010; Lerner, Düring, and Wyart, 2012; DeGiuli *et al.*, 2014; Yoshino and Zamponi, 2014).

In experiments, these scaling forms have also been used to analyze flow curves measured in a variety of systems. Using the exponents defined previously and assuming that power laws hold for the entire range of explored densities and shear rates, the flow curves measured for different volume fractions of a given system can be collapsed onto two master curves (one below and one above jamming) by rescaling both the stress and the shear rate with appropriate powers of the distance to the jamming transition ($\phi - \phi_J$) (Nordstrom *et al.*, 2010; Paredes,

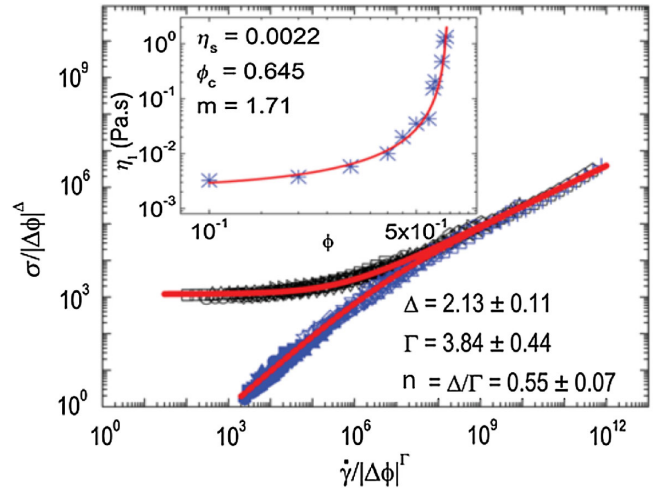


FIG. 10. Master curves showing a good collapse of the flow curves onto two branches, one for samples with $\phi < \phi_J$ and one for $\phi > \phi_J$, when stress and shear rate are rescaled with the distance to jamming to a certain power. The lines are supercritical and subcritical branches representing empirical fits of the master curve. The inset shows a fit of the low-shear viscosity to a power-law divergence. Flow curves were obtained for emulsions prepared with different volume fractions of the dispersed phase. From Paredes, Michels, and Bonn, 2013.

Michels, and Bonn, 2013; Dinkgreve *et al.*, 2015), as shown in Fig. 10. This type of data collapse is empirically useful, as it organizes the experimental data around the critical density ϕ_J , while using simple, but reasonable functional forms for their density dependence. This strategy was first employed in numerical work (Olsson and Teitel, 2007), for which it is now understood to be only approximately correct.

In all published cases (Nordstrom *et al.*, 2010; Paredes, Michels, and Bonn, 2013; Dinkgreve *et al.*, 2015), the rescaling appears to work well; $\Delta \approx 2$ and the exponent for the rescaling of the shear rate axis is $\Gamma \approx 4$. The observation that the rescaling collapses the Herschel-Bulkley flow curves above jamming then immediately implies that the shear-thinning exponent is $n = \Delta/\Gamma \approx 1/2$. The collapse of the Newtonian flow regime curves at low shear rates below jamming implies in turn that the exponent for the divergence of the viscosity is $m = \Gamma - \Delta \approx 2$ (Paredes, Michels, and Bonn, 2013); see the inset of Fig. 10. This rescaling with very similar exponents has now been observed for soft polymer particles (p-NIPAM and Carbopol), emulsions with mobile and immobile surfactants and foams (Nordstrom *et al.*, 2010; Paredes, Michels, and Bonn, 2013; Dinkgreve *et al.*, 2015), suggesting that either these systems have similar interactions, or that the exponents (Δ , notably) do not sensitively depend on the interactions, in contrast to theoretical predictions (Tighe *et al.*, 2010). Another possibility for the difference between experiments and simulations could be that the simulations and experiments use quite different regimes to determine the critical exponents (in general, in the simulations one is much closer to the jamming transition), so that experimentally determined values could represent “effective” values. Moreover, some of the analyzed systems (notably, microgels) are not fully athermal and should perhaps be described by

exponents characteristic of the glass transition (if exponents exist for this situation), which may be different from the exponents from the thermal jamming transition.

Finally, it is worth mentioning that other scaling analyses have been proposed that are also based on experimental data, e.g., for the evolution of the yield stress or the shear modulus (Mason, Bibette, and Weitz, 1996; Mohan, Bonnecaze, and Cloitre, 2013; Basu *et al.*, 2014; Scheffold *et al.*, 2014; Kim, Scheffold, and Mason, 2016). These remain interesting open questions and we refer to a recent publication (Dinkgreve *et al.*, 2015) for a compilation of the different jamming exponents in theory, experiment, and numerics.

III. PHYSICAL INSIGHTS FROM YIELD STRESS MEASUREMENTS

While the definition of the yield stress from a theoretical point of view, i.e., Eq. (7), looks very simple, its practical determination is known to raise challenging experimental problems. As discussed, aging and time dependences—most generically, thixotropy—have led to long-standing controversies in the rheology community. Other issues include instrument artifacts or slippage of the material at the walls of the measuring device. Such problems with the measurement of yield stress have been reviewed from an engineering point of view, for example, by Uhlherr *et al.* (2005), Nguyen *et al.* (2006), Møller *et al.* (2009), Balmforth, Frigaard, and Ovarlez (2014), and Coussot (2014). Here we try to clarify what experimentalists call the “yield stress,” what they exactly measure, and what physical mechanisms they actually probe in the various classical techniques. We will ignore techniques that involve complex geometries such as squeeze flows (Rabideau and Coussot, 2009), penetrometry tests (Boujlel and Coussot, 2012), or stop flows on inclined planes (de Kee *et al.*, 1990; Coussot and Boyer, 1995) in order to focus only on techniques that rely on the drag flow produced by a rheometer and show how their diversity proves relevant to address specific fundamental questions pertaining to yield stress behavior.

In rotational shear rheometry a shear stress σ is imposed and the corresponding shear rate $\dot{\gamma}$ (or strain γ) is recorded, or vice versa. Typical geometries used for performing this type of measurement include concentric cylinders, plate-plate, and cone-plate geometries (Barnes, Hutton, and Walters, 1989; Larson, 1999). In the following we first review methods that involve liquid-to-solid transitions to determine the yield stress and then those based on solid-to-liquid transitions (see Fig. 11).

A. Experiments probing the liquid-to-solid transition

1. Extrapolating the flow curve in the limit of vanishing shear rates

The experiment matching the definition of Eq. (7) consists of measuring the flow curve (σ vs $\dot{\gamma}$) by applying a *steady shear* and progressively ramping down the shear rate to reach the limit $\dot{\gamma} \rightarrow 0$. The material, liquidlike at first, is thus progressively brought into a solidlike state, ideally through a series of steady states. The extrapolation of the stress in the limit of vanishing shear rates points toward a stress value that is generally referred to as the *dynamic yield stress*. In practice,

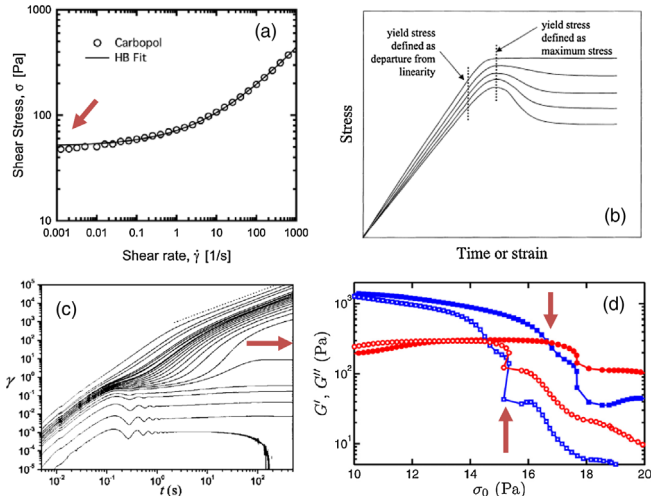


FIG. 11. Various methods to determine a yield stress experimentally. (a) Extrapolation of the flow curve in the limit of vanishing shear rates. Experiments performed on a Carbopol microgel using roughened cone-and-plate fixtures. The black line is the best Herschel-Bulkley fit. From Dimitriou, Ewoldt, and McKinley, 2013. (b) Sketch of the stress response to a shear start-up experiment. The yield stress can be defined as the stress corresponding to the end of the linear regime, as the stress maximum, or as the equilibrium stress. From Barnes and Nguyen, 2001. (c) Strain response to step stress experiments for various stresses ranging from 0.22 to 220 Pa. From Coussot *et al.*, 2006. (d) Oscillatory stress sweep experiment performed on a 6% wt carbon black gel at two different sweep rates: 7 (open) and 34 (filled) mPa s^{-1} . Here the yield stress, defined as the intersection of G' (dark gray, blue) and G'' (light gray, red), depends on the sweep rate. From Perge *et al.*, 2014.

however, this extrapolation can be problematic as it requires the establishment of a steady shear flow at arbitrarily low shear rates. An alternative is to fit the flow curve to a rheological model, such as the Bingham, Herschel-Bulkley, or Casson models [see Fig. 11(a)] (Nguyen and Boger, 1992). As noted, the Herschel-Bulkley model is observed to fit the experimental data properly over several decades in the case of dense assemblies of soft particles, such as emulsions, microgels, and foams (Ovarlez, Cohen-Addad *et al.*, 2013), and to provide a reproducible yield stress value. For this model, the most convincing representation of the flow curve is to plot the *viscous* stress, namely, the difference between the stress and the yield stress $\sigma - \sigma_y$ versus the shear rate $\dot{\gamma}$, which should show pure power-law behavior, as reported for instance by Katgert *et al.* (2009), Fall, Paredes, and Bonn (2010), Möbius, Katgert, and van Hecke (2010), Tighe *et al.* (2010), and Shukat, Sharma, and Joshi (2012).

However, this methodology suffers from several important limitations. First, wall slip can affect the flow at low shear rates, an issue that will be discussed in more detail in Sect. III.C. Second, time-dependent phenomena such as thixotropy cause the shape of the flow curve and therefore its extrapolation in the limit of vanishing shear rates to depend on the rate at which the shear rate is swept (Divoux, Grenard, and Manneville, 2013). For some materials such as various attractive colloidal gels (Ovarlez, Tocquer *et al.*, 2013), this may even be a subtle function of the previous flow history.

The dynamic yield stress obtained for a time-dependent material thus depends on the details of the experimental protocol. Furthermore, from a theoretical viewpoint it is unclear whether Eq. (7) strictly holds even for simple types of glassy materials, whereas very little is known for physical and nonequilibrium gels from computer simulations. Even for athermal systems characterized by a genuine jamming transition, extracting the yield stress using extrapolations to vanishing shear rates requires rheological measurements over a broad time window.

2. Determining the residual stress after flow cessation

In order to minimize the influence of previous flow history and thixotropy, some researchers prefer switching off the flow rather than progressively decreasing the shear rate. In such a flow cessation experiment, the sample is sheared at a given shear rate long enough to reach steady state. Then the shear rate is suddenly set to zero and the initially liquidlike material turns into a solid while the stress decreases toward a constant *residual* or *internal* stress σ_r ; see Fig. 12. Historically, this stress value has also been coined a yield stress by Michaels and Bolger (1962), Tiu and Boger (1974), Nguyen and Boger (1983), and Magnin and Piau (1990) but it was soon recognized that this residual stress was always much smaller than the dynamic yield stress (Keentok, 1982). In fact, the residual stress decreases for increasing values of the shear rate applied prior to flow cessation (Osaji, Kim, and Weitz, 2008; Lidon, Villa, and Manneville, 2016). Therefore σ_r is not a material constant but rather gives access to a history-dependent frozen-in quantity that accounts for the microstructural anisotropy imprinted to the material by previous shear.

Still, recent years have seen a renewed interest in internal stresses triggered by various theories for soft glasses and their predictions of the dynamics upon flow cessation. In dense assemblies of soft particles, the stress has been shown to relax through two distinct steps. A rapid relaxation, interpreted as the ballistic motion of the particles in the framework of a micromechanical model (Seth *et al.*, 2011), is followed by a slower relaxation of the elastic contact forces between the jammed particles (Mohan, Bonnecaze, and Cloitre, 2013) [see Fig. 12(a)]. Whereas such a slow relaxation due to aging dynamics is expected for the Brownian particles studied in these experiments, no such slow relaxation should exist for fully athermal soft particles, as there is no mechanism to induce fluctuations that would allow for a slow exploration of the complex free-energy landscape of the material. Simulations of the behavior of non-Brownian particles after shear is suddenly stopped confirm the rapid convergence of the residual stress to a finite value (Chaudhuri, Berthier, and Bocquet, 2012), with no slow relaxation involved in that relaxation process.

In hard-sphere colloidal glasses, the stress relaxes as a power law as predicted by the SGR model (Cates *et al.*, 2004) and is associated with subdiffusive motions of the particles (Ballauff *et al.*, 2013) [see Fig. 12(b)]. This is not surprising because the SGR model was initially devised as a rheological model to study the interplay of aging dynamics and shear flow in glassy materials (Sollich, 1998; Fielding, Sollich, and Cates, 2000). By contrast, the mode-coupling approach developed by Fuchs and Cates (2009) does not include aging

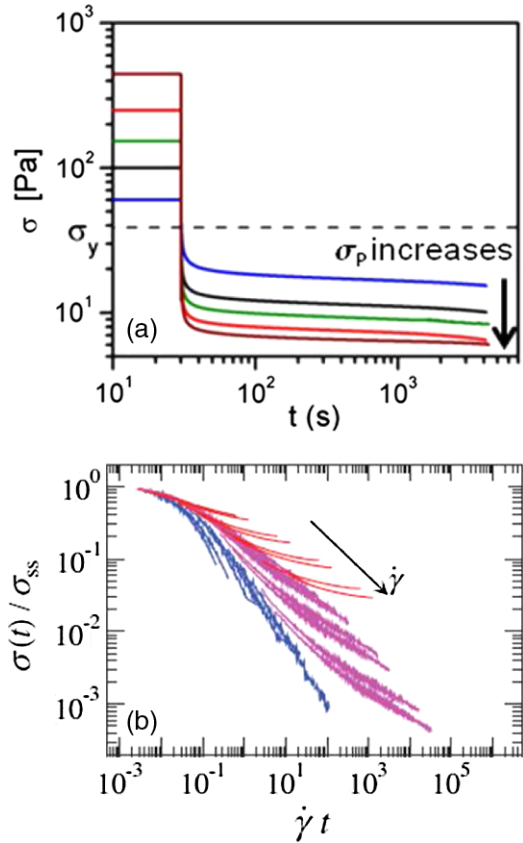


FIG. 12. (a) Stress relaxation upon flow cessation: experiments with microgels for different preshear stresses (from 60 to 443 Pa). The internal stress σ_r , defined by linear extrapolation of the stress measured over a short time interval (< 50 s) after flow cessation, is larger for smaller preshear stress and becomes quite significant for preshear stresses approaching the yield stress. From Mohan, Bonnecaze, and Cloitre, 2013. (b) Evolution of the stress after flow cessation normalized by the stress prior to flow cessation (σ_{ss}) as a function of $\dot{\gamma} t$ for a hard-sphere colloidal suspension. The curves correspond to various imposed shear rates $\dot{\gamma}$ prior to flow cessation, and different packing fractions. Glass states are shown in light gray (red), liquid states in dark gray (blue). From Ballauff *et al.*, 2013.

effects, and so it cannot describe the slow relaxation of the stress after flow cessation or the subdiffusive particle displacements observed in experiments (Ballauff *et al.*, 2013; Fritsch, Fuchs, and Voigtmann, 2014) and predicts instead a fast convergence to an arrested state with a finite residual stress.

Finally, aging laponite clay suspensions display a sigmoidal stress relaxation upon flow cessation with a characteristic time that scales inversely with the quench rate (Negi and Osaji, 2010b). The latter behavior contrasts with the simpler relaxation reported in dense systems with strong aging and remains to be interpreted from microscopic and/or theoretical points of view.

B. Experiments probing the solid-to-liquid transition

1. Analyzing the transient stress response during shear start-up

When an external shear rate $\dot{\gamma}$ is imposed on a soft solid at time $t = 0$ and is kept constant thereafter, the stress $\sigma(t)$ first

increases linearly with the strain $\gamma = \dot{\gamma}t$ which is indicative of elastic response [see Fig. 11(b)]. It then departs from linearity at intermediate strains, typically $\gamma \sim 0.1$ for bentonite suspensions (Nagase and Okada, 1986) and 0.2 for microgels (Divoux, Barentin, and Manneville, 2011a). Although a characteristic stress associated with departure from linearity can be inferred from this early-time stress response (Lin and Brodkey, 1985; Nagase and Okada, 1986), such a yield stress involves an arbitrary definition of how far from linearity the system should be. More importantly, this behavior may relate to local yielding events rather than to global yielding of the material. Nonetheless, this crossover from linear to nonlinear behavior is an interesting phenomenon for which experiments can be compared to theories and simulations perhaps more easily than for larger strains.

Upon entering the fully nonlinear regime, $\sigma(t)$ in general goes through a maximum before decreasing toward its steady-state value. Such a *stress overshoot* is observed in a large number of yield stress fluids such as foams (Khan, Schnepper, and Armstrong, 1988), emulsions (Papenhuijzen, 1972; Batista *et al.*, 2006), microgels (Divoux, Barentin, and Manneville, 2011a), clays (Nagase and Okada, 1986), and attractive gels (Lidell and Boger, 1996; Koumakis and Petekidis, 2011). The maximum value of the stress reached during shear start-up has been widely used as an estimate of the yield stress. However, it does not coincide with the definition of Eq. (7) and it is now referred to as the *static yield stress* (Varnik, Bocquet, and Barrat, 2004) in order to clearly distinguish it from the dynamic yield stress inferred from flow-curve measurements measured in the flowing regime. In particular, as they are performed at a finite shear rate, start-up experiments introduce the additional time scale $1/\dot{\gamma}$ and the subsequent nonlinear stress response is generally not a function of γ only but also depends on $\dot{\gamma}$. Although the static yield stress is not a material constant, the stress overshoot phenomenon still raises important fundamental questions: Does it have any simple microstructural interpretation? Can it be predicted from theory? The influence of the various experimental control parameters on the stress maximum, reviewed next, might give some clues.

First, if the effect of boundaries and the possibility of wall slip (see Sec. III.C) are ignored, the stress overshoot mainly depends on the value of $\dot{\gamma}$ (Nguyen and Boger, 1983). Experiments performed on stabilized suspensions of silica particles (Derec *et al.*, 2003), Carbopol microgels (Divoux, Barentin, and Manneville, 2011a), and attractive gels (Koumakis and Petekidis, 2011) report a power-law increase of the stress maximum with external shear, with an exponent ν in the range of 0.1–0.5. This power-law scaling is captured by fluidity models (Derec *et al.*, 2003), Stokesian simulations (West, Melrose, and Ball, 1994), and Brownian dynamics simulations of particle gels (Whittle and Dickinson, 1997; Park and Ahn, 2013), although the microscopic parameters controlling the exponent ν are still unclear. Power laws also contrast with the logarithmic increase reported for bidisperse Lennard-Jones mixtures for which the increase of the stress maximum can be interpreted in the framework of the Ree-Eyring viscosity theory (Varnik, Bocquet, and Barrat, 2004; Rottler and Robbins, 2005) and appears quite natural in the context of aging studies of glassy materials, in which

slow aging dynamics very often leads to logarithmic time dependences.

Second, for a given applied shear rate, the stress maximum increases with the “sample age,” i.e., the waiting time t_w between the preshear used to reset the fluid memory and the start-up of the shear. The overshoot eventually disappears for waiting times shorter than $1/\dot{\gamma}$ (Derec *et al.*, 2003; Letwimolnun *et al.*, 2007; Divoux, Barentin, and Manneville, 2011b). Such a behavior is well captured by the SGR (Fielding, Sollich, and Cates, 2000) and fluidity models (Moorecroft, Cates, and Fielding, 2011), although both models predict a logarithmic increase of the stress maximum with t_w , whereas experimental results rather point to a weak power-law dependence.

Finally, regarding the local behavior of the fluid during shear start-up, recent experimental and numerical studies have shed new light on the nature of the stress maximum. In Brownian colloidal systems, the stress maximum coincides with the maximum structural anisotropy (Mohraz and Solomon, 2005; Koumakis, Laurati *et al.*, 2012) [see Figs. 13(a) and 13(b)]. For attractive gels, the stress maximum corresponds to the rupture of the gel network, while for dense hard-sphere-like systems, individual colloids experience an (apparent) superdiffusive motion as they are being pushed out of their cage by shear (Zausch *et al.*, 2008; Koumakis, Laurati *et al.*, 2012), which can be readily interpreted in terms of a delayed onset of diffusive behavior. In the case of a jammed assembly of soft particles, the deformation is almost elastic and only a few rearrangements that are uniformly spatially distributed have been reported in foams (Kabla, Scheibert, and Debrégeas, 2007) [see Figs. 13(c) and 13(d)], while linear

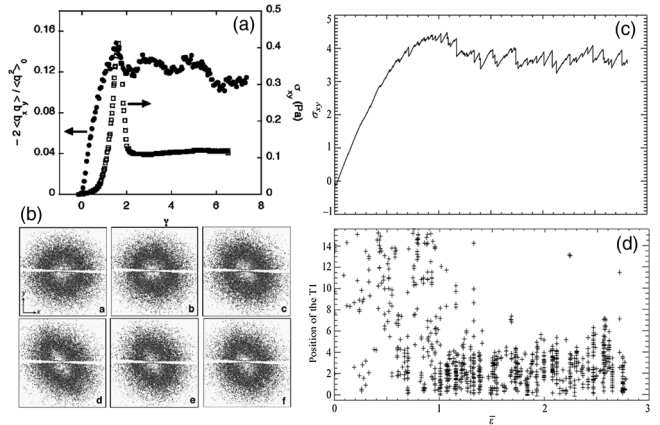


FIG. 13. (a) Normalized off-diagonal component of the second moment tensor of the dimensionless scattering vector \hat{q} weighted by the structure factor $\langle \hat{q} \hat{q} \rangle$, and shear stress σ_{xy} vs strain γ during a shear start-up experiment ($\dot{\gamma} = 0.17 \text{ s}^{-1}$) for a polystyrene gel ($\phi = 10^{-3}$). (b) Contour plots of a representative cascade of scattering patterns collected during a start-up experiment ($\dot{\gamma} = 0.56 \text{ s}^{-1}$) with a $t = 0.1$, b 1.1 , c 2.2 , d 3.5 , e 6.3 , and f 8.3 s. Maximum anisotropy is observed at $t = 3.5$ s. (a), (b) From Mohraz and Solomon, 2005. (c) Evolutions of the shear stress and (d) positions of the T1 events in a foam sheared in a 2D Couette cell as a function of the applied strain during a shear start-up experiment. Data from numerical simulations. From Kabla, Scheibert, and Debrégeas, 2007.

velocity profiles have been observed in microgels up to the stress maximum (Divoux, Barentin, and Manneville, 2011b). These recent local approaches show that shear start-up and more specifically the stress overshoot phenomenon are powerful tools to finely distinguish between various types of yield stress materials. Theoretical understanding of the full transient scenario is, however, still far from reach.

2. Creep experiments

In a creep experiment, a constant shear stress σ is applied from time $t = 0$ and the strain response $\gamma(t)$ is monitored. Although also a shear start-up experiment, this protocol does not necessarily fluidize the material which may remain solid, and the results may be qualitatively distinct from those discussed in Sec. III.B.1.

For stresses applied above the yield stress, the material eventually flows, i.e., $\gamma(t)$ increases linearly with time, whereas for stresses lower than the yield stress, the material behaves as a solid and $\gamma(t)$ tends toward a constant. Equivalently, the shear rate $\dot{\gamma}(t)$ reaches a nonzero steady-state value in the former case, while it vanishes in the latter case. Following the discussion in Sec. III.B.1, the yield stress measured by this approach should again provide an estimate of the static yield stress.

This “bifurcation” between a finite steady-state viscosity and an apparently infinite viscosity in principle provides a well-defined estimation of the yield stress as the critical stress separating these two regimes (Cousset *et al.*, 2002a, 2002b, 2006; Cruz *et al.*, 2002; Møller, Mewis, and Bonn, 2006) [see Fig. 11(c)]. This method is cumbersome, however, as the yield stress is obtained by dichotomy, and for each experiment the time for the material to flow increases as the applied shear stress gets closer to the yield stress (Møller, Fall, and Bonn, 2009). The question of deciding whether a steady state is reached and whether the system eventually flows or not becomes even more important in the case of very long transients and of so-called “delayed yielding,” where no apparent flow can be detected for long times before the material finally yields (Uhlherr *et al.*, 2005; Magda *et al.*, 2009; Gibaud, Frelat, and Manneville, 2010; Chaudhuri and Horbach, 2013).

Besides the determination of the yield stress, the transient strain or shear rate responses also provide potentially rich information on the physical processes at play in soft solids under constant stress. In particular, a robust feature of creep responses prior to fluidization is a power-law decrease of the shear rate (see Fig. 14) that strongly resembles the “Andrade creep” reported for hard solids (da C. Andrade, 1910), which has been attributed to collective dislocation dynamics (Miguel *et al.*, 2002; Csikor *et al.*, 2007; Miguel, Laurson, and Alava, 2008). Power-law creep has been reported for cellulose gels (Plazek, 1960) and more recently for various amorphous soft solids such as polycrystalline surfactant hexagonal phases (Bauer, Oberdisse, and Ramos, 2006), Carbopol microgels (Divoux, Barentin, and Manneville, 2011a; Lidon, Villa, and Manneville, 2016), core-shell p-NIPAM colloidal particles (Siebenbürger, Ballauf, and Voigtmann, 2012), thermoreversible protein gels (Brenner *et al.*, 2013), and colloidal glasses (Sentjabrskaja *et al.*, 2015). Yet, Andrade-like creep remains

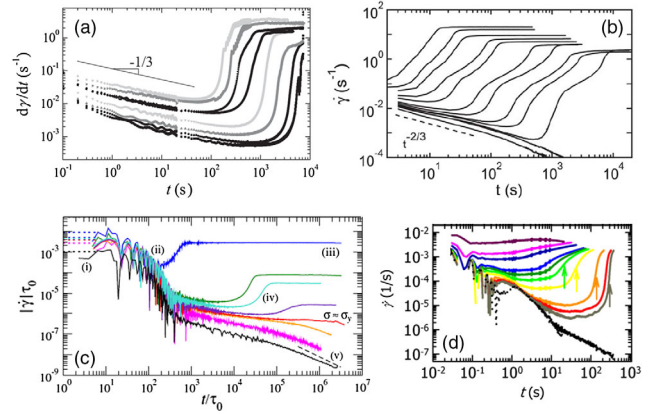


FIG. 14. Shear rate responses vs time for creep experiments at different imposed shear stresses in various materials: (a) polycrystalline hexagonal columnar phase. From Bauer, Oberdisse, and Ramos, 2006. (b) Carbopol microgel. From Divoux, Barentin, and Manneville, 2011a. (c) Core-shell PS-p-NIPAM particle glass. From Siebenbürger, Ballauf, and Voigtmann, 2012. (d) Carbon black gel at 8% wt. From Sprakel *et al.*, 2011.

mostly unexplored in soft materials such as yield stress fluids. Local velocimetry suggests that the strain field remains macroscopically homogeneous during this first regime (Divoux, Barentin, and Manneville, 2011a; Grenard *et al.*, 2014). Still, characterizations at finer, ideally microscopic, scales are needed to unveil the presence of plasticity or microcracks during the initial loading phase and to make a clear link between the physical mechanisms at play in the creep of ordered solids and of disordered soft materials. New insight can also be gained by adapting recent numerical models to creep situations (Colombo and Gado, 2014; Fusco, Albaret, and Tanguy, 2014).

Finally, for stresses above the yield stress, the initial power-law creep is followed by a gradual acceleration up to an abrupt fluidization of the material that later reaches a steady state. The dynamics associated with fluidization are discussed in Sec. IV.C.2 together with the characteristic time scales involved in the yielding process. For stresses below the yield stress, the interplay between creep deformation and aging leads to long-time strain responses that are more complex than pure power laws and strongly depend on the sample age, as reported for laponite clay suspensions (Negi and Osuji, 2010a; Baldewa and Joshi, 2012) and star glassy polymers (Christopoulou *et al.*, 2009).

3. Large-amplitude oscillatory shear experiments

So far, the yielding transition has been considered only from the point of view of a *steady* external shear. Yet, the solidlike versus liquidlike behavior of a complex material can also be quantified through *oscillatory* shear experiments. By imposing a sinusoidal shear strain of amplitude γ_0 and frequency ω , given by $\gamma(t) = \gamma_0 \sin(\omega t)$, and measuring the corresponding stress response $\sigma(t)$, the storage (G') and loss (G'') moduli can be defined from the amplitudes of the stress response that are, respectively, in phase and out of phase with $\gamma(t)$ at the excitation pulsation ω (Ferry, 1980). The solid-to-liquid transition of a yield stress material can thus be probed

by progressively increasing the amplitude γ_0 of the oscillatory strain. At low strain amplitudes, the solidlike material is elastically deformed and the storage modulus G' remains roughly constant and much larger than the loss modulus G'' . This corresponds to the linear regime of deformation referred to as “small-amplitude” oscillatory shear. At larger strain amplitudes, the material response gets nonlinear. Under such “large-amplitude” oscillatory shear (LAOS), G' typically decreases, then crosses G'' and becomes much smaller than G'' as the material becomes liquidlike [see Fig. 11(d)].

LAOS experiments allow for a number of different estimations of the yield point. By plotting G' and G'' as functions of either the strain amplitude γ_0 or the shear stress amplitude σ_0 , the stress amplitude σ_{0y} at which the material yields may be given by the point at which $G' = G''$, which has been called “characteristic modulus” by Larson (1999) [see Figs. 11(d) and 15(a)], or by the intersection of power-law fits of the moduli behaviors well above and well below the yielding point (Rouyer, Cohen-Addad, and Höller, 2005). Alternatively, σ_{0y} can be estimated by plotting σ_0 vs γ_0 from the intersection between a linear behavior with slope G' at low strains and a power-law fit at high strains (Mason, Bibette, and Weitz, 1996; Saint-Jalmes and Durian, 1999). These various estimates are discussed and compared in Dinkgreve *et al.*, 2016.

Clearly, contrary to steady-shear measurements, all LAOS estimates of the yield stress as σ_{0y} involve the additional time scale $1/\omega$ and thus do not comply with the definition of Eq. (7) unless vanishingly small frequencies are considered. Moreover, as already addressed in several rheology reviews (Wilhelm, 2002; Hyun *et al.*, 2011), the response to LAOS is intrinsically nonlinear and needs to be analyzed considering the full spectrum of strain or stress harmonics rather than the sole fundamental frequency through G' and G'' only. The various estimates of σ_{0y} should depend on both ω and the harmonic content of the stress or strain response, and there is no particular reason why they should coincide and correspond to the dynamic yield stress inferred from steady-state measurements. Finally, in the case of strongly time-dependent materials, the estimate of σ_{0y} is most likely to depend on the details of the LAOS ramp protocol, as illustrated in Fig. 11(d). Wall slip and/or bulk heterogeneous flows may complicate yielding under oscillatory shear even more (Walls *et al.*, 2003; Gibaud, Frelat, and Manneville, 2010; Perge *et al.*, 2014; Gibaud *et al.*, 2016).

Interest in LAOS has grown, leading to a surge in the number of experimental and theoretical studies over the last decade. First, LAOS has been used to unveil a striking difference between attractive and repulsive colloidal glasses. Whereas the elastic modulus decreases monotonically in dense hard-sphere-like systems, attractive glasses display a two-step yielding, which results from the existence of two distinct microscopic length scales in the system: the adhesion range (responsible for initiating phase separation) and the cage size in the dense glassy phase (responsible for the dynamic arrest) (Pham *et al.*, 2006; Laurati, Egelhaaf, and Petekidis, 2011; Chan and Mohraz, 2012; Koumakis, Brady, and Petekidis, 2013). Such a two-step scenario has been observed through strain-step experiments (Koumakis and Petekidis, 2011), but its interpretation still requires full confirmation

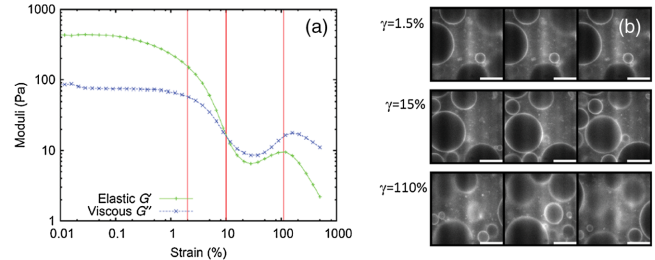


FIG. 15. (a) Evolution of the shear moduli of a Pickering emulsion stabilized by silica colloids during a LAOS strain amplitude sweep. The volume fraction of the oil is 65%. (b) Confocal images of the emulsion during shear taken 40 mm into the sample to avoid wall effects and obtained at different strains during the strain sweep. Scale bars correspond to 20 μm . For $\gamma_0 < 0.10$, the droplets slide along each other but remain trapped in the cages formed by their neighbors. For $\gamma_0 \approx 0.10$, the moduli intersect and the droplets can be seen to move irreversibly, although their displacement over a period is much less than their diameter. For $\gamma_0 > 0.30$, G' and G'' increase due to jamming, which results in apparent shear thickening, and the droplets move rapidly during each period, over distances larger than their own diameter. From Hermes and Clegg, 2013.

from direct local investigations. Of course, this two-step yielding process immediately leads to the question whether a yield stress or even two yield stresses should be defined.

Second, physical insights into the microscopic dynamics under LAOS have been gained by coupling oscillatory shear to other characterization techniques, such as structural measurements or local tracking of particle motion. The “light scattering echo” technique has allowed the quantification of the global amount of irreversible rearrangements (Hébraud *et al.*, 1997; Petekidis, Vlassopoulos, and Pusey, 2003; Laurati, Egelhaaf, and Petekidis, 2014). Direct optical imaging of the microstructure has recently been used to assess the transition to irreversibility with emphasis on the physical properties of rearrangements such as their correlation length (Nagamanasa *et al.*, 2014), the presence of dynamical heterogeneities (Knowlton, Pine, and Cipelletti, 2014), and cage breaking in repulsive versus attractive systems (Hermes and Clegg, 2013) [see Fig. 15(b)]. Along the same lines, time-resolved neutron and x-ray scattering now allows one to follow the evolution of shear-induced anisotropy in colloidal gels during one single LAOS cycle (Kim *et al.*, 2014; Min Kim *et al.*, 2014; Rogers *et al.*, 2014). Such measurements come as a crucial complement to recently proposed nonlinear analyses of rheological data during one oscillation cycle (Ewoldt, Hosoi, and McKinley, 2008; Rogers *et al.*, 2011; Dimitriou, Ewoldt, and McKinley, 2013; Ewoldt, 2013; Dimitriou and McKinley, 2014) and can be used as an additional tool to study the yielding behavior and hence the value of the yield stress.

Third, from a more theoretical point of view, recent advances in modeling and simulation of LAOS flows have also led to significant progress in unveiling the physical importance of caging effects in the yielding of both hard-sphere glasses (Brader *et al.*, 2010; Koumakis, Brady, and Petekidis, 2013) and dense assemblies of soft particles (Mohan *et al.*, 2013), and this situation was analyzed within

a mode-coupling approach (Seyboldt *et al.*, 2016). The idea has emerged that the yielding transition corresponds to a change in the dynamics at the microscopic scale between reversible particle trajectories at small applied stress and a chaotic dynamics beyond the yielding point (Fiocco, Foffi, and Sastry, 2013; Regev, Lookman, and Reichhardt, 2013; Kawasaki and Berthier, 2016). Whereas early numerical work seemed to predict a continuous phase transition between the two regimes characterized by power-law divergences (Brader *et al.*, 2010; Perchikov and Bouchbinder, 2014), more recent work (Kawasaki and Berthier, 2016) put forward the idea that the transition is indeed sharp but discontinuous, akin to a nonequilibrium first-order phase transition. In experiments, contrasting evidence has been reported on this point (Hermes and Clegg, 2013; Knowlton, Pine, and Cipelletti, 2014; Denisov *et al.*, 2015). Therefore, the nature of the yielding transition under oscillatory shear remains to be fully elucidated.

4. Nonviscometric flows

Many flows encountered in practice are not simple viscometric flows. A typical example is that of a sphere falling through a yield stress fluid; this has often been used as a benchmark, e.g., for numerics. The fluid around the sphere will be set in motion because of the stress exerted by the falling sphere, but the fluid far away will remain motionless; the question is where the yield surface (i.e., the transition from the flowing to the nonflowing material) is localized in space. Experiments on the flow of yield stress fluids around falling spheres far from any boundaries have revealed the location of the yield surface, but have also shown that the usual constitutive equations are unable to describe this situation. In a number of experiments, the loss of fore-aft symmetry (Gueslin *et al.*, 2006; Putz *et al.*, 2008) was observed. For thixotropic fluids (Gueslin *et al.*, 2006), this can easily be understood: where the sphere has passed through the material, it has liquefied. However, similar observations made on Carbopol gels (Putz *et al.*, 2008) cannot be explained by properly invariant 3D generalizations of classical models such as the Bingham and Herschel-Bulkley fluids (Putz *et al.*, 2008). Symmetry breaking may in fact be an elastic effect: the resemblance between the yield stress fluid flow around a sphere and the flow of viscoelastic polymer solutions has been noted. The notion of combining viscoelasticity and yield stress behavior has spurred Saramito (2007) and de Souza Mendes (2009, 2011) to attempt to add elasticity to the usual viscoplastic models and developed properly invariant continuum elastoviscoplastic constitutive equations. There has been some success in simulating the breaking of flow fore-aft symmetry by Cheddadi *et al.* (2011), Fonseca *et al.* (2013), and dos Santos *et al.* (2014). Notably, Fragedakis, Dimakopoulos, and Tsamopoulos (2016) have successfully simulated the flow of Carbopol solutions past isolated spheres by incorporating the plastic back pressure (Dimitriou, Ewoldt, and McKinley, 2013) into the Saramito model.

C. Wall slip in yield stress materials

As mentioned, in the vicinity of a *smooth* solid boundary, the velocity of a yield stress fluid (v_{sample}) may differ from the

velocity of the boundary (v_{wall}). One may observe either $v_{\text{sample}} < v_{\text{wall}}$ (e.g., in the case of a shearing device driven at constant velocity v_{wall}) or $v_{\text{sample}} > v_{\text{wall}} = 0$ (close to a fixed surface or in capillary or channel flows). In both cases, the apparent discontinuity in velocity at the wall is caused by a thin and highly sheared region adjacent to the wall of lower viscosity than the bulk material. This phenomenon, referred to as *apparent wall slip* or more often simply as *wall slip* in the literature, has first been described as an artifact that experimentalists should get rid of in order to avoid misinterpreting rheological measurements (Barnes, 1995). Although elucidating the exact microscopic structure of the lubrication layer remains an experimental challenge due to its small width (typically smaller than 1 μm), very high local shear rate, and proximity to a solid boundary, it is presumably composed of a pure solvent in the case of colloidal gels or suspensions (Hartman Kok *et al.*, 2002, 2004) or of a film of continuous phase in emulsions (Princen, 1985). The emergence of local techniques to quantify slip velocities has brought about a better understanding of the behavior of yield stress materials near boundaries, allowing the development of successful microscopic models in the case of dense assemblies of soft particles (Seth *et al.*, 2011). In the case of attractive gels, a recent body of evidence suggests that the dynamics close to a wall may not be easily decoupled from the bulk dynamics and that wall slip is not merely a rheometric complication, as recently pointed out by Buscall (2010). This section addresses the various issues related to wall slip in yield stress fluids in light of such recent developments.

1. Impact on flow-curve measurements

In the presence of wall slip, the measured apparent shear rate overestimates the true shear rate within the material (or, correspondingly, the strain indicated by a rheometer overestimates the true deformation experienced by the bulk of the material). Consequently, the apparent flow curve is shifted to higher shear rates compared to the actual constitutive equation of the bulk material. In general, at low shear rates, where wall-slip effects are most pronounced, the apparent flow curve displays a kink and/or a plateau at a stress lower than the yield stress estimated in the absence of wall slip [see Fig. 16(a) for examples]. This signature has been reported in the literature as early as 1975 in the pioneering work of Vinogradov *et al.* (1975) and, since then, for a broad range of yield stress materials including colloidal gels (Buscall, McGowan, and MortonJones, 1993; Mas and Magnin, 1994), dense Brownian suspensions (Ballesta *et al.*, 2008, 2012), emulsions and microgels (Meeker, Bonnecaze, and Cloitre, 2004a, 2004b), and foams (Marze, Langevin, and Saint-Jalmes, 2008). In particular, wall slip leads to significant deviations from the Herschel-Bulkley behavior at low shear rates, and the apparent flow curve is strongly surface dependent in this limit (Seth, Cloitre, and Bonnecaze, 2008).

2. Physical origin of wall slip in yield stress fluids

Direct flow visualization coupled to rheology has made it possible to go one step further in interpreting the apparent lower stress plateau in the presence of wall slip. The seminal work of Magnin and Piau (1990) on Carbopol microgels,

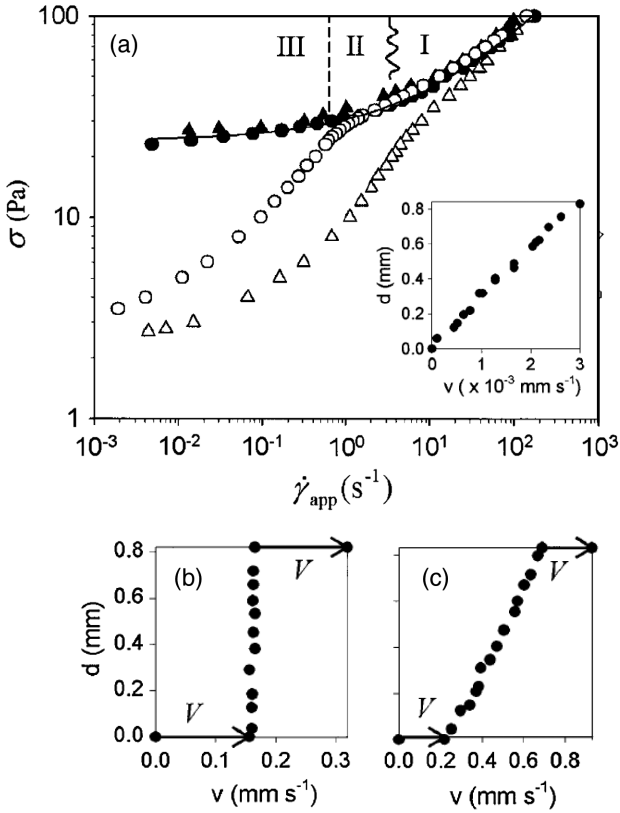


FIG. 16. (a) Stress σ vs the apparent shear rate $\dot{\gamma}_{\text{app}}$ for a microgel paste (open and solid circles) and an emulsion (open and solid triangles) of packing fraction $\phi \approx 0.77$ obtained in a cone-and-plate device for smooth (open symbols) and rough (closed symbols) surfaces. Regimes I–III refer to microgel slip behavior discussed in the text. The inset shows the velocity profile measured with rough surfaces for $\sigma/\sigma_y = 1.05 \pm 0.1$. (b), (c) Velocity profiles measured with smooth surfaces for (b) $\sigma/\sigma_y = 0.9 \pm 0.1$ and (c) 1.3 ± 0.1 . Adapted from Meeker, Bonnecaze, and Cloitre, 2004b.

coupling rheology to direct observations of the strain field, has inspired numerous subsequent studies coupling flow visualization to standard rheology (Kalyon *et al.*, 1993; Aral and Kalyon, 1994; Persello *et al.*, 1994). Subsequently, combinations of rheology and other local measurement techniques, such as light scattering velocimetry in a Couette geometry (Salmon, Bécu *et al.*, 2003) and particle tracking velocimetry in cone-and-plate (Meeker, Bonnecaze, and Cloitre, 2004a, 2004b; Ballesta *et al.*, 2008, 2012; Paredes, Shahidzadeh-Bonn, and Bonn, 2011) and plate-plate geometries (Seth *et al.*, 2012), have provided quantitative measurements of slip velocities (defined as $v_s = |v_{\text{sample}} - v_{\text{wall}}|$) and wall-slip scenarios for the different yield stress materials. Let us first discuss the case of yield stress fluids composed of soft deformable particles before turning to rigid particles.

a. Wall slip in the case of soft particles

In yield stress fluids made of soft particles, the solid behavior results from the tightly packed structure of deformable objects, and the lubrication layers that develop at smooth walls are intimately related to the particle deformability. For

shear rates such that $\sigma < \sigma_y$ [see regime III in Fig. 16(a)], the bulk remains unsheared and the apparent motion is entirely due to wall slip [see Fig. 16(b)]. This situation is referred to as “total” wall slip or “pluglike” flow. In this regime, v_s has been shown to increase as a power law of the excess stress (i.e., the stress at the wall minus the apparent yield stress σ_s inferred from the extrapolation of the flow curve to vanishing shear rates in the smooth geometry) $v_s \propto (\sigma - \sigma_s)^p$, where the exponent p does not depend significantly on the packing fraction but is strongly influenced by the chemical nature of the walls. The slip velocity v_s displays a nearly quadratic scaling, i.e., $p \approx 2$, in the case of attractive or nonwetting surfaces, whereas $p = 1$ for repulsive and/or wetting walls (Seth, Cloitre, and Bonnecaze, 2008; Seth *et al.*, 2012) [see Fig. 17(a)]. Both exponents $p = 1$ and 2 have been successfully described at the scale of single particles by elastohydrodynamic lubrication theory as the result of a balance between bulk osmotic pressure and viscous dissipation taking place in the thin lubrication layer that separates the squeezed particles from the wall (Meeker, Bonnecaze, and Cloitre, 2004a; Seth, Cloitre, and Bonnecaze, 2008). The upper limit of this total wall-slip regime generally correlates well with the stress drop or “kink” on steady-state macroscopic measurements.

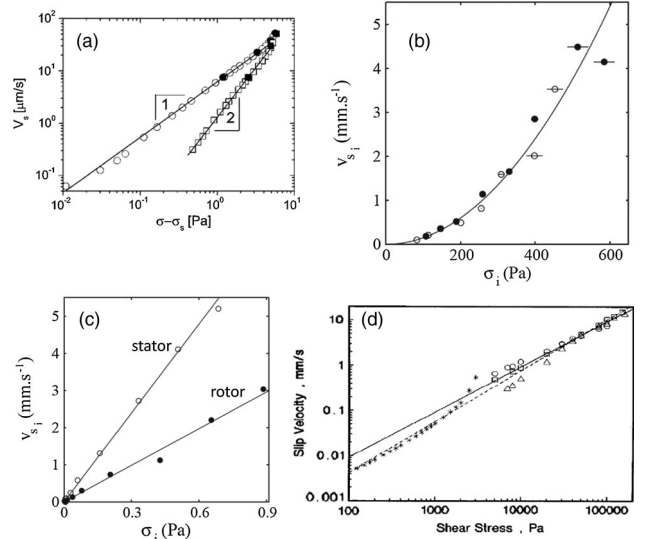


FIG. 17. (a) Slip velocity vs excess stress in a dense emulsion for stresses below the yield stress in a plate-plate geometry. The top plate is coated with either a weakly adhering polymer surface (open and solid squares) or a nonadhering glass surface (open and solid circles). The wetting properties of the boundary conditions strongly impact the behavior of the slip velocity. From Seth *et al.*, 2012. (b), (c) Slip velocity vs shear stress at the rotor (solid circles) and stator (open circles) for (b) a dense emulsion $\phi = 0.75$ and (c) a dilute emulsion $\phi = 0.2$. The slip velocity is linear in the dilute regime and quadratic for dense packing for stresses above the yield stress. From Salmon, Bécu *et al.*, 2003. (d) Slip velocity vs shear stress in a suspension of ammonium sulfate particles in poly(butadiene acrylonitrile acrylic acid) terpolymer (PBAN). Data obtained in capillary flows with dies (extrusion nozzles) of various aspect ratios (open symbols) and a plate-plate geometry (stars). The solid line corresponds to a linear behavior. From Yilmazer and Kalyon, 1989.

For larger shear rates such that $\sigma > \sigma_y$, the bulk material is sheared but wall slip remains significant, at least for $\sigma \gtrsim \sigma_y$ [see regimes I and II in Figs. 16(a) and 16(c)]. In this partial wall-slip regime, it appears that the slip velocity scales as a power law of the slip stress only (i.e., stress at the wall). Here the physical picture is much less clear. Both the absolute value of v_s and the exponent p depend strongly on the geometry. For instance, in similar systems, $p \approx 1$ has been reported for a plate-plate geometry (Seth *et al.*, 2012) while $p \approx 2$ for a smooth Couette cell (Salmon, Béchu *et al.*, 2003) [see Fig. 17(b)] and for rough microchannels (Geraud, Bocquet, and Barentin, 2013). We note that in this regime the influence of the packing fraction in the glassy state and the impact of the chemical nature of the walls have not been systematically explored. Yet, as seen in Figs. 17(b) and 17(c), one finds $p \approx 2$ above jamming to $p \approx 1$ for low packing fractions where soft particles are no longer compressed against each other and the yield stress vanishes. The exponent $p = 1$ is also found in liquidlike suspensions of rigid particles as discussed in the next section. From a recent study on soft thermoresponsive particles conducted at different temperatures in a Couette cell, it appears that the scaling of the slip velocity depends mainly on the packing fraction (Divoux *et al.*, 2015). Nonetheless, more experiments in other geometries are required to provide a truly universal scaling to the slip velocity across the jamming transition.

b. Wall slip in the case of hard particles

Concerning wall slip in suspensions of hard particles, a great deal of work has been done on non-Brownian systems, which corresponds to large Péclet numbers. Over a wide range of packing fractions, wall slip is associated with a depletion layer near the wall, where the thickness depends on the particle size and decreases roughly linearly with increasing bulk packing fraction (Kalyon, 2005). The latter result may not hold for polydisperse samples (Soltani and Yilmazer, 1998) and appears to be affected by migration effects (Jana, Kapoor, and Acrivos, 1995), which shows that the detailed mechanism for slip in non-Brownian systems is not fully understood. Nonetheless, the slip velocity at the wall scales linearly with the slip stress in a remarkably robust fashion (Yilmazer and Kalyon, 1989; Aral and Kalyon, 1994; Jana, Kapoor, and Acrivos, 1995; Soltani and Yilmazer, 1998) [see Fig. 17(d)]. The chemical properties of both the particle surface and boundary conditions seem to affect wall slip (van Kao, Nielsen, and Hill, 1975) although their quantitative impact on $v_s(\sigma)$ remains to be determined.

For Brownian hard spheres, the thickness of the depletion layer depends weakly on the Péclet number (Hartman Kok *et al.*, 2004) and decreases for increasing packing fractions (Ballesta *et al.*, 2008). The slip velocity scales linearly with the slip stress for both dilute and glassy assemblies. Moreover, wall slip in glassy samples is characterized at low shear rates by a stress kink on the macroscopic flow curve together with pluglike velocity profiles (Ballesta *et al.*, 2012). The latter result is strikingly similar to the one reported for soft particles in contact with nonadhering surfaces in Fig. 16(a), suggesting that a common mechanism might be at work. Attractive colloidal gels display the same phenomenology as glassy

suspensions over a broader range of packing fractions, down to very low values of ϕ . However, both the kink and wall slip tend to disappear as the polydispersity is increased (Ballesta *et al.*, 2013). Particle migration is also more likely to play a major role in these yield stress fluids with low packing fractions by promoting concentration gradients and/or segregation. One can thus anticipate that wall slip in attractive gels originates from the combined effects of migration and polydispersity, with a strong dependence on the shearing geometry, including stress gradients.

3. Dealing with wall slip in practice

Two types of practical approaches toward wall slip have been proposed in the literature: either to quantify the effect of wall slip from the experimentally determined flow curve or to eliminate it. An elegant solution due to Mooney (1931) and further extended by Yoshimura and Prud'homme (1988), Kiljański (1989), and Wein and Tovchigrechko (1992) consists of determining the relationship between the apparent shear stress and rate for gaps of different sizes. Combining at least two measurements and assuming that (i) the slip velocity is a function of stress only and (ii) slippage is the same at both walls, one can recover the constitutive relationship $\sigma(\dot{\gamma})$ corrected for wall slip (see Fig. 18). This method has been applied to various yield stress fluids, including emulsions (Yoshimura and Prud'homme, 1988), microgels (Meeker, Bonnecaze, and Cloitre, 2004a), and dense suspensions (Yilmazer and Kalyon, 1989; Kalyon *et al.*, 1993; Hartman Kok *et al.*, 2002, 2004; Kalyon, 2005) although the two assumptions on which it relies have been verified by local measurements of slip velocities only in a few cases (Salmon, Béchu *et al.*, 2003; Meeker, Bonnecaze, and Cloitre, 2004a; Habibi *et al.*, 2016).

To prevent wall slip, the nature of the wall needs to be modified. The use of rough boundary conditions allows one to properly determine constitutive equations without wall slip (Vinogradov *et al.*, 1975). The roughness of the wall has been tuned from a few microns to hundreds of microns by using sandblasted surfaces (Buscall, McGowan, and MortonJones,

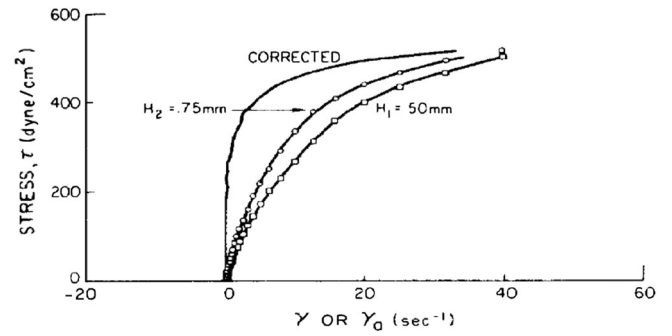


FIG. 18. Shear stress vs shear rate for a dense emulsion ($\phi = 0.923$) measured in a plate-plate geometry with smooth boundary conditions for two different gap sizes (500 and 750 μm , respectively). The stress vs the shear rate computed from the method developed by Mooney and extended by Yoshimura and Prud'homme displays a yield stress, while this is not obvious from the raw measurements. From Yoshimura and Prud'homme, 1988.

1993), grooved surfaces (Magnin and Piau, 1990), serrated tools (Nickerson and Kornfield, 2005), or by gluing waterproof sandpaper (Seth, Cloitre, and Bonnecaze, 2008; Seth *et al.*, 2012) or a monolayer of particles on the cell walls (Isa, Besseling, and Poon, 2007). The accepted paradigm is that the roughness of the surface should be comparable to the size of the microstructure, since a lower roughness would not be efficient, and a higher roughness, including vane cup geometries, may trigger secondary flows (Ovarlez *et al.*, 2011). In that respect, recent attempts to systematically explore the effect of the roughness-to-particle-size ratio (Mansard and Colin, 2012) look promising in order to go beyond empirical knowledge. Last but not least, the chemical nature and wetting properties of the walls can also be tuned to force the adhesion of the material even for smooth interfaces. This has been successfully achieved for colloidal silica gels at low deformations using hydrophobic boundaries (Walls *et al.*, 2003) and for aqueous microgels and oil-in-water emulsions using silicon boundaries (Seth, Cloitre, and Bonnecaze, 2008; Seth *et al.*, 2012) and chemical treatment of PMMA (Christel *et al.*, 2012) or glass surfaces (Paredes, Shahidzadeh, and Bonn, 2015), as illustrated in Fig. 19.

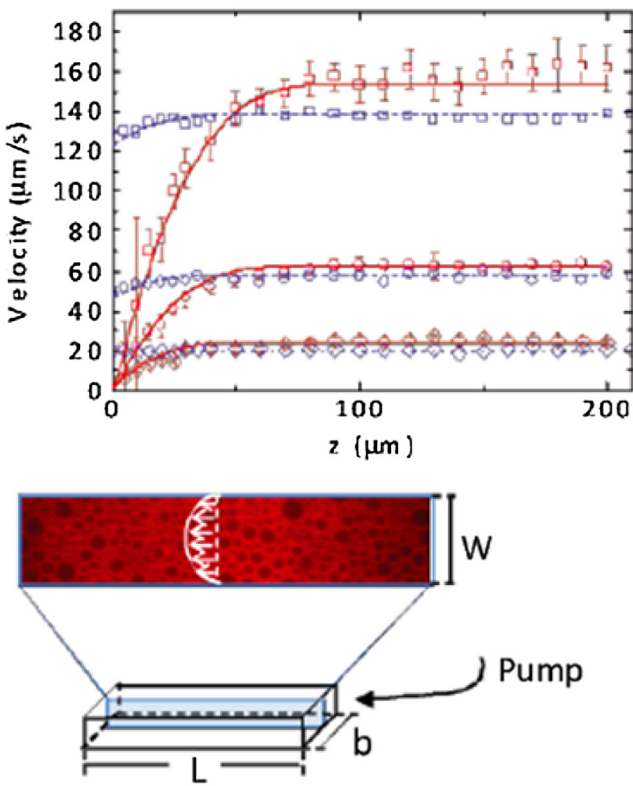


FIG. 19. Velocity profiles of a dense emulsion flowing in a rectangular microchannel (gap $w = 400 \mu\text{m}$). Images obtained by confocal microscopy. Velocity profiles in blue (dashed lines) correspond to smooth boundary conditions treated with a piranha solution. The oil droplets experience wall slip. Velocity profiles in red (continuous lines) correspond to smooth, silanized boundary conditions. The oil droplets stick to the surface, creating an effectively rough boundary condition. Flow rates: 0.2, 0.5, and $1.2 \times 10^{-2} \text{ mL}/\text{min}$. From Paredes, Shahidzadeh, and Bonn, 2015.

IV. STEADY-STATE FLOW DYNAMICS OF YIELD STRESS FLUIDS: FLOW CURVES AND SHEAR BANDING

This section is devoted to the dynamics of yield stress materials in the case where a stress above the yield stress is applied. After briefly reviewing methods to experimentally distinguish between simple and thixotropic yield stress fluids, we examine the current interpretations and models for the steady-state shear-banding flows generally observed in thixotropic materials. We close this section with two topics that have emerged within the last few years on the flow of yield stress fluids under confinement and the time scales involved in transient regimes of yield stress fluid flow.

A. Flow curves of simple and thixotropic yield stress fluids

As discussed in Sec. II.D, yield stress fluids can be broadly divided into simple yield stress fluids (microgels, dense emulsions, and foams) and thixotropic yield stress fluids (clays, fiber suspensions, and colloidal gels) (Bonn and Denn, 2009; Møller *et al.*, 2009; Ovarlez *et al.*, 2009; Ovarlez, Cohen-Addad *et al.*, 2013). Here we review how the distinction can be made experimentally, before turning to the most recent ideas.

1. Distinction between flow curves

Steady-state flow curves $\sigma(\dot{\gamma})$ can be used to distinguish between the two types of yield stress materials (Møller *et al.*, 2009) as follows:

- Simple yield stress fluids exhibit a *continuous* and monotonic constitutive equation, which is well fitted by the phenomenological Herschel-Bulkley law $\sigma = \sigma_y + A\dot{\gamma}^n$ [Fig. 20(a)]. As a consequence, whatever the applied shear rate, even in the limit of vanishing values, there is always a finite shear stress above σ_y at which the material flows. Conversely, whatever the applied shear stress above σ_y , there is always a finite shear rate reached by the material.
- In contrast, thixotropic yield stress fluids are characterized by a *discontinuous* underlying flow curve [Fig. 20(b)] with a pronounced time dependence. Indeed, in addition to a yield stress σ_y , these materials are also characterized by a critical shear rate $\dot{\gamma}_c$, below which they cannot flow steadily in homogeneous conditions when imposing the shear rate (Coussot, Raynaud *et al.*, 2002).

At this stage, it is tempting to draw an analogy with equilibrium phase transitions, where such a discontinuous flow curve would correspond to a first-order solid-to-fluid transition while a continuous flow curve would correspond to a second-order solid-to-fluid transition. However, in practice it may be difficult to discriminate between these two categories on the sole basis of the steady-state flow curve (Dennin, 2008). This is because the flow may become unstable and heterogeneous at low imposed shear rates ($\dot{\gamma} < \dot{\gamma}_c$), leading to an *apparent* flow curve that does not necessarily reflect the unstable constitutive behavior of the material.

2. Existence of a “viscosity bifurcation”

A practical consequence of the existence of a critical shear rate $\dot{\gamma}_c$ is the striking avalanchelike behavior of thixotropic

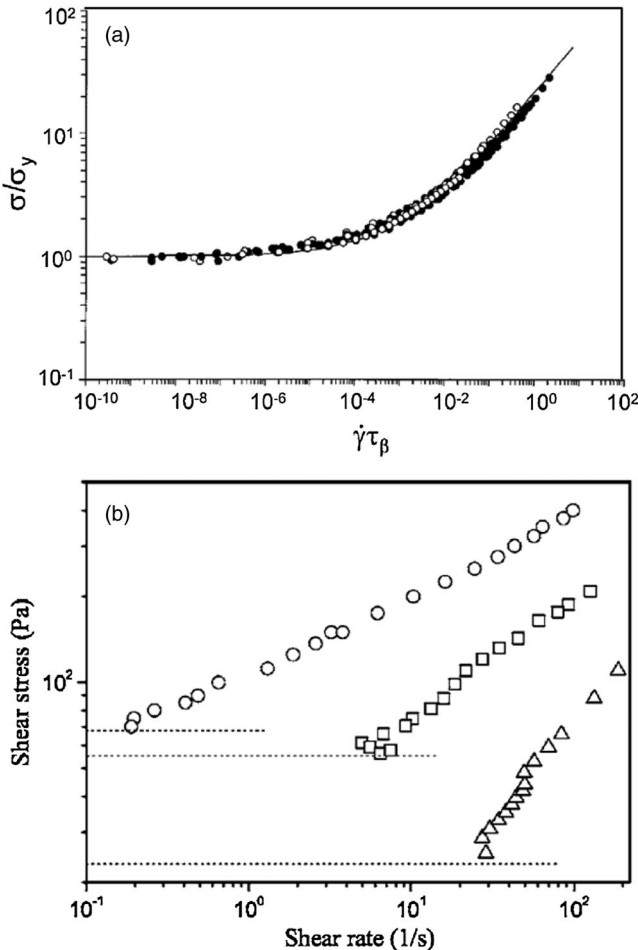


FIG. 20. Representative flow curves for (a) a simple yield stress fluid, here microgels of different cross-link densities and concentrations. The solid line is the equation $\sigma/\sigma_y = 1 + (\dot{\gamma}\tau_\beta/\gamma_0)^{0.45}$, where τ_β is the fluid relaxation time. From Cloitre, Borrega, and Leibler, 2003. (b) Three different thixotropic materials. From top to bottom: a hair gel, a commercial mustard, and a bentonite suspension. Note that each of these materials displays a minimum shear rate $\dot{\gamma}_c$ below which no steady flow is possible. The horizontal dotted lines indicate the yield stresses of the different materials. From Coussot *et al.*, 2006.

yield stress fluids under an applied shear stress in the vicinity of the yield stress (Coussot *et al.*, 2002a, 2002b; Cruz *et al.*, 2002). Within a narrow range of stresses of a few pascals around the yield stress, two very different macroscopic responses can be observed [see Fig. 21]: for $\sigma < \sigma_y$, the material deforms and progressively stops flowing as the viscosity takes up ever-increasing values, whereas for $\sigma > \sigma_y$ the material experiences an abrupt fluidization, characterized by an increase of the shear rate up to a finite steady-state value, which recalls avalanche behavior.

This behavior is characteristic of thixotropic yield stress fluids and has been coined a viscosity bifurcation in the sense that the yield stress separates two regimes characterized by widely different values of the steady-state viscosity. The terminology is, however, somewhat unfortunate since a divergence of the viscosity is also expected for $\sigma \rightarrow \sigma_y^+$ or $\dot{\gamma} \rightarrow 0$ in simple yield stress fluids. For these materials, the

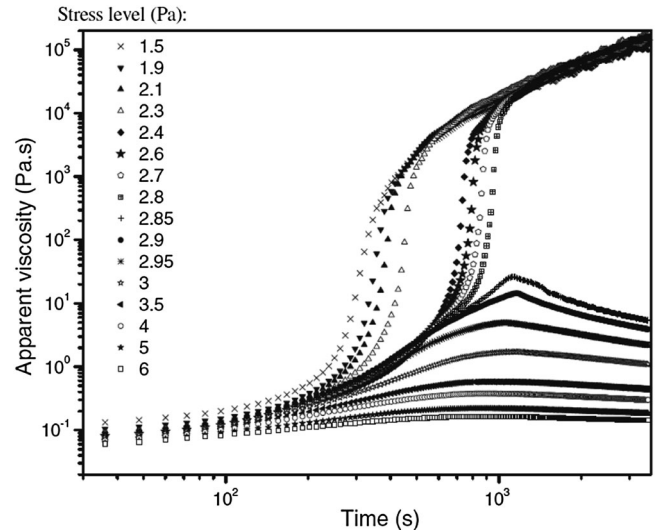


FIG. 21. Temporal evolution of the apparent viscosity $\eta = \sigma/\dot{\gamma}$ of a drilling mud for various applied shear stresses below and above the yield stress $\sigma_y \approx 2.82$ Pa. The drastic change of behavior within a range of less than 0.1 Pa around the yield stress illustrates the viscosity bifurcation scenario. From Ragouilliaux *et al.*, 2006.

divergence is continuous and any (arbitrarily large) value of the final viscosity can be reached close to the yield stress without any forbidden shear rate range. In the language of bifurcations, yielding in simple yield stress fluids would therefore be analogous to a *supercritical* bifurcation while in thixotropic yield stress fluids it would correspond to a *subcritical* bifurcation.

3. Consequences for local measurements

Within the last two decades, a number of different tools have emerged to measure the local velocity field within standard rheological geometries, including particle tracking, dynamic light scattering, magnetic resonance, and ultrasonic imaging (Salmon, Manneville *et al.*, 2003; Manneville, Béguin, and Colin, 2004; Bonn *et al.*, 2008; Callaghan, 2008; Manneville, 2008; Besseling *et al.*, 2009; Gallot *et al.*, 2013). As reviewed elsewhere (Ovarlez, Cohen-Addad *et al.*, 2013), local velocity profiles under shear allow one to make a clearer distinction between simple and thixotropic yield stress materials. It has been shown that, as expected from their monotonic macroscopic rheology, simple yield stress fluids display homogeneous velocity profiles in steady state, at least in experimental geometries with small enough stress heterogeneity. In this case, the local rheology, given by the local shear stress $\sigma(\mathbf{r})$ as a function of the local shear rate $\dot{\gamma}(\mathbf{r})$ derived from the velocity $v(\mathbf{r})$, perfectly matches the global rheology (Divoux *et al.*, 2012; Ovarlez, Cohen-Addad *et al.*, 2013). In the case of wide-gap geometries, $\sigma(\mathbf{r})$ may vary so much that it falls below the yield stress. This leads to a heterogeneous flow where a solid region characterized by a pluglike flow [where $\sigma(\mathbf{r}) < \sigma_y$] coexists with a flowing region [where $\sigma(\mathbf{r}) > \sigma_y$]. Similar pluglike flow is observed in the case of channel flows of simple yield stress fluids, where the local stress necessarily vanishes in the center of the

channel (Pérez-González *et al.*, 2012; Poumaere *et al.*, 2014). Such a shear localization due to large stress heterogeneity does not contradict the continuous solid-fluid transition of simple yield stress fluids. It is now clearly distinguished from the intrinsic shear localization, referred to as “shear banding,” observed in thixotropic yield stress fluids and discussed next (Ovarlez *et al.*, 2009; Ovarlez, Cohen-Addad *et al.*, 2013). Finally, even more subtle effects were recently discovered in simple yield stress fluids that are made to flow in confined geometries or during transient regimes close to the yield stress. These effects are reviewed in Sec. IV.C.

Contrary to simple yield stress fluids, thixotropic yield stress materials have been shown either to flow homogeneously (for $\dot{\gamma} > \dot{\gamma}_c$) or to display heterogeneous velocity profiles (for $\dot{\gamma} < \dot{\gamma}_c$). In the latter case, a solidlike region coexists with a liquidlike band sheared at $\dot{\gamma} = \dot{\gamma}_c$ (Møller *et al.*, 2008) and the relative extent of both bands ensures that the average shear rate coincides with the macroscopic applied shear rate (Cousset, Raynaud *et al.*, 2002; Ovarlez *et al.*, 2009). As seen in Fig. 22(a) for the case of a colloidal gel, the amount of fluidlike material increases proportionally to the global applied shear rate for $0 < \dot{\gamma} < \dot{\gamma}_c$. This points to an equivalent of a “lever rule” for solid-fluid coexistence and once again emphasizes the analogy between yielding in thixotropic materials and a first-order phase transition. It corresponds to true shear localization, i.e., to shear banding, in the sense that it

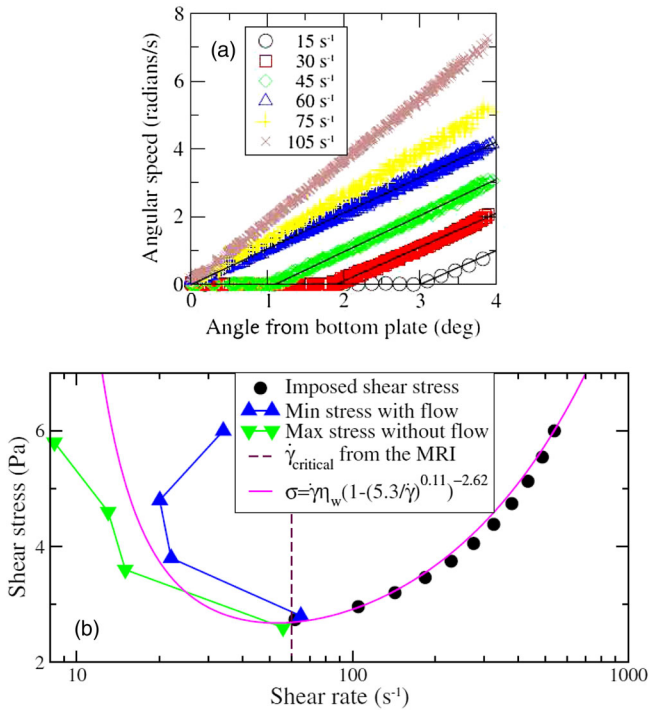


FIG. 22. Example of shear-banded flows. (a) Velocity profiles in a 4° cone-and-plate geometry of a colloidal silica suspension (Ludox TM-40) for shear rates ranging from 15 to 105 s⁻¹. (b) Steady-state flow curve determined by two different types of measurements. The branch at larger shear rates is obtained under constant external stress. The branches at lower shear rates are determined by estimating the minimum (respectively, maximum) shear stress with (respectively, without) flow. From Møller *et al.*, 2008.

TABLE I. Different types of shear localization in simple and thixotropic yield stress fluids (YSF).

Origin of shear localization	Simple YSF	Thixotropic YSF
From critical shear rate	Not possible	Possible
From stress heterogeneity	Possible	Possible
Wall slip	Possible	Possible

is observed independently of any geometry-dependent stress heterogeneity. Table I summarizes the distinction between shear banding (due to the existence of a critical shear rate) and shear localization (due to stress heterogeneity). It also recalls that in both cases, apparent slippage at the walls, which can be seen as an extreme kind of shear localization, may come into play as discussed in Sec. III.C.

B. Causes of steady-state shear banding

1. Competition between aging and shear rejuvenation

The existence of a critical shear rate $\dot{\gamma}_c$ in thixotropic yield stress materials has been explained in terms of an underlying decreasing branch of the flow curve at low shear rates (Olmsted, 2008; Divoux *et al.*, 2016), as discussed for viscoelastic “wormlike micelle” surfactant solutions (Spenley, Cates, and McLeish, 1993). In such a scenario, the constitutive relation of the material is actually a decreasing function for shear rates ranging from 0 to $\dot{\gamma}_c$. In this shear rate range, the flow is mechanically unstable, which leads to some sort of phase separation into an arrested region that coexists with a flowing band sheared at $\dot{\gamma}_c$ (Picard *et al.*, 2002). This coexistence is expected to correspond to a flat portion of the steady-state flow curve, analogous to the Maxwell plateau in first-order phase transitions, where the size of the flowing band should follow the lever rule mentioned in Sec. IV.A.3. Transient measurements in the unstable shear rate range can be used to unveil the underlying decreasing flow curve [see Fig. 22(b)].

The unstable part of the flow curve is most often interpreted and modeled as the result of competition between spontaneous aging and shear-induced rejuvenation, although only indirect evidence for such a competition has been reported up to now. Aging processes arise from particle aggregation in systems with microscopic attractive interactions, e.g., clays and attractive colloidal gels, or from the thermally activated reorganization toward minimal energy in dense systems, such as dense emulsions or microgels (Sollich *et al.*, 1997; Cloitre, Borrega, and Leibler, 2000; Viasnoff and Lequeux, 2002; Cousset, 2007). Such physical aging may occur over a wide range of time scales and is different in nature from the chemical aging due to slow chemical reactions, such as the release of Na⁺ ions in laponite clays, which cannot be reversed by shear (Shahin and Joshi, 2010; Shahin and Joshi, 2012). While attractive interactions have been shown to be a sufficient ingredient to induce shear banding (Bécu, Manneville, and Colin, 2006; Ragouilliaux *et al.*, 2007; Fall, Paredes, and Bonn, 2010; Paredes, Shahidzadeh-Bonn, and Bonn, 2011), the minimal amount of attraction necessary to permanently form banded profiles is still an open issue. A better understanding of the role of microscopic interactions

should be gained from experiments where the attraction between microscopic constituents is continuously tuned, e.g., in a model system of colloids or deformable droplets (Saunders and Vincent, 1999).

The simplest phenomenological model based on the idea of a competition between aging and shear rejuvenation is the toy model known in the literature as the “ λ model” (Cousset *et al.*, 2002a; Mujumdar, Beris, and Metzner, 2002). The basic assumptions of this model are (i) there exists a structural parameter λ that describes the local degree of interconnection of the microstructure, (ii) the viscosity η increases with increasing λ , and (iii) for an aging system at low (or zero) shear rate $\dot{\gamma}$ increases, while at sufficiently high shear rates the flow breaks down the structure so that λ decreases to a low steady-state value. For certain parameter values, this model is easily shown to predict flow curves with a minimum at a critical shear rate $\dot{\gamma}_c$, therefore qualitatively reproducing the case of a thixotropic yield stress material showing a viscosity bifurcation and steady-state shear banding. More refined versions of the λ model have been proposed in the literature, e.g., for fractal colloidal gels (Møller *et al.*, 2008) and elastoviscoplastic structured fluids (de Souza Mendes, 2011; de Souza Mendes and Thompson, 2013), leading to similar results. The kinematic hardening model used by Dimitriou, Ewoldt, and McKinley (2013) incorporates a back stress that evolves dynamically and affects the mechanics in the neighborhood of yielding. This back stress can be viewed as a λ parameter in simple shear flow and causes the location of the yield surface to adjust, depending on the deformation state.

In order to achieve a more realistic picture of the effects of aging that accounts for the viscoelasticity of the material, a simplified mean-field argument was proposed based on two time scales (Cousset and Ovarlez, 2010): a macroscopic relaxation time τ_{rel} , equivalent to the viscoelastic time, which can easily be measured through step-strain or stress relaxation experiments, and a microscopic restructuring time τ_{age} associated with the fluid spontaneous aging. This model produces a simple expression for the flow curve:

$$\frac{\sigma}{G\dot{\gamma}_c} = \tau_{\text{rel}} \frac{\dot{\gamma}}{\dot{\gamma}_c} + \frac{1}{1 + \tau_{\text{age}}\dot{\gamma}/\dot{\gamma}_c}, \quad (9)$$

where G is the characteristic elastic modulus of elements that break above a critical strain $\dot{\gamma}_c$. Interestingly, the predicted flow curve has a minimum at a critical shear rate for $\tau_{\text{rel}} < \tau_{\text{age}}$, i.e., for a sufficiently long restructuring time, while simple yield stress behavior sets in when restructuring becomes faster than viscoelastic relaxation, i.e., for $\tau_{\text{age}} < \tau_{\text{rel}}$ (see Fig. 23). In this model, one can thus continuously go from a monotonic flow curve to a nonmonotonic flow curve, i.e., from a simple to a thixotropic yield stress fluid, by increasing the duration of the restructuring time.

The idea of a competition between a restructuring time scale and shear flow was implemented in the elastoplastic coarse-grained modeling initiated by Picard *et al.* (2004). The influence of the time scale competition between structural rearrangement and elastic recovery was explored in full detail by Martens, Bocquet, and Barrat (2012); see also Benzi *et al.* (2016). This study not only confirms the nonmonotonic

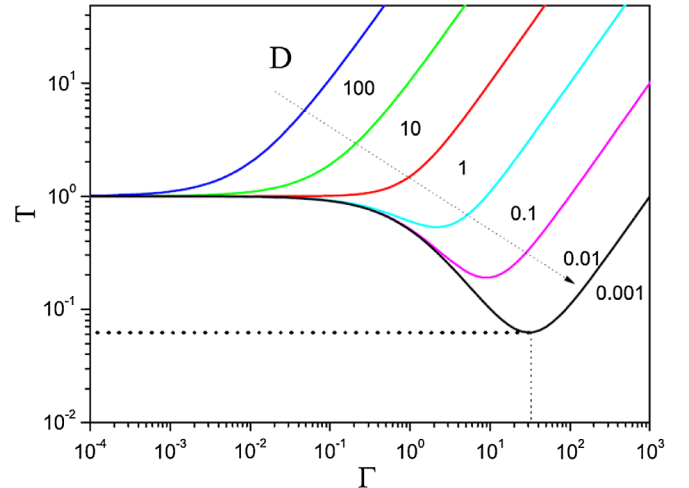


FIG. 23. Dimensionless flow curves (stress T vs shear rate Γ) for different values of the ratio D of the fluid relaxation time τ_{rel} over the restructuration time τ_{age} , i.e., the time for a microscopic link to reform after being broken. From Cousset and Ovarlez, 2010.

character of the global flow curves for a certain set of control parameters, but also explores the spatial consequences of the nonmonotonicity in a realistic geometry. In particular, the emergence of a “phase separation” between flowing and nonflowing regions in the system, i.e., permanent shear bands, was clearly observed, thus putting the ideas of Cousset and Ovarlez (2010) on firmer grounds. Similar ideas involving a self-consistent dynamics following structural reorganization have been explored in various modeling contexts; see, for instance, Jagla (2007), Fielding, Cates, and Sollich (2009), Cheddadi, Saramito, and Graner (2012), Maki and Renardy (2012), and Joshi (2015).

Although these models all give a consistent picture of a time scale competition leading to nonmonotonic flow curves in some well-chosen regimes, and thus may give rise to shear bands and viscosity bifurcation, very little progress has been made toward understanding at a more microscopic level both the physical origin of these time scales and how to control their evolution by tuning, for instance, the interaction between colloidal particles. A notable exception is recent work exploring the athermal rheology of sticky particles in the vicinity of the jamming transition (Irani, Chaudhuri, and Heussinger, 2014). Here it was shown that stickiness may promote a yield stress even below jamming, which is however easily disrupted by a slow shear flow. At larger shear rate, particles are pushed against each other, and therefore repulsive forces should produce an increase of the shear stress. For a narrow range of control parameters, this competition produces a nonmonotonic flow curve, very much in the spirit of Fig. 23.

2. Static versus dynamic yielding

Whereas nonmonotonic flow curves necessarily give rise to shear bands (Olmsted, 2008), as observed in a variety of complex fluids, a simpler scenario can also hold in the specific context of yield stress materials. Because the shear bands observed in a yield stress material delimit a flowing phase from an arrested phase (and not two different fluids as in more

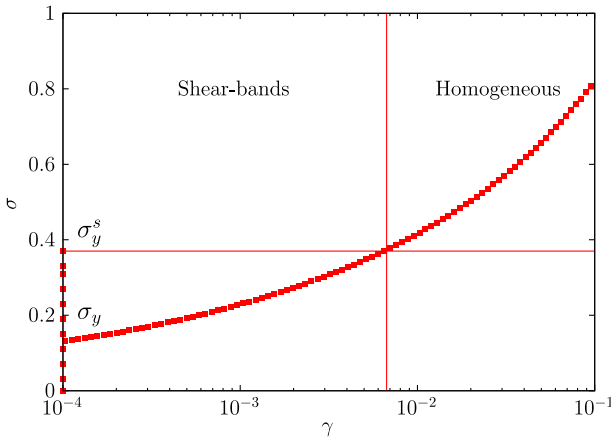


FIG. 24. Scenario for shear banding in yield stress materials. A monotonic flow curve with a finite dynamic yield stress σ_y coexists with a static branch at $\dot{\gamma} = 0$ and $\sigma < \sigma_y^s$, where σ_y^s is the static yield stress. The shear rate is bi-valued for a range of shear stresses $\sigma \in [\sigma_y, \sigma_y^s]$, which may lead to shear bands. Adapted from Berthier, 2003.

traditional complex fluids), shear banding can be explained by a simple picture where a monotonic global flow curve of the Herschel-Bulkley type with a finite dynamic yield stress σ_y [as in Eq. (3)] coexists with a static branch at $\dot{\gamma} = 0$ existing for $\sigma < \sigma_y^s$, where σ_y^s is a static yield stress. In that case, a strict inequality $\sigma_y^s > \sigma_y$ directly ensures the existence of a finite stress regime $\sigma \in [\sigma_y, \sigma_y^s]$, where the shear rate is bi-valued and can be either zero or finite; see Fig. 24.

This scenario was explored theoretically by Berthier (2003), where the two phases were shown to correspond to two different families of dynamical solutions under the same external stress values in the context of a specific driven glassy model. These solutions, respectively, correspond to a fluid and an arrested phase. A similar explanation was shown to account for the presence of permanent (or at least very long-lived) shear bands in the computer simulation of a glass-forming liquid in the glassy region below the glass transition temperature (Varnik *et al.*, 2003). There, again, a clear separation was observed between the dynamic extrapolation of the homogeneous flow curve and the direct determination of the static yield stress value. Detailed numerical studies have shown, however, that carefully measuring these two yield stress values is not an easy task (Xu and O'Hern, 2006; Peyneau and Roux, 2008).

The validity of this scenario was demonstrated in a numerical study of concentrated assemblies of soft particles where the degree of particle adhesion was tuned continuously (Chaudhuri, Berthier, and Bocquet, 2012), in analogy with the experimental investigations described previously (Béguin, Manneville, and Colin, 2006; Ragouilliaux *et al.*, 2006; Ovarlez *et al.*, 2008; Fall, Paredes, and Bonn, 2010). In this numerical study, the emergence of flow inhomogeneity was again directly connected to a discontinuity of the flow curve at $\dot{\gamma} = 0$, which was moreover observed to be strongly enhanced by adhesive forces, thus establishing a direct link between increasing the adhesion and promoting shear-banding behavior (Chaudhuri, Berthier, and Bocquet, 2012).

Although the flow curves depicted in Figs. 23 and 24 appear qualitatively distinct at first sight, they may become more similar in the case where the minimum of the flow curves in Fig. 23 occurs at the lower end of the accessible experimental range, in which case the remaining part of the flow curve at small $\dot{\gamma}$ is “compressed” along the $\dot{\gamma} = 0$ axis, very much as in Fig. 24. In addition, in both cases a shear band may appear where a slow (or arrested) flowing phase and a fast flowing phase coexist, and it may be experimentally challenging to distinguish between both scenarios unless non-banded, steady-state flows can also be characterized at very low shear rates. The distinction could be easier in computer simulations, where it is possible to impose a global shear rate and follow either set of flow curves shown in Figs. 23 and 24 down to arbitrary low shear rates.

3. Flow-concentration coupling

In the case of suspensions of dense and rigid noncolloidal particles, shear banding may also result from volume fraction heterogeneities. As particles are denser than the surrounding fluid, there is a competition between sedimentation and shear-induced resuspension (Ovarlez, Bertrand, and Rodts, 2006; Fall *et al.*, 2009). If shear-induced resuspension is not efficient enough, contacts between particles trigger the formation of a percolated network and of heterogeneous volume fraction profiles, leading to shear banding. Interestingly, such a flow-concentration coupling argument has also been invoked to account for shear banding in colloidal glasses (Besseling *et al.*, 2010). The underlying idea is that, despite a homogeneous stress field, minute local variations of the volume fraction ϕ may result in significant changes in the yield stress value, which for a homogeneous system strongly depends on the overall volume fraction ϕ . At low applied shear rates in sufficiently dense packings, the flow may become unstable (Schmitt, Marques, and Lequeux, 1995): fluctuations trigger the jamming of a region of the material, which further turns into steady-state shear banding. This type of localization could therefore be interpreted as a precursor to shear-induced thickening (Fall *et al.*, 2010), although more experimental work is needed to draw an overall conclusion.

C. Emerging topics: Confinement and transient regimes

In the following we focus on two questions that have recently attracted growing interest as examples of current challenges toward understanding the dynamics of yield stress fluids.

1. Yield stress materials in confined geometries

Flow properties of yield stress fluids have been discussed up to now in the context of “large” geometries, i.e., with gaps much larger than the granularity of the fluid microstructure, typically by at least 2 orders of magnitude. In this limit, the macroscopic behavior does not depend on the gap size. However, when the gap size becomes comparable to the mesoscopic scale characteristic of the fluid microstructure, i.e., in a *confined* geometry, rheological data have been reported to depend on the gap width (Clasen and McKinley, 2004; Davies and Stokes, 2008; Yan *et al.*,

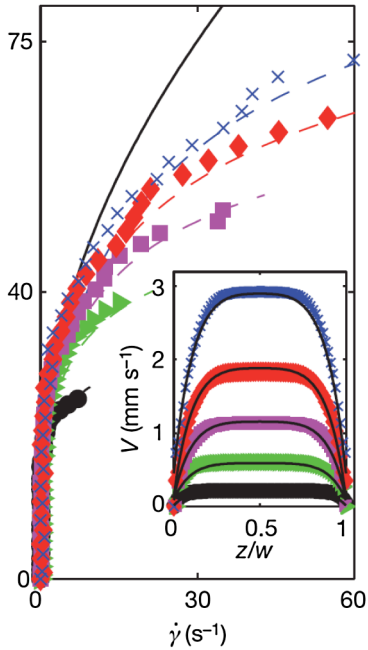


FIG. 25. Global and local flow curves (black solid line and symbols, respectively) for a dense emulsion ($\phi = 0.75$ and 20% polydispersity). Global data are obtained in a wide-gap Taylor-Couette cell, while local flow curves are deduced from velocity profiles measured in a $w = 250 \mu\text{m}$ thick microchannel with rough surfaces, for various pressure drops ranging from 300 to 900 mbar (inset). No overlap of the local flow curves is observed. Dashed lines are predictions for the local flow curves at the given pressure drop, as obtained from the nonlocal rheological model [see Eq. (10)] with a flow cooperativity length $\xi = 22.3 \mu\text{m}$. Inset: solid lines are the velocity profiles predicted by the nonlocal rheological model. The y axis for the main figure is the stress in Pa and the figure thus represents the flow curve; the important observation is that the flow curves for different driving pressures no longer overlap due to collective effects. From Goyon *et al.*, 2008.

2010). Accordingly, the local rheology in confined geometries no longer follows the Herschel-Bulkley model valid for large gaps (see Fig. 25), as demonstrated for emulsions (Goyon *et al.*, 2008; Goyon, Colin, and Bocquet, 2010) and Carbopol microgels (Geraud, Bocquet, and Barentin, 2013) in small microchannels.

a. Cooperative effects in simple yield stress fluids

In such a confined geometry, the effect of shear-induced local rearrangement spans over a range larger than the single grain, drop, or bubble scale and can become comparable to the gap size, in which case finite-size effects influence the measured viscosity. The idea that the flow occurs through successive plastic events over a certain “cooperativity” length ξ has led to the development of so-called nonlocal models (Bocquet, Colin, and Ajdari, 2009). The simplest such model is a spatial version of the “fluidity model” (Derec *et al.*, 2003), where the number of plastic events per unit time (or fluidity) taken as $f = \dot{\gamma}/\sigma$ is influenced both by the local contribution of the flow and by plastic events taking place at distances smaller

than ξ . In the simplest case of a one-dimensional planar shear, this leads to the following simple differential equation for f :

$$\xi^2 \frac{\partial^2 f}{\partial x^2} + (f_{\text{bulk}} - f) = 0, \quad (10)$$

where x is the direction of the stress gradient and f_{bulk} denotes the “bulk” fluidity value, i.e., the fluidity expected in a large-gap geometry in the absence of nonlocal effects. Here “nonlocality” stems from the double spatial derivative in $\partial^2 f / \partial x^2$ that involves the local fluidity over a typical size ξ . The solution to Eq. (10) successfully accounts for experimental flow profiles (see the inset of Fig. 25) and for dynamical arrest in confined geometries (Chaudhuri *et al.*, 2012).

Recently the local fluidity was related to the local shear rate fluctuations $\delta\dot{\gamma}(x)$ (Jop *et al.*, 2012; Benzi *et al.*, 2014). In particular, the study by Jop *et al.* suggests that the nonlocal rheology originates in the mechanical noise induced by the flow. Such a modification of the rheology due to confinement is not specific to yield stress materials since it also affects for instance the flow of surfactant wormlike micelles (Masselon, Salmon, and Colin, 2008). In fact, the leftmost term in Eq. (10) was first introduced to model shear banding in these systems (Dhont, 1999; Yuan, 1999). More details on current issues raised by confinement of yield stress fluids are summarized in the review by Mansard and Colin (2012). Here we emphasize only that the question of whether cooperative effects may be at play during start-up flows should also be addressed. Indeed, in a partially fluidized material undergoing a transient regime, the fluid at rest is confined between the wall and the flowing band. This point, which raises the question of whether the (possibly slow) dynamics of cooperative effects might be related to the diverging duration of transient regimes, is discussed in the next section.

b. Shear-induced structuration of attractive yield stress fluids

Another striking effect of confinement on yield stress fluids is the spectacular shear-induced structuration observed in the case of attractive particle systems at moderate shear rates, typically $0.1 < \dot{\gamma} < 10 \text{ s}^{-1}$. Examples include colloid-polymer mixtures (DeGroot *et al.*, 1994), flocculated magnetic suspensions (Navarrete, Scriven, and Macosko, 1996), carbon nanotubes (Lin-Gibson *et al.*, 2004), attractive emulsions (Montesi, Peña, and Pasquali, 2004), carbon black and alumina dispersions (Osugi, Kim, and Weitz, 2008; Negi and Osugi, 2009; Grenard, Taberlet, and Manneville, 2011), and micro-fibrillated cellulose (Karppinen *et al.*, 2012) (see Fig. 26). In all these thixotropic yield stress fluids, the microstructure fully rearranges into a striped pattern of log-rolling flocs aligned along the vorticity direction, as demonstrated indirectly either through light scattering measurements (DeGroot *et al.*, 1994) or through scanning electron microscopy (Navarrete, Scriven, and Macosko, 1996) and optical microscopy (Lin-Gibson *et al.*, 2004; Montesi, Peña, and Pasquali, 2004; Osugi, Kim, and Weitz, 2008; Negi and Osugi, 2009; Grenard, Taberlet, and Manneville, 2011; Karppinen *et al.*, 2012).

In some of these attractive systems, shear-induced structuration has been linked to the emergence of negative normal stresses (Lin-Gibson *et al.*, 2004; Montesi, Peña, and Pasquali,

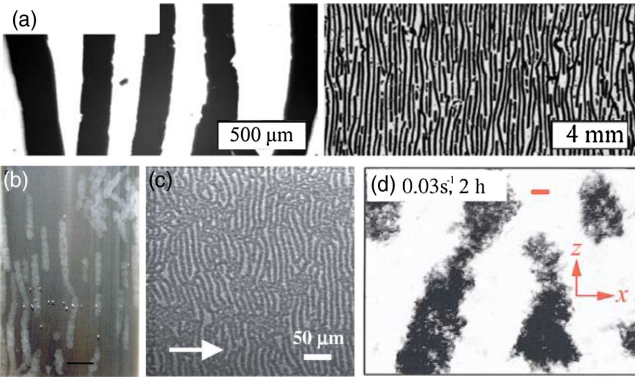


FIG. 26. Shear-induced patterns observed in various yield stress fluids under shear in confined geometries. (a) Carbon black gel under simple shear with a gap thickness of $173\text{ }\mu\text{m}$ as seen with optical microscopy with large and low magnifications (left and right, respectively). From Grenard, Taberlet, and Manneville, 2011. (b) Suspension of microfibrillated cellulose at 0.1% wt after shearing 10 min at 0.5 s^{-1} in a Taylor-Couette cell. From Karppinen *et al.*, 2012. (c) Emulsions under simple shear for a gap thickness of $12\text{ }\mu\text{m}$. The arrow indicates the direction of shear. From Montesi, Peña, and Pasquali, 2004. (d) Optical micrograph of a quiescent semidilute non-Brownian colloidal nanotube suspension at 0.5% wt. The gray (red) scale bar is $10\text{ }\mu\text{m}$ and the gap thickness is $50\text{ }\mu\text{m}$. From Lin-Gibson *et al.*, 2004.

2004; Negi and Osuji, 2009) and it was proposed to interpret vorticity alignment as the consequence of an elastic instability that would occur locally within individual flocs (Lin-Gibson *et al.*, 2004; Montesi, Peña, and Pasquali, 2004). However, clear experimental evidence for such an interpretation and a detailed theory to prove the link between an elastic instability and shear-induced structuration are still lacking.

Moreover, shear-induced structuration occurs only within a certain range of shear rates. On the one hand, for very low shear, wall slip becomes predominant and generally prevents the system from being sheared in the bulk so that it remains in a homogeneous solidlike state. On the other hand, structuration does not occur above some critical shear rate, most probably due to the predominance of viscous forces and particle resuspension by shear. Coming up with a theory to provide a complete physical mechanism for the present shear-induced pattern formation and to predict both their characteristics and the shear rate limits where they appear is an important future challenge. Indeed, the striking effect of confinement not only affects the interpretation of rheological measurements but may also be of prime importance in applications involving confined flows of attractive particle systems. Finally, it is still unclear whether the structural instability that leads to pattern formation in attractive, thixotropic yield stress materials is related in any way to the mechanical noise which triggers flow cooperativity in simple yield stress fluids.

2. Origin and scaling of the yielding time scales

So far, emphasis has been put on the steady state achieved by yield stress materials under a given shear rate or shear stress. However, it is quite obvious that such a steady state is

not reached instantaneously and that transient regimes, e.g., from solidlike behavior at rest to liquidlike behavior above yielding, convey tremendous physical information on the yielding process.

In particular, it can be expected that upon approaching the yield stress the time needed to reach a flowing steady state can grow longer and longer, possibly pointing to a divergence of some characteristic time scale. If this time scale can be reliably estimated as a function of the various control parameters (applied stress or shear rate, packing fraction, temperature), then the question is whether physically relevant information can be inferred on the yielding transition from such scalings. The aim of this section is to review recent work focusing on the time scales associated with yielding, open questions, and opportunities for the future.

a. Power-law scalings of the fluidization time and transient shear banding

It has been reported that transient regimes may become surprisingly long lived in the vicinity of the yield stress. As mentioned, it is not surprising that the dynamics becomes increasingly slow upon approaching the yield stress, which has been reported often (Aral and Kalyon, 1994; Gopalakrishnan and Zukoski, 2007; Caton and Baravian, 2008; Rogers, Vlassopoulos, and Callaghan, 2008). More quantitative and local insights have been gained from recent velocimetry experiments during shear start-up and creep experiments of simple yield stress fluids, namely, Carbopol microgels (Divoux *et al.*, 2010, 2012; Divoux, Barentin, and Manneville, 2011b) and, to a lesser extent, emulsions (Bégu *et al.*, 2005; Perge, 2014). These experiments revealed that the expected homogeneous velocity profiles are reached after a transient regime that involves shear-banded velocity profiles (see Fig. 27). In Carbopol microgels, the fluidization time τ_f ,

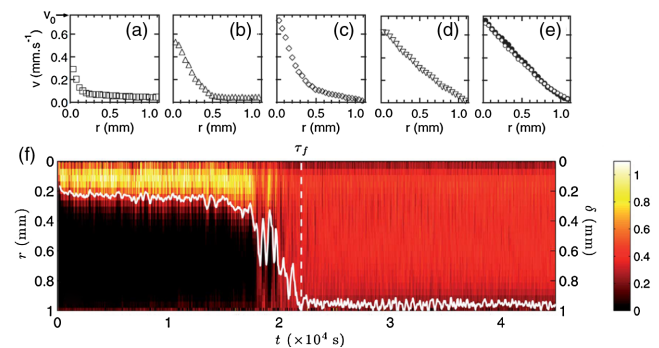


FIG. 27. Transient shear banding in a Carbopol microgel in the Taylor-Couette geometry. (a)–(e) Velocity profiles $v(r)$, where r is the distance to the rotor, in a rough geometry at different times during the stress relaxation for an applied shear rate of 0.7 s^{-1} . From Divoux *et al.*, 2010. (f) Spatiotemporal diagram of the local shear rate $\dot{\gamma}(r, t)$ in a smooth geometry for an applied shear rate of 0.5 s^{-1} . The white curve traces the position $\delta(t)$ of the interface between the fluidized band and the solidlike region. The vertical dashed line indicates the fluidization time τ_f , i.e., the time at which the shear rate field becomes homogeneous. From Divoux *et al.*, 2012.

i.e., the duration of the transient shear-banding regime, was shown to follow power-law scalings $\tau_f \sim A/\dot{\gamma}^\alpha$ and $\tau_f \sim B/(\sigma - \sigma_y)^\beta$ with $\alpha \approx 2-3$ and $\beta \approx 4-6$ under imposed shear rate and shear stress, respectively (Divoux *et al.*, 2010, 2012; Divoux, Barentin, and Manneville, 2011a). In all cases, the final homogeneous flow is consistent with the global steady-state rheology indicating simple yield stress behavior [see Fig. 27(e)]. Interestingly, assuming that the fluidization times under imposed shear rate and shear stress are simply proportional, the above power-law scalings naturally lead to a constitutive equation $\sigma(\dot{\gamma})$ that coincides with the Herschel-Bulkley equation [Eq. (3)] in which the phenomenological exponent n is given by $n = \alpha/\beta \approx 1/2$ (Divoux, Barentin, and Manneville, 2011a). Therefore, the exponents governing the transient regimes possess a striking link with the exponent that characterizes the steady-state behavior. Such a link has been interpreted in terms of a critical-like phenomenon (Divoux *et al.*, 2012; Chaudhuri and Horbach, 2013).

It is important to clearly distinguish the transient shear-banding phenomenology from the time-dependent behavior of thixotropic materials. Here, rather than a competition between aging and shear rejuvenation, the transition from a solidlike to a liquidlike state seems to involve plastic events and damage accumulation in a way that resembles hard solids. Indeed, the flowing band can be observed to slowly “erode” the material at rest before the whole material experiences a rather sudden fluidization. This induction phase suggests that erosion by the fluidized band somehow fragilizes the bulk-arrested microgel, bringing it to a critical state before complete, sudden fluidization occurs. Such a critical state could be analogous to the one reached by a colloidal gel experiencing “delayed sedimentation” right before its collapse (Buscall *et al.*, 2009; Teece, Faers, and Bartlett, 2011; Barlett, Teece, and Faers, 2012). However, more experiments that provide access to the structure of the band at rest are needed to confirm such a picture. Moreover, a systematic comparison with recent molecular dynamic simulations of disordered systems could help to bridge the gap between yield stress fluids and amorphous solids (Fusco, Albaret, and Tanguy, 2014).

From a theoretical point of view, a general criterion for the formation of transient shear bands has been proposed (Moorcroft, Cates, and Fielding, 2011; Moorcroft and Fielding, 2013), providing a connection with either the stress overshoot under an imposed shear rate or the delayed yielding under creep in yield stress fluids or viscoelastic fluids. In this approach the power-law scaling for the fluidization time under creep is recovered, but with a smaller exponent $\beta \approx 1$ (Moorcroft and Fielding, 2013). Another promising approach consists of a structural model of colloidal aggregates that incorporates viscoelasticity (Illa *et al.*, 2013; Lehtinen *et al.*, 2013; Mohtaschemi *et al.*, 2014). Such a phenomenological model recovers power-law scalings but predicts only trivial exponents $\alpha = \beta = 1$ and thus fails to capture the link between both transients and the steady-state rheology observed in microgels. Finally, theories at a more microscopic level, such as the STZ theory, suggest that the transient shear banding and sudden fluidization is primarily a result of microstructural disordering originating from structural heterogeneities (Hinkle and Falk, 2016). The latter results

remain to be confirmed and extended by supplemental measurements on purely repulsive systems through simpler numerical approaches such as molecular dynamics simulations.

b. Exponential scalings: Activated processes and brittlelike failure

Whereas rather few papers have focused on transient fluidization under an applied shear rate, creep experiments have revealed long-lived transients in numerous yield stress fluids, including attractive gels such as carbon black gels (Gibaud, Frelat, and Manneville, 2010; Grenard *et al.*, 2014), coated silica particles (Gopalakrishnan and Zukoski, 2007; Sprakel *et al.*, 2011), and colloidal glasses (Siebenbürger, Ballauf, and Voigtmann, 2012). The time at which the strain rate increases by several orders of magnitude defines a fluidization time τ_f , which coincides with the establishment of homogeneous velocity profiles (Gibaud, Frelat, and Manneville, 2010; Grenard *et al.*, 2014). Interestingly, in attractive colloidal systems, τ_f generally decreases exponentially with the applied shear stress (Gopalakrishnan and Zukoski, 2007; Gibaud, Frelat, and Manneville, 2010; Sprakel *et al.*, 2011; Grenard *et al.*, 2014). Such a scaling $\tau_f \sim \exp(-\sigma/\sigma_0)$ involves a characteristic stress σ_0 , which has been interpreted and modeled in the framework of bond breaking through thermally activated processes (Gopalakrishnan and Zukoski, 2007; Lindström *et al.*, 2012).

Alternative exponential scalings, such as the Griffith-like scalings $\tau_f \sim \exp(\sigma_0/\sigma)^p$ with $p = 1, 2$, or 4 (Griffith, 1921; Pomeau, 1992; Lawn, 1993; Vanel, Ciliberto, and Cortet, 2009), have been proposed in the context of yield stress fluids (Caton and Baravian, 2008) and transient networks (Tabuteau *et al.*, 2009; Mora, 2011). They hint at fracturelike dynamics, although it may be difficult to discriminate between various exponential—or even power-law—scalings due to the limited range of experimentally accessible shear stresses (Gibaud *et al.*, 2016). This raises the question of the “brittleness” of yield stress fluids: while the physics of yielding in concentrated, jammed assemblies of soft particles such as microgels or emulsions appears to rely on (microscale) plasticity associated with (macroscale) shear banding, early studies based on direct visualization of the sample edges have shown some colloidal systems, such as Laponite suspensions (Magnin and Piau, 1990; Pignon, Magnin, and Piau, 1996) and concentrated suspensions (Aral and Kalyon, 1994; Persello *et al.*, 1994), prone to fracturelike behavior. Revisiting these pioneering works with modern temporally and spatially resolved techniques could classify such strain localization in terms of fracture, wall slip, or shear banding and sort out the possible effects of the experimental geometry on the flow dynamics.

c. Dynamics induced by wall slip in transient and steady-state flows

In Sec. III.C we considered wall slip only through its effect on steady-state flow curves and velocity profiles. However, it has long been known, most prominently in the context of polymers, that wall slip often comes with instabilities and complex time dependences (Graham, 1995; Denn, 2001, 2008). In light of the previous discussion on fluidization time scales, it also seems natural to ask whether slippage at the walls shows interesting variations, both during transient

regimes and at steady state. Surprisingly only a handful of papers have dealt with the dynamics of wall slip in yield stress fluids. Various start-up experiments in smooth geometries, e.g., on emulsions (Béchu *et al.*, 2005), Carbopol microgels (Divoux *et al.*, 2010), and laponite clay suspensions (Gibaud *et al.*, 2009), have reported slip velocities that are strongly correlated to the fluidization dynamics and to the temporal evolution of the shear stress as well as stick-slip oscillations in the steady state (Pignon, Magnin, and Piau, 1996; Ianni *et al.*, 2008; Divoux, Barentin, and Manneville, 2011a). Recent experiments of unsteady pipe flows reported a similar coupling between the solid-to-fluid transition and wall slip, including strongly fluctuating behaviors (Poumaere *et al.*, 2014).

Importantly, the work by Gibaud, Barentin, and Manneville (2008) and Gibaud *et al.* (2009) on laponite suspensions illustrates that boundary conditions not only strongly affect the transient fluidization process but may also lead to totally different steady states—in this case, shear banded flows versus homogeneous flows. Recent numerical modeling suggests that the internal stress distribution prior to shear start-up affects the steady state (Cheddadi, Saramito, and Graner, 2012). These results reveal the influence of both the boundary conditions and the initial conditions on the steady state reached after yielding, an issue that remains to be fully explored in experiments and models.

D. Open questions

We close this section by listing the open questions that represent the most pressing issues in current research into the dynamics of yield stress materials.

- How does nonlocality due to confinement set in during transient material response?
- Is there any plasticity occurring during initial Andrade-like creep? If so, where is it localized?
- What is the physical mechanism responsible for shear-induced structuration in confined attractive yield stress fluids?
- What are the differences (if any) between the material microstructure in the transient shear band and in the rest of the sample?
- What is the nature of the wall-fluid interactions that drive slip phenomena and how can they affect bulk flow?

V. SUMMARY AND OUTLOOK

We have reviewed recent progress in the understanding of yield stress fluids. Most of the recent experimental advances are due to simultaneous measurements of flow structure and mechanical properties. Techniques that allow one to elucidate the flow structure such as magnetic resonance imaging, ultrasound, or optical microscopy have revealed a richness in the behavior of yield stress materials that was hitherto unsuspected and have allowed for some novel physical insight.

On the theoretical side, much progress has been accomplished to account for the physical origin of solid behavior in

amorphous materials across a broad range of interparticle interactions producing glassy, jammed, and gel behaviors. Simultaneously, computer simulations have demonstrated their efficiency in producing convincing particle-based models of yield stress materials and allowed detailed investigations of the rheological behavior of these systems in various geometries. By construction, such simulations allow for a direct study of both the macroscopic rheological response and the microscopic dynamics. These studies have in turn allowed the development of a new family of coarse-grained elasto-plastic models of yield stress materials, where exploration of larger-scale phenomena (such as shear-banding and time-dependent flows) is better facilitated than through particle-resolved simulations.

For many decades it has been questioned whether the yield stress actually exists. It is now well established that it does, in any case on experimentally relevant time scales. Different techniques of determining the yield stress produce similar values, provided care is taken to account for wall slip, flow heterogeneity, and time dependences. Indeed, one of the novel insights is that not all yield stress materials behave ideally and that a distinction needs to be made between two types of yield stress fluids: simple and thixotropic. Simple yield stress fluids show a flow behavior that is well reproduced by the Herschel-Bulkley law, with no significant time dependence, while thixotropic ones show a pronounced time dependence that arises from aging and shear rejuvenation phenomena. Adequate experimental protocols need to be employed that take into account the time evolution of these materials in order to get reproducible experimental estimates for the yield stress.

Tied in with the discussion of the yield stress is the shear localization that is generically observed in yield stress fluids. For simple yield stress fluids, shear banding is in general due to stress heterogeneity, and if not, it is only transient. For thixotropic materials, the situation is qualitatively different: due to the interplay between aging and shear rejuvenation, there exists a critical shear rate below which no stable homogeneous flow is possible. If a shear rate is then imposed macroscopically within the unstable regime, a shear band is formed in which the material flows at the critical shear rate, and the rest of the material remains motionless.

In addition, wall slip is commonly observed in yield stress materials and needs to be accounted for. In rheological measurements, wall slip is usually detected through variations of the viscosity with the size of the gap of the measurement geometry, which distinguishes it from the two types of shear localization discussed previously. The correction can be done by comparing measurements with different gap sizes and extrapolating to an infinite gap. Besides complicating the interpretation of rheological measurements, wall slip also raises fascinating fundamental questions. Reaching a general understanding of the physics of slippage phenomena in yield stress materials appears to be a challenging task for the future.

Recently, a different type of gap-dependent viscosity was uncovered for very small gaps, e.g., for microchannels with a size close to that of the microstructural elements. Here, gap dependence was attributed to collective effects or “spatial cooperativity” when the range of shear-induced rearrangements spans the whole system. There is still a lot of discussion

on this topic, but it may challenge the simple view of yield stress materials sketched previously.

One last burning issue concerns the full characterization and understanding of the transient flow behavior of both categories of yield stress fluids. The way such materials *start* to flow is indeed of great practical interest. In spite of notable recent progress this question of the yielding dynamics mostly remains to be explored at both microscopic and mesoscopic levels, and both experimentally and theoretically.

What is also crucial, especially for engineering purposes, is to have a predictive constitutive equation that allows for a general description of the flow (or not) of yield stress materials. For polymer systems a large number of such models have been derived from statistical mechanical approaches and are extensively used in practice. For yield stress fluids it is clear that three-dimensional invariant versions of the inelastic Bingham and Herschel-Bulkley models are inadequate, because they cannot reproduce the loss of fore-aft flow symmetry in geometries with fore-aft symmetry. Empirical models based on equations developed for polymeric liquids have shown promise in a few applications to complex flows, especially creeping flow past an isolated sphere, but, unlike the polymer counterparts, these models are not based on microstructural considerations and have not been tested against a full range of rheological measurements. Our limited understanding of plasticity is also a factor in incorporating pre-yield behavior into continuum models. One promising research direction to solve this problem is to borrow statistical mechanical models from the glass transition and soft-matter physics communities such as mode-coupling theory or the soft glassy rheology model. These would automatically also include ageing and shear rejuvenation as these are general features of the glass transition and could thus in the end be the answer to the many remaining questions posed in this review.

ACKNOWLEDGMENTS

We thank numerous colleagues for discussions on these matters over the years. We especially thank Catherine Barentin, Jean-Louis Barrat, Annie Colin, Philippe Coussot, Abdouaye Fall, Marc-Antoine Fardin, Thomas Gibaud, Atsushi Ikeda, Sara Jabbari, Hamid Kellay, Jorge Kurchan, Anke Lindner, Lisa Manning, Jacques Meunier, Jan Mewis, Thijs Michels, Peder Moller, Guillaume Ovarlez, Peter Sollich, and Hajime Tanaka for interactions on this topic. The research leading to these results has received funding from the European Research Council under the European Unions Seventh Framework Programme (Grant No. FP7/2007-2013)/ERC Grant Agreements No. 306845 and No. 258803.

REFERENCES

- Amann, C. P., M. Siebenbürger, M. Ballauff, and M. Fuchs, 2015, *J. Phys. Condens. Matter* **27**, 194121.
- Amann, C., M. Siebenbürger, M. Krüger, F. Weysser, M. Ballauff, and M. Fuchs, 2013, *J. Rheol.* **57**, 149.
- Andreotti, B., J.-L. Barrat, and C. Heussinger, 2012, *Phys. Rev. Lett.* **109**, 105901.
- Andreotti, B., Y. Forterre, and O. Pouliquen, 2013, *Granular media: between fluid and solid* (Cambridge University Press, Cambridge, England).
- Aral, B., and D. Kalyon, 1994, *J. Rheol.* **38**, 957.
- Astarita, G., 1990, *J. Rheol.* **34**, 275.
- Baldeua, B., and Y. M. Joshi, 2012, *Soft Matter* **8**, 789.
- Ballauff, M., *et al.*, 2013, *Phys. Rev. Lett.* **110**, 215701.
- Ballesta, P., R. Besseling, L. Isa, G. Petekidis, and W. C. K. Poon, 2008, *Phys. Rev. Lett.* **101**, 258301.
- Ballesta, P., N. Koumakis, R. Besseling, W. Poon, and G. Petekidis, 2013, *Soft Matter* **9**, 3237.
- Ballesta, P., G. Petekidis, L. Isa, W. Poon, and R. Besseling, 2012, *J. Rheol.* **56**, 1005.
- Balmforth, N. J., I. A. Frigaard, and G. Ovarlez, 2014, *Annu. Rev. Fluid Mech.* **46**, 121.
- Baret, J., D. Vandembroucq, and S. Roux, 2002, *Phys. Rev. Lett.* **89**, 195506.
- Barlett, P., L. Teece, and M. Faers, 2012, *Phys. Rev. E* **85**, 021404.
- Barnes, H., 2007, *Applied Rheology* **17**, 43110.
- Barnes, H., and Q. Nguyen, 2001, *J. Non-Newtonian Fluid Mech.* **98**, 1.
- Barnes, H. A., 1995, *J. Non-Newtonian Fluid Mech.* **56**, 221.
- Barnes, H. A., 1999, *J. Non-Newtonian Fluid Mech.* **81**, 133.
- Barnes, H. A., J. F. Hutton, and K. Walters, 1989, *An Introduction to Rheology* (Elsevier Amsterdam).
- Barnes, H. A., and K. Walters, 1985, *Rheol. Acta* **24**, 323.
- Barrat, J.-L., and A. Lemaître, 2011, “Heterogeneities in amorphous systems under shear,” in *Dynamical Heterogeneities in Glasses, Colloids, and Granular Media* (Oxford University Press, Oxford), pp. 264–297.
- Basu, A., Y. Xu, T. Still, P. E. Arratia, Z. Zhang, K. N. Nordstrom, J. M. Rieser, J. P. Gollub, D. J. Durian, and A. G. Yodh, 2014, *Soft Matter* **10**, 3027.
- Batista, A., A. Raymundo, I. Sousa, J. Empis, and J. Franco, 2006, *Food Biophys.* **1**, 216.
- Bauer, T., J. Oberdisse, and L. Ramos, 2006, *Phys. Rev. Lett.* **97**, 258303.
- Bécu, L., P. Grondin, S. Manneville, and A. Colin, 2005, *Colloids Surf., A* **263**, 146.
- Bécu, L., S. Manneville, and A. Colin, 2006, *Phys. Rev. Lett.* **96**, 138302.
- Bengtzelius, U., W. Götze, and A. Sjolander, 1984, *J. Phys. C* **17**, 5915.
- Benzi, R., M. Sbragaglia, M. Bernaschi, S. Succi, and F. Toschi, 2014 *Soft Matter* **10**, 4615.
- Benzi, R., M. Sbragaglia, M. Bernaschi, S. Succi, and F. Toschi, 2016 *Soft Matter* **12**, 514.
- Bernal, J. D., and J. Mason, 1960, *Nature (London)* **188**, 910.
- Berthier, L., 2003, *J. Phys. Condens. Matter* **15**, S933.
- Berthier, L., and J.-L. Barrat, 2002, *Phys. Rev. Lett.* **89**, 095702.
- Berthier, L., J.-L. Barrat, and J. Kurchan, 2000, *Phys. Rev. E* **61**, 5464.
- Berthier, L., and G. Biroli, 2011 *Rev. Mod. Phys.* **83**, 587.
- Berthier, L., and G. Tarjus, 2009 *Phys. Rev. Lett.* **103**, 170601.
- Berthier, L., and G. Tarjus, 2011 *J. Chem. Phys.* **134**, 214503.
- Berthier, L., and T. A. Witten, 2009, *Phys. Rev. E* **80**, 021502.
- Bertola, V., F. Bertrand, H. Tabuteau, D. Bonn, and P. Coussot, 2003, *J. Rheol.* **47**, 1211.
- Besseling, R., L. I. P. Ballesta, G. Petekidis, M. Cates, and W. Poon, 2010, *Phys. Rev. Lett.* **105**, 268301.
- Besseling, R., L. Isa, E. R. Weeks, and W. C. K. Poon, 2009, *Adv. Colloid Interface Sci.* **146**, 1.

- Bingham, E. C., 1922, *Fluidity and Plasticity* (McGraw-Hill, New York).
- Bocquet, L., A. Colin, and A. Ajdari, 2009, *Phys. Rev. Lett.* **103**, 036001.
- Bonn, D., P. Coussot, H. T. Huynh, F. Bertrand, and G. Debrégeas, 2002, *Europhys. Lett.* **59**, 786.
- Bonn, D., and M. Denn, 2009, *Science* **324**, 1401.
- Bonn, D., H. Kellay, H. Tanaka, G. Wegdam, and J. Meunier, 1999, *Langmuir* **15**, 7534.
- Bonn, D., S. Rodts, M. Groenink, S. Rafaï, N. Shahidzadeh-Bonn, and P. Coussot, 2008, *Annu. Rev. Fluid Mech.* **40**, 209.
- Bonn, D., S. Tanase, B. Abou, H. Tanaka, and J. Meunier, 2002, *Phys. Rev. Lett.* **89**, 015701.
- Bonnecaze, R., and M. Cloitre, 2010, *Adv. Polym. Sci.* **236**, 117.
- Bouchaud, J.-P., 1992, *J. Phys. I (France)* **2**, 1705.
- Bouchaud, J.-P., and D. S. Dean, 1995, *J. Phys. I (France)* **5**, 265.
- Bouchbinder, E., and J. S. Langer, 2009a, *Phys. Rev. E* **80**, 031131.
- Bouchbinder, E., and J. S. Langer, 2009b, *Phys. Rev. E* **80**, 031132.
- Bouchbinder, E., and J. S. Langer, 2009c, *Phys. Rev. E* **80**, 031133.
- Boujlel, J., and P. Coussot, 2012, *Rheol. Acta* **51**, 867.
- Boyer, F., E. Guazzelli, and O. Pouliquen, 2011, *Phys. Rev. Lett.* **107**, 188301.
- Brader, J. M., M. Siebenbürger, M. Ballauff, K. Reinheimer, M. Wilhelm, S. J. Frey, F. Weysser, and M. Fuchs, 2010, *Phys. Rev. E* **82**, 061401.
- Brader, J. M., T. Voigtmann, M. E. Cates, and M. Fuchs, 2007, *Phys. Rev. Lett.* **98**, 058301.
- Brambilla, G., D. E. Masri, M. Pierno, G. Petekidis, A. B. Schofield, L. Berthier, and L. Cipelletti, 2009, *Phys. Rev. Lett.* **102**, 085703.
- Brenner, T., S. Matsukawa, K. Nishinari, and R. Johannsson, 2013, *J. Non-Newtonian Fluid Mech.* **196**, 1.
- Buscall, R., 2010, *J. Rheol.* **54**, 1177.
- Buscall, R., T. H. Choudhury, M. A. Faers, J. W. Goodwin, P. A. Luckham, and S. J. Partridge, 2009, *Soft Matter* **5**, 1345.
- Buscall, R., J. McGowan, and A. MortonJones, 1993, *J. Rheol.* **37**, 621.
- Callaghan, P. T., 2008, *Rheol. Acta* **47**, 243.
- Capellmann, R. F., N. E. Valadez-Pérez, B. Simon, S. U. Egelhaaf, M. Laurati, and R. Castaneda-Priego, 2016, *Soft Matter* **12**, 9303.
- Cates, M. E., M. Fuchs, K. Kroy, W. C. K. Poon, and A. M. Puertas, 2004, *J. Phys. Condens. Matter* **16**, S4861.
- Caton, F., and C. Baravian, 2008, *Rheol. Acta* **47**, 601.
- Chan, H., and A. Mohraz, 2012, *Phys. Rev. E* **85**, 041403.
- Chang, C., Q. D. Nguyen, and H. Rønning, 1999, *J. Non-Newtonian Fluid Mech.* **87**, 127.
- Charbonneau, P., 2014, *Nat. Commun.* **5**, 3725.
- Chaudhuri, P., L. Berthier, and L. Bocquet, 2012, *Phys. Rev. E* **85**, 021503.
- Chaudhuri, P., L. Berthier, and S. Sastry, 2010, *Phys. Rev. Lett.* **104**, 165701.
- Chaudhuri, P., and J. Horbach, 2013, *Phys. Rev. E* **88**, 040301(R).
- Chaudhuri, P., L. B. P. I. Hurtado, and W. Kob, 2010, *Phys. Rev. E* **81**, 040502.
- Chaudhuri, P., V. Mansard, A. Colin, and L. Bocquet, 2012, *Phys. Rev. Lett.* **109**, 036001.
- Cheddadi, I., P. Saramito, B. Dollet, C. Raufaste, and F. Graner, 2011, *Eur. Phys. J. E* **34**, 1.
- Cheddadi, I., P. Saramito, and F. Graner, 2012, *J. Rheol.* **56**, 213.
- Cheng, Z., J. Zhu, P. M. Chaikin, S.-E. Phan, and W. B. Russel, 2002, *Phys. Rev. E* **65**, 041405.
- Christel, M., R. Yahya, M. Albert, and B. A. Antoine, 2012, *Soft Matter* **8**, 7365.
- Christopoulou, C., G. Petekidis, B. Erwin, M. Cloitre, and D. Vlassopoulos, 2009, *Phil. Trans. R. Soc. A* **367**, 5051.
- Clasen, C., and G. McKinley, 2004, *J. Non-Newtonian Fluid Mech.* **124**, 1.
- Cloitre, M., and R. T. Bonnecaze, 2017, *Rheol. Acta* **56**, 283.
- Cloitre, M., R. Borrega, and F. M. L. Leibler, 2003, *Phys. Rev. Lett.* **90**, 068303.
- Cloitre, M., R. Borrega, and L. Leibler, 2000, *Phys. Rev. Lett.* **85**, 4819.
- Colombo, J., and E. D. Gado, 2014, *J. Rheol.* **58**, 1089.
- Coussot, P., 2005, *Rheometry of pastes, suspensions, and granular materials* (Wiley, New York).
- Coussot, P., 2007, *Soft Matter* **3**, 528.
- Coussot, P., 2014, *J. Non-Newtonian Fluid Mech.* **211**, 31.
- Coussot, P., 2017, *Rheol. Acta* **56**, 163.
- Coussot, P., and S. Boyer, 1995, *Rheol. Acta* **34**, 534.
- Coussot, P., A. Y. Malkin, and G. Ovarlez, 2017, *Rheol. Acta* **56**, 161.
- Coussot, P., Q. D. Nguyen, H. T. Huynh, and D. Bonn, 2002a, *Phys. Rev. Lett.* **88**, 175501.
- Coussot, P., Q. D. Nguyen, H. T. Huynh, and D. Bonn, 2002b, *J. Rheol.* **46**, 573.
- Coussot, P., and G. Ovarlez, 2010, *Eur. Phys. J. E* **33**, 183.
- Coussot, P., J. S. Raynaud, F. Bertrand, P. Moucheront, J. P. Guilbaud, H. T. Huynh, S. Jarny, and D. Lesueur, 2002, *Phys. Rev. Lett.* **88**, 218301.
- Coussot, P., H. Tabuteau, X. Chateau, L. Tocquer, and G. Ovarlez, 2006, *J. Rheol.* **50**, 975.
- Cruz, F. D., F. Chevoir, D. Bonn, and P. Coussot, 2002, *Phys. Rev. E* **66**, 051305.
- Csikor, F., C. Motz, D. Weygand, M. Zaiser, and S. Zapperi, 2007, *Science* **318**, 251.
- Cugliandolo, L., J. Kurchan, and L. Peliti, 1997, *Phys. Rev. E* **55**, 3898.
- Cugliandolo, L. F., and J. Kurchan, 1993, *Phys. Rev. Lett.* **71**, 173.
- Cugliandolo, L. F., J. Kurchan, P. L. Doussal, and L. Peliti, 1997, *Phys. Rev. Lett.* **78**, 350.
- da C. Andrade, E. N., 1910, *Proc. R. Soc. A* **84**, 1.
- Data, S., D. Gerrard, T. Rhodes, T. G. Mason, and D. Weitz, 2011, *Phys. Rev. E* **84**, 041404.
- Davies, G., and J. Stokes, 2008, *J. Non-Newtonian Fluid Mech.* **148**, 73.
- Dawson, K., G. Foffi, M. Fuchs, W. Gotze, F. Sciortino, M. Sperl, P. Tartaglia, T. Voigtmann, and E. Zaccarelli, 2000, *Phys. Rev. E* **63**, 011401.
- DeGiuli, E., E. Lerner, C. Brito, and M. Wyart, 2014, *Proc. Natl. Acad. Sci. U.S.A.* **111**, 17054.
- DeGroot, J. J. V., C. W. Macosko, T. Kume, and T. Hashimoto, 1994, *J. Colloid Interface Sci.* **166**, 404.
- de Kee, D., R. Chhabra, M. Powley, and S. Roy, 1990, *Chem. Eng. Commun.* **96**, 229.
- Denisov, D. V., M. T. Dang, B. Struth, A. Zacccone, G. H. Wegdam, and P. Schall, 2015, *Sci. Rep.* **5**, 14359.
- Denn, M., 2008, *Polymer melt processing: foundations in fluid mechanics and heat transfer* (Cambridge University Press, New York).
- Denn, M., and D. Bonn, 2011, *Rheol. Acta* **50**, 307.
- Denn, M. M., 2001, *Annu. Rev. Fluid Mech.* **33**, 265.
- Dennin, M., 2008, *J. Phys. Condens. Matter* **20**, 283103.
- Derec, C., G. Ducouret, A. Ajdari, and F. Lequeux, 2003, *Phys. Rev. E* **67**, 061403.
- de Souza Mendes, P., 2009, *J. Non-Newtonian Fluid Mech.* **164**, 66.
- de Souza Mendes, P., 2011, *Soft Matter* **7**, 2471.
- de Souza Mendes, P., and R. Thompson, 2013, *Rheol. Acta* **52**, 673.

- Dhont, J. K. G., 1999, *Phys. Rev. E* **60**, 4534.
- Dimitriou, C., R. Ewoldt, and G. McKinley, 2013, *J. Rheol.* **57**, 27.
- Dimitriou, C., and G. H. McKinley, 2014, *Soft Matter* **10**, 6619.
- Dinkgreve, M., M. M. Denn, and D. Bonn, 2017, *Rheol. Acta* **56**, 189.
- Dinkgreve, M., J. Paredes, M. M. Denn, and D. Bonn, 2016, *J. Non-Newtonian Fluid Mech.* **238**, 233.
- Dinkgreve, M., J. Paredes, M. A. J. Michels, and D. Bonn, 2015, *Phys. Rev. E* **92**, 012305.
- Divoux, T., C. Barentin, and S. Manneville, 2011a, *Soft Matter* **7**, 8409.
- Divoux, T., C. Barentin, and S. Manneville, 2011b, *Soft Matter* **7**, 9335.
- Divoux, T., M. A. Fardin, S. Manneville, and S. Lerouge, 2016, *Annu. Rev. Fluid Mech.* **48**, 81.
- Divoux, T., V. Grenard, and S. Manneville, 2013, *Phys. Rev. Lett.* **110**, 018304.
- Divoux, T., V. Lapeyre, V. Ravaine, and S. Manneville, 2015, *Phys. Rev. E* **92**, 060301.
- Divoux, T., D. Tamarii, C. Barentin, and S. Manneville, 2010, *Phys. Rev. Lett.* **104**, 208301.
- Divoux, T., D. Tamarii, C. Barentin, S. Teitel, and S. Manneville, 2012, *Soft Matter* **8**, 4151.
- Donev, A., S. Torquato, F. H. Stillinger, and R. Connelly, 2004, *Phys. Rev. E* **70**, 043301.
- dos Santos, D., S. Frey, M. Naccache, and P. de Souza Mendes, 2014, *Rheol. Acta* **53**, 31.
- Durian, D. J., 1995, *Phys. Rev. Lett.* **75**, 4780.
- Evans, I. D., 1992, *J. Rheol.* **36**, 1313.
- Ewoldt, R. H., 2013, *J. Rheol.* **57**, 177.
- Ewoldt, R. H., A. E. Hosoi, and G. H. McKinley, 2008, *J. Rheol.* **52**, 1427.
- Ewoldt, R. H., and G. H. McKinley, 2017, *Rheol. Acta* **56**, 195.
- Fabbian, L., W. Götze, F. Sciortino, P. Tartaglia, and F. Thiery, 1999, *Phys. Rev. E* **59**, R1347.
- Falk, M. L., and J. S. Langer, 1998, *Phys. Rev. E* **57**, 7192.
- Falk, M. L., and J. S. Langer, 2011, *Annu. Rev. Condens. Matter Phys.* **2**, 353.
- Falk, M. L., J. S. Langer, and L. Pechenik, 2004, *Phys. Rev. E* **70**, 011507.
- Fall, A., F. Bertrand, G. Ovarlez, and D. Bonn, 2009, *Phys. Rev. Lett.* **103**, 178301.
- Fall, A., H. de Cagny, D. Bonn, G. Ovarlez, E. Wandersman, J. A. Dijksman, and M. van Hecke, 2013, *J. Rheol.* **57**, 1237.
- Fall, A., A. Lemaître, F. B. B. Bonn, and G. Ovarlez, 2010, *Phys. Rev. Lett.* **105**, 268303.
- Fall, A., J. Paredes, and D. Bonn, 2010, *Phys. Rev. Lett.* **105**, 225502.
- Ferry, J., 1980, *Viscoelastic Properties of Polymers* (John Wiley & Sons, Inc., New York).
- Fielding, S. M., M. E. Cates, and P. Sollich, 2009, *Soft Matter* **5**, 2378.
- Fielding, S. M., P. Sollich, and M. E. Cates, 2000, *J. Rheol.* **44**, 323.
- Fiocco, D., G. Foffi, and S. Sastry, 2013, *Phys. Rev. E* **88**, 020301.
- Foffi, G., C. de Michele, F. Sciortino, and P. Tartaglia, 2005, *J. Chem. Phys.* **122**, 224903.
- Fonseca, C., S. Frey, M. Naccache, and P. de Souza Mendes, 2013, *J. Non-Newtonian Fluid Mech.* **193**, 80.
- Fraggedakis, D., D. Dimakopoulos, and J. Tsamopoulos, 2016, *Soft Matter* **12**, 5378.
- Frigaard, I. A., K. G. Paso, and P. R. de Souza Mendes, 2017, *Rheol. Acta* **56**, 259.
- Fritsch, S., M. Fuchs, and T. Voigtmann, 2014, *Soft Matter* **10**, 4822.
- Fuchs, M., and M. E. Cates, 2002, *Phys. Rev. Lett.* **89**, 248304.
- Fuchs, M., and M. E. Cates, 2003, *Faraday Discuss.* **123**, 267.
- Fuchs, M., and M. E. Cates, 2009, *J. Rheol.* **53**, 957.
- Fusco, C., T. Albaret, and A. Tanguy, 2014, *Eur. Phys. J. E* **37**, 43.
- Gallot, T., C. Perge, V. Grenard, M.-A. Fardin, N. Taberlet, and S. Manneville, 2013, *Rev. Sci. Instrum.* **84**, 045107.
- Geraud, B., L. Bocquet, and C. Barentin, 2013, *Eur. Phys. J. E* **36**, 30.
- Gibaud, T., C. Barentin, and S. Manneville, 2008, *Phys. Rev. Lett.* **101**, 258302.
- Gibaud, T., C. Barentin, N. Taberlet, and S. Manneville, 2009, *Soft Matter* **5**, 3026.
- Gibaud, T., D. Frelat, and S. Manneville, 2010, *Soft Matter* **6**, 3482.
- Gibaud, T., C. Perge, S. B. Lindström, N. Taberlet, and S. Manneville, 2016, *Soft Matter* **12**, 1701.
- Gilbreth, C., S. Sullivan, and M. Dennin, 2006, *Phys. Rev. E* **74**, 051406.
- Gopalakrishnan, V., and C. Zukoski, 2007, *J. Rheol.* **51**, 623.
- Götze, W., 2008, *Complex Dynamics of Glass-Forming Liquids: A Mode-Coupling Theory* (Oxford University Press, Oxford).
- Goyon, J., A. Colin, and L. Bocquet, 2010, *Soft Matter* **6**, 2668.
- Goyon, J., A. Colin, G. Ovarlez, A. Ajdari, and L. Bocquet, 2008, *Nature (London)* **454**, 84.
- Graham, M., 1995, *J. Rheol.* **39**, 697.
- Grenard, V., T. Divoux, N. Taberlet, and S. Manneville, 2014, *Soft Matter* **10**, 1555.
- Grenard, V., N. Taberlet, and S. Manneville, 2011, *Soft Matter* **7**, 3920.
- Griffith, A., 1921, *Phil. Trans. R. Soc. A* **221**, 163.
- Gueslin, B., L. Talini, B. Herzhaft, Y. Peysson, and C. Allain, 2006, *Phys. Fluids* **18**, 103101.
- Gutowski, I., D. Lee, J. de Bruyn, and B. Frisken, 2012, *Rheol. Acta* **51**, 441.
- Habibi, M., M. Dinkgreve, J. Paredes, M. M. Denn, and D. Bonn, 2016, *J. Non-Newtonian Fluid Mech.* **238**, 33.
- Hansen, J. P., and I. R. McDonald, 2006, *Theory of Simple Liquids* (Academic, London).
- Hartman Kok, P., S. Kazarian, B. Briscoe, and C. Lawrence, 2004, *J. Colloid Interface Sci.* **280**, 511.
- Hartman Kok, P., S. Kazarian, C. Lawrence, and B. Briscoe, 2002, *J. Rheol.* **46**, 481.
- Hartnett, J., and R. Hu, 1989, *J. Rheol.* **33**, 671.
- Hatano, T., 2010, *Prog. Theor. Phys. Suppl.* **184**, 143.
- Hébraud, P., and F. Lequeux, 1998, *Phys. Rev. Lett.* **81**, 2934.
- Hébraud, P., F. Lequeux, J.-P. Munch, and D. J. Pine, 1997, *Phys. Rev. Lett.* **78**, 4657.
- Helal, A., T. Divoux, and G. H. McKinley, 2016, *Phys. Rev. Applied* **6**, 064004.
- Helgeson, M. E., Y. Gao, S. E. Moran, J. Lee, M. Godfrin, A. Tripathi, A. Bossee, and P. S. Doyleb, 2014, *Soft Matter* **10**, 3122.
- Hermes, M., and P. Clegg, 2013, *Soft Matter* **9**, 7568.
- Hermes, M., and M. Dijkstra, 2010, *Europhys. Lett.* **89**, 38005.
- Herschel, W., and R. Bulkley, 1926, *Kolloid Z.* **39**, 291.
- Hinkle, A. R., and M. L. Falk, 2016, *J. Rheol.* **60**, 873.
- Höhler, R., and S. Cohen-Addad, 2005, *J. Phys. Condens. Matter* **17**, R1041.
- Huang, N., G. Ovarlez, F. Bertrand, S. Rodts, P. Coussot, and D. Bonn, 2005, *Phys. Rev. Lett.* **94**, 028301.
- Hunter, G. L., and E. R. Weeks, 2012, *Rep. Prog. Phys.* **75**, 066501.
- Hyun, K., M. Wilhelm, C. Klein, K. Cho, J. Nam, K. Ahn, S. Lee, R. Ewoldt, and G. McKinley, 2011, *Prog. Polym. Sci.* **36**, 1697.
- Ianni, F., R. D. Leonardo, S. Gentilini, and G. Ruocco, 2007, *Phys. Rev. E* **75**, 011408.
- Ianni, F., R. D. Leonardo, S. Gentilini, and G. Ruocco, 2008, *Phys. Rev. E* **77**, 031406.

- Ikeda, A., and L. Berthier, 2013, *Phys. Rev. E* **88**, 052305.
- Ikeda, A., L. Berthier, and P. Sollich, 2012, *Phys. Rev. Lett.* **109**, 018301.
- Ikeda, A., L. Berthier, and P. Sollich, 2013, *Soft Matter* **9**, 7669.
- Ikeda, A., L. Berthier, and P. Sollich, 2016, *Phys. Rev. Lett.* **116**, 179801.
- Illa, X., A. Puisto, A. Lehtinen, M. Mohtaschemi, and M. Alava, 2013, *Phys. Rev. E* **87**, 022307.
- Irani, E., P. Chaudhuri, and C. Heussinger, 2014, *Phys. Rev. Lett.* **112**, 188303.
- Isa, L., R. Besseling, and W. C. K. Poon, 2007, *Phys. Rev. Lett.* **98**, 198305.
- Jagla, E. A., 2007, *Phys. Rev. E* **76**, 046119.
- James, A., D. Williams, and P. Williams, 1987, *Rheol. Acta* **26**, 437.
- Jana, S., B. Kapoor, and A. Acrivos, 1995, *J. Rheol.* **39**, 1123.
- Jop, P., V. Mansard, P. Chaudhuri, L. Bocquet, and A. Colin, 2012, *Phys. Rev. Lett.* **108**, 148301.
- Joshi, Y. M., 2015, *Soft Matter* **11**, 3198.
- Kabla, A., J. Scheibert, and G. Debrégeas, 2007, *J. Fluid Mech.* **587**, 45.
- Kalyon, D., 2005, *J. Rheol.* **49**, 621.
- Kalyon, D., P. Yaras, B. Aral, and U. Yilmazer, 1993, *J. Rheol.* **37**, 35.
- Karppinen, A., T. Saarinen, J. Salmela, A. Laukkanen, M. Nuopponen, and J. Seppälä, 2012, *Cellulose* **19**, 1807.
- Katgert, G., A. Latka, M. Möbius, and M. van Hecke, 2009, *Phys. Rev. E* **79**, 066318.
- Katgert, G., M. Möbius, and M. van Hecke, 2008, *Phys. Rev. Lett.* **101**, 058301.
- Kawasaki, T., D. Coslovich, A. Ikeda, and L. Berthier, 2015, *Phys. Rev. E* **91**, 012203.
- Kawasaki, Takeshi, and Ludovic Berthier, 2016, *Phys. Rev. E* **94**, 022615.
- Keentok, M., 1982, *Rheol. Acta* **21**, 325.
- Khan, S. A., C. A. Schnepper, and R. C. Armstrong, 1988, *J. Rheol.* **32**, 69.
- Kiljański, T., 1989, *Rheol. Acta* **28**, 61.
- Kim, H. S., F. Scheffold, and T. G. Mason, 2016, *Rheol. Acta* **55**, 683.
- Kim, J., D. Merger, M. Wilhelm, and M. E. Helgeson, 2014, *J. Rheol.* **58**, 1359.
- Kirkpatrick, T. R., and D. Thirumalai, 1987, *Phys. Rev. Lett.* **58**, 2091.
- Knowlton, E. D., D. J. Pine, and L. Cipelletti, 2014, *Soft Matter* **10**, 6931.
- Kogan, M., L. Ducloué, J. Goyon, X. Chateau, O. Pitois, and G. Ovarlez, 2013, *Rheol. Acta* **52**, 237.
- Koumakis, N., J. F. Brady, and G. Petekidis, 2013, *Phys. Rev. Lett.* **110**, 178301.
- Koumakis, N., M. Laurati, S. Egelhaaf, J. Brady, and G. Petekidis, 2012, *Phys. Rev. Lett.* **108**, 098303.
- Koumakis, N., E. Moghimi, R. Besseling, W. C. K. Poon, J. F. Brady, and G. Petekidis, 2015, *Soft Matter* **11**, 4640.
- Koumakis, N., A. Pamvouxoglou, A. Poulos, and G. Petekidis, 2012, *Soft Matter* **8**, 4271.
- Koumakis, N., and G. Petekidis, 2011, *Soft Matter* **7**, 2456.
- Kurchan, J., and L. Laloux, 1996, *J. Phys. A* **29**, 1929.
- Kurokawa, A., V. Vidal, K. Kurita, T. Divoux, and S. Manneville, 2015, *Soft Matter* **11**, 9026.
- Langer, J. S., 2004, *Phys. Rev. E* **70**, 041502.
- Langer, J. S., and M. L. Manning, 2007, *Phys. Rev. E* **76**, 056107.
- Larson, R. G., 1999, *The Structure and Rheology of Complex Fluids* (Oxford University Press, New York).
- Laurati, M., S. Egelhaaf, and G. Petekidis, 2011, *J. Rheol.* **55**, 673.
- Laurati, M., S. U. Egelhaaf, and G. Petekidis, 2014, *J. Rheol.* **58**, 1395.
- Lawn, B., 1993, *Fracture of Brittle Solids* (Cambridge University Press, Cambridge, England).
- Lehtinen, A., A. Puisto, X. Illa, M. Mohtaschemi, and M. J. Alava, 2013, *Soft Matter* **9**, 8041.
- Lequeux, F., and A. Ajdari, 2001, *Phys. Rev. E* **63**, 030502.
- Lerner, E., G. Düring, and M. Wyart, 2012, *Proc. Natl. Acad. Sci. U.S.A.* **109**, 4798.
- Letwimolnun, W., B. Vergnes, G. Ausias, and P. Carreau, 2007, *J. Non-Newtonian Fluid Mech.* **141**, 167.
- Lidell, P., and D. V. Boger, 1996, *J. Non-Newtonian Fluid Mech.* **63**, 235.
- Lidon, P., L. Villa, and S. Manneville, 2017, *Rheol. Acta* **56**, 307.
- Lin, S.-F., and R. Brodkey, 1985, *J. Rheol.* **29**, 147.
- Lindström, S., T. Kodger, J. Sprakler, and D. Weitz, 2012, *Soft Matter* **8**, 3657.
- Lin-Gibson, S., J. A. Pathak, E. A. Grulke, H. Wang, and E. K. Hobbie, 2004, *Phys. Rev. Lett.* **92**, 048302.
- Liu, A., and S. R. Nagel, 1998, *Nature (London)* **396**, 21.
- Liu, A. J., and S. R. Nagel, 2001, Eds., *Jamming and Rheology* (Taylor and Francis, London).
- Liu, A. J., and S. R. Nagel, 2010, *Annu. Rev. Condens. Matter Phys.* **1**, 347.
- Lois, G., J. Blawzdziewicz, and C. S. O'Hern, 2008, *Phys. Rev. Lett.* **100**, 028001.
- Lu, P., E. Zaccarelli, F. Ciulla, A. B. Schofield, F. Sciortino, and D. A. Weitz, 2008, *Nature (London)* **453**, 499.
- Lubchenko, V., and P. G. Wolynes, 2007, *Annu. Rev. Phys. Chem.* **58**, 235.
- Macosko, C., 1994, *Rheology. Principles, measurements, and applications.* (Wiley—VCH, New York).
- Magda, J. J., H. El-Gendy, K. Oh, M. D. Deo, A. Montesi, and R. Venkatesan, 2009, *Energy Fuels* **23**, 1311.
- Magnin, A., and J. Piau, 1990, *J. Non-Newtonian Fluid Mech.* **36**, 85.
- Maki, K., and Y. Renardy, 2012, *J. Non-Newtonian Fluid Mech.* **181–182**, 30.
- Maloney, C. E., and A. Lemaître, 2006, *Phys. Rev. E* **74**, 016118.
- Malkin, A., V. Kulichikhin, and S. Ilyin, 2017, *Rheol. Acta* **56**, 177.
- Manley, S., H. M. Wyss, K. Miyazaki, J. C. Conrad, V. Trappe, L. J. Kaufman, and D. R. Reichman, 2005, *Phys. Rev. Lett.* **95**, 238302.
- Manneville, S., 2008, *Rheol. Acta* **47**, 301.
- Manneville, S., L. Bécu, and A. Colin, 2004, *Eur. Phys. J. Appl. Phys.* **28**, 361.
- Manning, M. L., E. G. Daub, J. S. Langer, and J. M. Carlson, 2009, *Phys. Rev. E* **79**, 016110.
- Manning, M. L., J. S. Langer, and J. M. Carlson, 2007, *Phys. Rev. E* **76**, 056106.
- Mansard, V., and A. Colin, 2012, *Soft Matter* **8**, 4025.
- Martens, K., L. Bocquet, and J.-L. Barrat, 2012, *Soft Matter* **8**, 4197.
- Marze, S., D. Langevin, and A. Saint-Jalmes, 2008, *J. Rheol.* **52**, 1091.
- Mas, R., and A. Magnin, 1994, *J. Rheol.* **38**, 889.
- Mason, T. G., J. Bibette, and D. A. Weitz, 1996, *J. Colloid Interface Sci.* **179**, 439.
- Masschaele, K., J. Fransaer, and J. Vermant, 2011, *Soft Matter* **7**, 7717.
- Masselon, C., J.-B. Salmon, and A. Colin, 2008, *Phys. Rev. Lett.* **100**, 038301.

- Meeker, S. P., R. T. Bonnecaze, and M. Cloitre, 2004a, *J. Rheol.* **48**, 1295.
- Meeker, S. P., R. T. Bonnecaze, and M. Cloitre, 2004b, *Phys. Rev. Lett.* **92**, 198302.
- Mewis, J., and N. J. Wagner, 2009, *Adv. Colloid Interface Sci.* **147–148**, 214.
- Mézard, M., G. Parisi, and M. A. Virasoro, 1988, *Spin Glass Theory and Beyond* (World Scientific, Singapore).
- Michaels, A., and J. Bolger, 1962, *Ind. Eng. Chem. Fundam.* **1**, 153.
- MiDi, G., 2004, *Eur. Phys. J. E* **14**, 341.
- Miguel, M.-C., L. Laurson, and M. Alava, 2008, *Eur. Phys. J. B* **64**, 443.
- Miguel, M.-C., A. Vespignani, M. Zaiser, and S. Zapperi, 2002, *Phys. Rev. Lett.* **89**, 165501.
- Min Kim, J., A. P. R. Eberle, A. Kate Gurnon, L. Porcar, and N. J. Wagner, 2014, *J. Rheol.* **58**, 1301.
- Mitsoulis, E., and J. Tsamopoulos, 2017, *Rheol. Acta* **56**, 231.
- Miyazaki, K., and D. R. Reichman, 2002, *Phys. Rev. E* **66**, 050501.
- Möbius, M. E., G. Katgert, and M. van Hecke, 2010, *Europhys. Lett.* **90**, 44003.
- Mohan, L., R. Bonnecaze, and M. Cloitre, 2013, *Phys. Rev. Lett.* **111**, 268301.
- Mohan, L., C. Pellet, M. Cloitre, and R. Bonnecaze, 2013, *J. Rheol.* **57**, 1023.
- Mohraz, A., and M. Solomon, 2005, *J. Rheol.* **49**, 657.
- Mohtaschemi, M., A. Puisto, X. Illa, and M. J. Alava, 2014, *Soft Matter* **10**, 2971.
- Møller, P. C. F., A. Fall, and D. Bonn, 2009, *Europhys. Lett.* **87**, 38004.
- Møller, P. C. F., A. Fall, V. Chikkadi, D. Derk, and D. Bonn, 2009, *Phil. Trans. R. Soc. A* **367**, 5139.
- Møller, P. C. F., J. Mewis, and D. Bonn, 2006, *Soft Matter* **2**, 274.
- Møller, P. C. F., S. Rodts, M. A. J. Michels, and D. Bonn, 2008, *Phys. Rev. E* **77**, 041507.
- Montesi, A., A. A. Peña, and M. Pasquali, 2004, *Phys. Rev. Lett.* **92**, 058303.
- Mooney, M., 1931, *J. Rheol.* **2**, 210.
- Moorcroft, R., M. Cates, and S. Fielding, 2011, *Phys. Rev. Lett.* **106**, 055502.
- Moorcroft, R., and S. Fielding, 2013, *Phys. Rev. Lett.* **110**, 086001.
- Mora, S., 2011, *Soft Matter* **7**, 4908.
- Mujumdar, A., A. N. Beris, and B. Metzner, 2002, *J. Non-Newtonian Fluid Mech.* **102**, 157.
- Nagamanasa, K. H., S. Gokhale, A. K. Sood, and R. Ganapathy, 2014, *Phys. Rev. E* **89**, 062308.
- Nagase, Y., and K. Okada, 1986, *J. Rheol.* **30**, 1123.
- Navarrete, R., L. Scriven, and C. Macosko, 1996, *J. Colloid Interface Sci.* **180**, 200.
- Negi, A., and C. Osuji, 2009, *Rheol. Acta* **48**, 871.
- Negi, A., and C. Osuji, 2010a, *Europhys. Lett.* **90**, 28003.
- Negi, A., and C. Osuji, 2010b, *J. Rheol.* **54**, 943.
- Nguyen, Q., T. Akroyd, D. de Kee, and L. Zhu, 2006, *Korea-Australia Rheol. J.* **18**, 15 [<https://www.cheric.org/research/tech/periodicals/view.php?seq=540568>].
- Nguyen, Q., and D. Boger, 1983, *J. Rheol.* **27**, 321.
- Nguyen, Q., and D. Boger, 1992, *Annu. Rev. Fluid Mech.* **24**, 47.
- Nickerson, C., and J. Kornfield, 2005, *J. Rheol.* **49**, 865.
- Nicolas, A., K. Martens, and J.-L. Barrat, 2014, *Europhys. Lett.* **107**, 44003.
- Nordstrom, K., E. Verneuil, P. Arratia, A. Basu, Z. Zhang, A. Yodh, J. Gollub, and D. Durian, 2010, *Phys. Rev. Lett.* **105**, 175701.
- O'Hern, C. S., L. E. Silbert, A. J. Liu, and S. R. Nagel, 2003, *Phys. Rev. E* **68**, 011306.
- Olmsted, P. D., 2008, *Rheol. Acta* **47**, 283.
- Olsson, P., and S. Teitel, 2007, *Phys. Rev. Lett.* **99**, 178001.
- Olsson, P., and S. Teitel, 2011, *Phys. Rev. E* **83**, 030302.
- Olsson, P., and S. Teitel, 2012, *Phys. Rev. Lett.* **109**, 108001.
- Oppong, F. K., L. Rubatat, B. J. Friske, A. E. Bailey, and J. R. de Bruyn, 2006, *Phys. Rev. E* **73**, 041405.
- Osuji, C. O., C. Kim, and D. A. Weitz, 2008, *Phys. Rev. E* **77**, 060402(R).
- Ovarlez, G., F. Bertrand, and S. Rodts, 2006, *J. Rheol.* **50**, 259.
- Ovarlez, G., and X. Chateau, 2008, *Phys. Rev. E* **77**, 061403.
- Ovarlez, G., S. Cohen-Addad, K. Krishan, J. Goyon, and P. Coussot, 2013, *J. Non-Newtonian Fluid Mech.* **193**, 68.
- Ovarlez, G., F. Mahaut, F. Bertrand, and X. Chateau, 2011, *J. Rheol.* **55**, 197.
- Ovarlez, G., S. Rodts, X. Chateau, and P. Coussot, 2009, *Rheol. Acta* **48**, 831.
- Ovarlez, G., S. Rodts, A. Ragouilliaux, P. Coussot, J. Goyon, and A. Colin, 2008, *Phys. Rev. E* **78**, 036307.
- Ovarlez, G., L. Tocquer, F. Bertrand, and P. Coussot, 2013, *Soft Matter* **9**, 5540.
- Papenhuijzen, J., 1972, *Rheol. Acta* **11**, 73.
- Paredes, J., M. A. J. Michels, and D. Bonn, 2013, *Phys. Rev. Lett.* **111**, 015701.
- Paredes, J., N. Shahidzadeh, and D. Bonn, 2015, *Phys. Rev. E* **92**, 042313.
- Paredes, J., N. Shahidzadeh-Bonn, and D. Bonn, 2011, *J. Phys. Condens. Matter* **23**, 284116.
- Parisi, G., and F. Zamponi, 2010, *Rev. Mod. Phys.* **82**, 789.
- Park, J., and K. Ahn, 2013, *Soft Matter* **9**, 11650.
- Perchikov, N., and E. Bouchbinder, 2014, *Phys. Rev. E* **89**, 062307.
- Pérez-González, J., J. López-Durán, B. Marín-Santibáñez, and F. Rodríguez-González, 2012, *Rheol. Acta* **51**, 937.
- Perge, C., 2014, “Ultrasonic imaging in soft materials,” Ph.D. thesis (École Normale Supérieure de Lyon).
- Perge, C., N. Taberlet, T. Gibaud, and S. Manneville, 2014, *J. Rheol.* **58**, 1331.
- Persello, J., A. Magnin, J. Chang, J. Piau, and B. Cabane, 1994, *J. Rheol.* **38**, 1845.
- Petekidis, G., D. Vlassopoulos, and P. Pusey, 2003, *Faraday Discuss.* **123**, 287.
- Petekidis, G., D. Vlassopoulos, and P. Pusey, 2004, *J. Phys. Condens. Matter* **16**, S3955.
- Peyneau, P.-E., and J.-N. Roux, 2008, *Phys. Rev. E* **78**, 011307.
- Pham, K., G. Petekidis, D. Vlassopoulos, S. Egelhaaf, P. Pusey, and W. Poon, 2006, *Europhys. Lett.* **75**, 624.
- Pham, K. N., S. U. Egelhaaf, P. N. Pusey, and W. C. K. Poon, 2004, *Phys. Rev. E* **69**, 011503.
- Pham, K. N., A. M. Puertas, J. Bergenholz, S. U. Egelhaaf, A. Moussaïd, P. N. Pusey, A. B. Schofield, M. E. Cates, M. Fuchs, and W. C. K. Poon, 2002, *Science* **296**, 104.
- Picard, G., A. Ajdari, L. Bocquet, and F. Lequeux, 2002, *Phys. Rev. E* **66**, 051501.
- Picard, G., A. Ajdari, F. Lequeux, and L. Bocquet, 2004, *Eur. Phys. J. E* **15**, 371.
- Picard, G., A. Ajdari, F. Lequeux, and L. Bocquet, 2005, *Phys. Rev. E* **71**, 010501(R).
- Pignon, F., A. Magnin, and J.-M. Piau, 1996, *J. Rheol.* **40**, 573.
- Plazek, D., 1960, *J. Colloid Sci.* **15**, 50.
- Pomeau, Y., 2002, *C.R. Mec.* **330**, 249.
- Poumaere, A., M. Moyers-González, C. Castelain, and T. Burghelea, 2014, *J. Non-Newtonian Fluid Mech.* **205**, 28.
- Pratt, E., and M. Dennin, 2003, *Phys. Rev. E* **67**, 051402.
- Princen, H. M., 1985, *J. Colloid Interface Sci.* **105**, 150.

- Princen, H. M., and A. D. Kiss, 1989, *J. Colloid Interface Sci.* **128**, 176.
- Puertas, A. M., and M. Fuchs, 2009, in *Structure and functional properties of colloidal systems*, edited by R. Hidalgo-Alvarez (Taylor and Francis, London).
- Puertas, A. M., E. Zaccarelli, and F. Sciortino, 2005, *J. Phys. Condens. Matter* **17**, L271.
- Pusey, P. N., and W. van Megen, 1986, *Nature (London)* **320**, 340.
- Pusey, P. N., and W. van Megen, 1987, *Phys. Rev. Lett.* **59**, 2083.
- Putz, A., T. Burghelea, I. Frigaard, and D. Martinez, 2008, *Phys. Fluids* **20**, 033102.
- Rabideau, B., and C. L. L. Coussot, 2009, *Rheol. Acta* **48**, 517.
- Ragouilliaux, A., B. Herzhaft, F. Bertrand, and P. Coussot, 2006, *Rheol. Acta* **46**, 261.
- Ragouilliaux, A., G. Ovarlez, N. Shahidzadeh-Bonn, B. Herzhaft, T. Palermo, and P. Coussot, 2007, *Phys. Rev. E* **76**, 051408.
- Rainone, C., P. Urbani, H. Yoshino, and F. Zamponi, 2015, *Phys. Rev. Lett.* **114**, 015701.
- Regev, I., T. Lookman, and C. Reichhardt, 2013, *Phys. Rev. E* **88**, 062401.
- Roberts, G., and H. Barnes, 2001, *Rheol. Acta* **40**, 499.
- Rodney, D., A. Tangy, and D. Vandembroucq, 2011, *Modelling Simul. Mater. Sci. Eng.* **19**, 083001 [<http://iopscience.iop.org/article/10.1088/0956-0393/19/8/083001/meta>].
- Rogers, M., K. Chen, L. Andrzejewski, S. Narayanan, S. Ramakrishnan, R. Leheny, and J. Harden, 2014, *Phys. Rev. E* **90**, 062310.
- Rogers, S. A., B. M. Erwin, D. Vlassopoulos, and M. Cloitre, 2011, *J. Rheol.* **55**, 435.
- Rogers, S. A., D. Vlassopoulos, and P. T. Callaghan, 2008, *Phys. Rev. Lett.* **100**, 128304.
- Romer, S., H. Bissig, P. Schurtenberger, and F. Scheffold, 2014, *Europhys. Lett.* **108**, 48006.
- Rottler, J., and M. O. Robbins, 2005, *Phys. Rev. Lett.* **95**, 225504.
- Rouyer, F., S. Cohen-Addad, and R. Höhler, 2005, *Colloids Surf. A* **263**, 111.
- Royall, C., W. Poon, and E. Weeks, 2013, *Soft Matter* **9**, 17.
- Royall, C. P., S. R. Williams, T. Ohtsuka, and H. Tanaka, 2008, *Nat. Mater.* **7**, 556.
- Royall, C. P., S. R. Williams, and H. Tanaka, 2015, “The nature of the glass and gel transitions in sticky spheres,” [arXiv:1409.5469](https://arxiv.org/abs/1409.5469).
- Rycroft, C. H., and E. Bouchbinder, 2012, *Phys. Rev. Lett.* **109**, 194301.
- Saint-Jalme, A., and D. Durian, 1999, *J. Rheol.* **43**, 1411.
- Salmon, J.-B., L. Bégu, S. Manneville, and A. Colin, 2003, *Eur. Phys. J. E* **10**, 209.
- Salmon, J.-B., S. Manneville, A. Colin, and B. Pouliquen, 2003, *Eur. Phys. J. Appl. Phys.* **22**, 143.
- Saramito, P., 2007, *J. Non-Newtonian Fluid Mech.* **145**, 1.
- Saramito, P., and A. Wachs, 2017, *Rheol. Acta* **56**, 211.
- Saunders, B., and B. Vincent, 1999, *Adv. Colloid Interface Sci.* **80**, 1.
- Sausset, F., G. Biroli, and J. Kurchan, 2010, *J. Stat. Phys.* **140**, 718.
- Schall, P., D. A. Weitz, and F. Spaepen, 2007, *Science* **318**, 1895.
- Scheffold, F., J. N. Wilking, J. Haberko, F. Cardinaux, and T. G. Mason, 2014, *Soft Matter* **10**, 5040.
- Schmitt, V., C. M. Marques, and F. Lequeux, 1995, *Phys. Rev. E* **52**, 4009.
- Schurz, J., 1990, *Rheol. Acta* **29**, 170.
- Schwartz, L., and H. Princen, 1987, *J. Colloid Interface Sci.* **118**, 201.
- Sciortino, F., 2002, *Nat. Mater.* **1**, 145.
- Sciortino, F., and P. Tartaglia, 2005, *Adv. Phys.* **54**, 471.
- Sciortino, F., P. Tartaglia, and E. Zaccarelli, 2003, *Phys. Rev. Lett.* **91**, 268301.
- Sentjabrskaja, T., P. Chaudhuri, M. Hermes, W. C. K. Poon, J. Horbach, S. U. Egelhaaf, and M. Laurati, 2015, *Sci. Rep.* **5**, 11884.
- Seth, J., M. Cloitre, and R. Bonnecaze, 2008, *J. Rheol.* **52**, 1241.
- Seth, J., C. Locatelli-Champagne, F. Monti, R. Bonnecaze, and M. Cloitre, 2012, *Soft Matter* **8**, 140.
- Seth, J., L. Mohan, C. Locatelli-Champagne, M. Cloitre, and R. Bonnecaze, 2011, *Nat. Mater.* **10**, 838.
- Seyboldt, R., D. Merger, F. Coupette, M. Siebenburger, and M. Ballauff, M. Wilhelm, and M. Fuchs, 2016, *Soft Matter* **12**, 8825.
- Shahin, A., and Y. Joshi, 2010, *Langmuir* **26**, 4219.
- Shahin, A., and Y. Joshi, 2012, *Langmuir* **28**, 15674.
- Shaukat, A., A. Sharma, and Y. M. Joshi, 2012, *J. Non-Newtonian Fluid Mech.* **167–168**, 9.
- Shi, Y., M. B. Katz, H. Li, and M. L. Falk, 2007, *Phys. Rev. Lett.* **98**, 185505.
- Siebenbürger, M., M. Ballauf, and T. Voigtmann, 2012, *Phys. Rev. Lett.* **108**, 255701.
- Siebenbürger, M., M. Fuchs, and M. Ballauf, 2012, *Soft Matter* **8**, 4014.
- Sollich, P., 1998, *Phys. Rev. E* **58**, 738.
- Sollich, P., and M. E. Cates, 2012, *Phys. Rev. E* **85**, 031127.
- Sollich, P., F. Lequeux, P. Hébraud, and M. E. Cates, 1997, *Phys. Rev. Lett.* **78**, 2020.
- Soltani, F., and U. Yilmazer, 1998, *J. Appl. Polym. Sci.* **70**, 515.
- Spaans, R., and M. Williams, 1995, *J. Rheol.* **39**, 241.
- Spenley, A., M. E. Cates, and T. C. B. McLeish, 1993, *Phys. Rev. Lett.* **71**, 939.
- Sprakler, J., S. Lindström, T. Kodger, and D. Weitz, 2011, *Phys. Rev. Lett.* **106**, 248303.
- Szamel, G., 2010, *Europhys. Lett.* **91**, 56004.
- Tabuteau, H., S. Mora, G. Porte, M. Abkarian, and C. Ligoure, 2009, *Phys. Rev. Lett.* **102**, 155501.
- Tanaka, H., J. Meunier, and D. Bonn, 2004, *Phys. Rev. E* **69**, 031404.
- Tanguy, A., F. Leonforte, and J.-L. Barrat, 2006, *Eur. Phys. J. E* **20**, 355.
- Teece, L. J., M. A. Faers, and P. Bartlett, 2011, *Soft Matter* **7**, 1341.
- Testard, V., L. Berthier, and W. Kob, 2011, *Phys. Rev. Lett.* **106**, 125702.
- Tighe, B. P., E. Woldhuis, J. J. C. Remmers, W. van Saarloos, and M. van Hecke, 2010, *Phys. Rev. Lett.* **105**, 088303.
- Tiu, C., and D. Boger, 1974, *J. Texture Stud.* **5**, 329.
- Torquato, S., and F. H. Stillinger, 2010, *Rev. Mod. Phys.* **82**, 2633.
- Trappe, V., V. Prasad, L. Cipelletti, L. Cipelletti, P. N. Segre, and D. A. Weitz, 2001, *Nature (London)* **411**, 772.
- Uhlherr, P., J. Guo, C. Tiu, X.-M. Zhang, J.-Q. Zhou, and T.-N. Fang, 2005, *J. Non-Newtonian Fluid Mech.* **125**, 101.
- Urbani, F., and F. Zamponi, 2017, *Phys. Rev. Lett.* **118**, 038001.
- Vagberg, D., P. Olsson, and S. Teitel, 2014, *Phys. Rev. Lett.* **113**, 148002.
- Vagberg, D., D. Valdez-Balderas, M. A. Moore, P. Olsson, and S. Teitel, 2011, *Phys. Rev. E* **83**, 030303.
- van Aken, G., 2001, *Colloids Surf. A* **190**, 333.
- Vandembroucq, D., and S. Roux, 2011, *Phys. Rev. B* **84**, 134210.
- van der Vaart, K., Y. Rahmani, R. Zargar, Z. Hu, D. Bonn, and P. Schall, 2013, *J. Rheol.* **57**, 1195.
- Vanel, L., S. Ciliberto, and P.-P. Cortet, 2009, *J. Phys. D* **42**, 214007.
- Vanel, L., D. Howell, D. Clark, R. P. Behringer, and E. Clément, 1999, *Phys. Rev. E* **60**, R5040.
- van Hecke, M., 2010, *J. Phys. Condens. Matter* **22**, 033101.
- van Kao, S., L. Nielsen, and C. Hill, 1975, *J. Colloid Interface Sci.* **53**, 358.
- Varnik, F., L. Bocquet, and J.-L. Barrat, 2004, *J. Chem. Phys.* **120**, 2788.
- Varnik, F., L. Bocquet, J.-L. Barrat, and L. Berthier, 2003, *Phys. Rev. Lett.* **90**, 095702.

- Varnik, F., and O. Henrich, 2006, *Phys. Rev. B* **73**, 174209.
- Viasnoff, V., and F. Lequeux, 2002, *Phys. Rev. Lett.* **89**, 065701.
- Vinogradov, G., G. Froishteter, and K. Trilisky, 1978, *Rheol. Acta* **17**, 156.
- Vinogradov, G., G. Froishteter, K. Trilisky, and Y. Smorodinsky, 1975, *Rheol. Acta* **14**, 765.
- Voigtmann, T., 2011, *Eur. Phys. J. E* **34**, 106.
- Voigtmann, T., 2014, *Curr. Opin. Colloid Interface Sci.* **19**, 549.
- Walls, H., S. Caines, A. Sanchez, and S. Khan, 2003, *J. Rheol.* **47**, 847.
- Wein, O., and V. Tovchigrechko, 1992, *J. Rheol.* **36**, 821.
- West, A., J. Melrose, and R. Ball, 1994, *Phys. Rev. E* **49**, 4237.
- Whittle, M., and E. Dickinson, 1997, *J. Chem. Phys.* **107**, 10191.
- Wilhelm, M., 2002, *Macromol. Mater. Eng.* **287**, 83.
- Wittmer, J. P., H. Xu, P. Polińska, F. Weysser, and J. Baschnagel, 2013, *J. Chem. Phys.* **138**, 12A533.
- Xu, N., and C. S. O'Hern, 2006, *Phys. Rev. E* **73**, 061303.
- Yamamoto, R., and A. Onuki, 1997, *Europhys. Lett.* **40**, 61.
- Yan, Y., Z. Z. Z. Cheneler, J. Stokes, and M. Adams, 2010, *Rheol. Acta* **49**, 255.
- Yilmazer, U., and D. Kalyon, 1989, *J. Rheol.* **33**, 1197.
- Yoshimura, A. S., and R. K. Prud'homme, 1988, *J. Rheol.* **32**, 53.
- Yoshino, H., and M. Mézard, 2010, *Phys. Rev. Lett.* **105**, 015504.
- Yoshino, H., and F. Zamponi, 2014, *Phys. Rev. E* **90**, 022302.
- Yuan, X.-F., 1999, *Europhys. Lett.* **46**, 542.
- Zaccarelli, E., 2007, *J. Phys. Condens. Matter* **19**, 323101.
- Zaccarelli, E., S. V. Buldyrev, E. L. Nave, A. J. Moreno, I. Saika-Voivod, F. Sciortino, and P. Tartaglia, 2005, *Phys. Rev. Lett.* **94**, 218301.
- Zaccarelli, E., and W. C. K. Poon, 2009, *Proc. Natl. Acad. Sci. U.S.A.* **106**, 15203.
- Zausch, J., J. Horbach, M. Laurati, S. Egelhaaf, J. Brader, T. Voigtmann, and M. Fuchs, 2008, *J. Phys. Condens. Matter* **20**, 404210.
- Zhu, L., N. Sun, K. Papadopoulos, and D. D. Kee, 2001, *J. Rheol.* **45**, 1105.
- Zia, R., B. J. Landrum, and W. B. Russel, 2014, *J. Rheol.* **58**, 1121.